university of groningen

Multi-Level Control in an Electric Vehicle Smart Parking Lot

MSc Thesis
Industrial Engineering and Management

Author:
M.G. van Ruitenbeek

Supervisors:
Dr. S. Trip
Prof. Dr. Ir. J.M.A. Scherpen
Prof. Dr. Ir. M. Cao

April 16, 2018

Abstract

The combination of a fast growing renewable energy sector, an increasing shift towards electric energy in the transport sector, and an expected increase in the sales of electric vehicles (EVs) asks for an improved infrastructure for charging these vehicles using renewable energy. A concept which responds to the needs of charging using renewable energy sources, is described in literature as an Electric Vehicle Smart Parking Lot (EVSPL) which generates, stores and distributes energy.

In this thesis a Multi-Level control method is proposed for an EVSPL, which balances the network while taking into account the unpredictability of renewable energy. A Higher-Level controller, based on the Model-Predictive Control methodology, creates setpoints for the chargers in the EVSPL. These chargers are controlled by a Lower-Level control method based on second-order Sliding Mode Control.

After testing the different controllers on a constructed simulation of an EVSPL, it is clear that Sliding Mode Control is able to provide stability for the network. Moreover, the Higher-Level controller shows promising results when future time steps are incorporated. Although combining both control methods comes with great computation loads, a Multi-Level control approach shows adequate stability in the linear and nonlinear area of the charging curve.

It should be noted that the used time frames are very short and further research should reveal whether the Multi-Level control method is also able to keep the stability for a larger time span. Suggested improvements imply the implementation of adaptive second-order Sliding Mode Control and a more detailed MPC model which is used in the Higher-Level controller. The final step would be testing this Multi-Level control method in an experimental setup.

Contents

Acronyms

AC	Alternating Current
BESS	Battery Energy Storage System
CS	Charging Station
DC	Direct Current
DES	Distributed Energy Source
DNI	Direct Normal Irradiance
DSO	Distribution System Operator
EV	(Fully) Electric Vehicle
EVSPL	Electric Vehicle Smart Parking Lot
FCHEV	Fuel Cell Hybrid Electric Vehicle
GHG	Greenhouse Gases
HEV	Hybrid Electric Vehicle
HLC	Higher-Level Control
HRES	Hybrid Renewable Energy System
IEA	International Energy Agency
IGBT	Insulated Gate Bipolar Transistor
LLC	Lower-Level Control
MG	Micro-Grid
MILP	Mixed Integer Linear Programming
MLC	Multi-Level Control
MINLP	Mixed Integer Non-Linear Programming
MPC	Model Predictive Control
PI Control	Proportional-Integral Control
PID Control	Proportional-Integral-Derivative Control
PHEV	Plug-in-Hybrid Electric Vehicle
PV Arrays	Photovoltaic Arrays
PWM	Pulse Width Modulation
RES	Renewable Energy Source
SG	Smart-Grid
SMC	Sliding Mode Control
SOC	State-of-Charge
TSO	Transmission System Operator
V2G	Vehicle-to-Grid
V2V	Vehicle-to-Vehicle

1 Introduction

The world energy consumption is growing yearly, while shifting more and more towards electric energy which is mostly produced using fossil fuels (68%), resulting in the emission an enormous amount of harmful Greenhouse Gases (GHG) (EIA, 2017). Fortunately, the fastest growing energy sector is the sector of renewable energy (EIA, 2017) creating huge possibilities in terms of energy production. An impression of these possibilities is the amount of solar power received by earth in one single hour, which is equivalent to the energy consumption of all human activities in one year (EIA, 2014). Next to these possibilities, challenges arise as well. One of these challenges is balancing the power fluctuations caused by the unpredictability of Renewable Energy Sources (RES). Therefore, more time and energy is devoted to researching balancing energy networks to distribute the energy as efficiently as possible. Smart algorithms are designed to solve the optimal power flow problem and thereby reduce power losses, voltage deviations, network costs and emissions (Elsayed et al., 2015).

Another heavy contributor to the emission of GHGs is the transport sector with a quarter of the total emissions around the globe (Nunes et al., 2016). In need of environmental improvement in the transport sector, Electric Vehicles (EVs) have been developed. The electric motors have an higher efficiency than the internal combustion engines (ICE) of ordinary vehicles. This results in lower energy losses and cleaner emissions, as long as RES are used to produce electricity. In Naceur and Gagné (2017), the International Energy Agency (IEA) has reported that the stocks in the EV industry have increased over the last years, as shown in Figure 1.

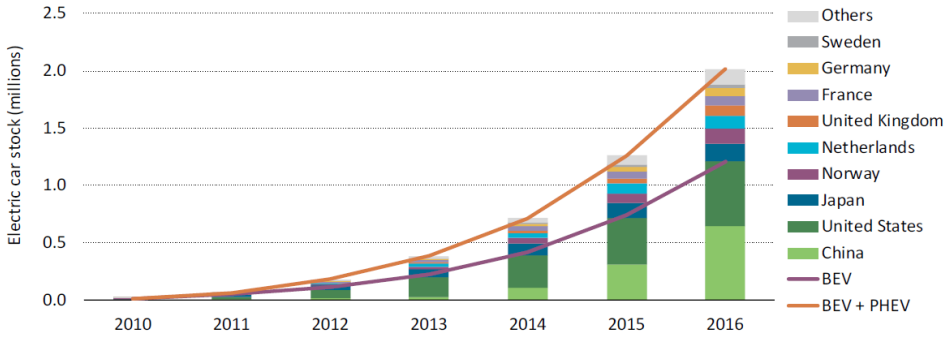

Fig. 1: The evolution of the amount of EVs by country from 2010-2016 (Naceur and Gagné, 2017). Globally, 95% of the sales take place in just ten countries; Norway, the UK, France, Germany, the Netherlands, Sweden, China, the USA, Japan, and Canada.

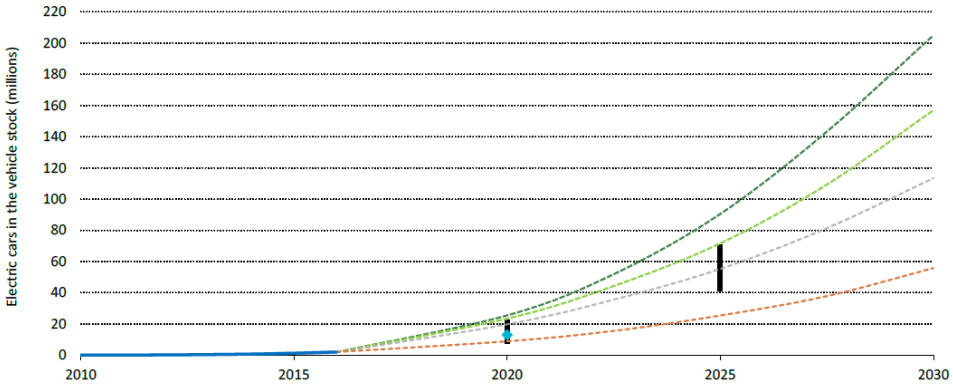

Fig. 2: The prospect of the coming 15 years shows a huge increase in the sales of EVs. Four scenarios are drawn based on the different global agreements (e.g. the Paris Agreement, which is represented by the violet dotted line). A more in-depth analysis can be found in Naceur and Gagné (2017).

The prospect of the coming 15 years, is a huge increase of at least sixty times the amount of sales in 2016 as shown in Figure 2. This trend creates huge opportunities for reducing emission and the emerging of new business models, but also comes with concerns for the charging infrastructure and the increased loads to the utility grid. A solution might be found in the smart distribution of energy.

To summarise, a fast growing renewable energy sector, an increasing shift towards electric energy in the transport sector, and an expected increase in the sales of EVs asks for an improved infrastructure for charging EVs using renewable energy. The energy must be distributed in the most efficient way using smart algorithms to make sure EVs are charged using RESs. A concept which responds to the needs of charging using RESs is described in literature as an **Electric Vehicle Smart Parking Lot** (EVSPL) which generates, stores and distributes energy (Nunes et al., 2016), (Bhatti et al., 2016), (Babic et al., 2017).

Thesis Outline

Nowadays a lot of research is done on balancing electricity networks and the optimal power flow problem at the Engineering and Technology Institute Groningen of the University of Groningen. As described in the introduction, electricity networks will alter in the future due to the rise of electric vehicles. One of the hot topics regarding charging those vehicles is the concept of smart-parking lots which generate, store and distribute energy. Insight on this relative new concept and its impact on electricity network is limited which leads to the following problem statement;

Problem Definition: *Insight in the operational issues of an EVSPL and its control, is limited.*

First of all, section 2 will provide an extended literature study which summarises the current status of EVSPLs in literature. The benefits and challenges are discussed, different charging strategies are revised and a general overview of different case studies is provided. The section is concluded with the knowledge gap which results in the research goal of the thesis and its associated research questions in section 3. This section also explains the basic configuration of an EVSPL, including the assumptions made.

This basic configuration is translated in a model of an EVSPL in section 4. The model will represent the real world and is designed using the power systems tools MATLAB's Simulink. The model will be used to test different control strategies which are introduced in section 5 and section 6. The design choices will be explained carefully.

The simulation model will be controlled using Multi-Level Control (MLC), which is categorised in Lower-Level Control (LLC) and Higher-Level Control (HLC), which are further clarified in section 5 and section 4 respectively. In this thesis, LLC implies the regulation of converters to distribute the electricity as desired, and the HLCer will consists of a controller which uses the Model Predictive Control methodology to generate setpoints for the LLCer.

Moreover, section 7 will be devoted to the actual testing of the designed control methods in three different scenarios. The first scenario will focus on the stability of the power flows and investigates whether Proportional-Integral (PI) control will be able to provide a higher stability compared to econd-order Sliding Mode Control (SMC). The second scenario will study the effects of the HLCer for different prediction horizons and disturbances regarding the environment. The last scenario will be devoted to the effects of a combination of both controllers in an EVSPL by testing the MLC strategy on the constructed EVSPL model.

The thesis will be concluded with summarising the options for further research in section 8 and the reflection upon the goal in section 9.

2 Literature Review

In this section, the current status of EVSPLs in literature will be illustrated. With help of the reviews of Nunes et al. (2016), Bhatti et al. (2016) and Mwasilu et al. (2014) a clear overview will be established.

2.1 Electric Vehicle Smart Parking Lot

An EVSPL is described by Nunes et al. (2016) as a Micro-Grid (MG) which is connected to the local grid, makes use of RESs of its own, and is able to control the distribution of the electricity to parked EVs. As seen in all Micro-Grids (MGs), local reliability is enhanced, emission is reduced, power quality is improved by reducing voltage dips and potentially costs are saved due to lower amount of losses (Hatziargyriou et al., 2014). As an EVSPL can be seen as a MG, the controlled distribution of energy has impact on electricity prices and imbalances on the utility grid. Therefore, EVSPLs act as a pivot between the utility grid, the energy markets and the EV owners.

In many cases, Photovoltaic (PV) arrays are chosen as RES over e.g. wind energy, due to the following benefits; PV energy has lower spatial and temporal variation and PV arrays account for a non-dispatchable and time-floating energy supply which can be coupled to controllable loads and energy storage in terms of EVs well (Nunes et al., 2015) (Widén et al., 2015). A Battery Energy Storage System (BESS) is often introduced to store the energy if the PV array produces more energy than the charging demand of the EVs. A control centre will allocate the energy throughout the MG with the goal of optimal charging which provides the EVSPL with the name 'smart'. Different parameters will play a role regarding the optimal charging policy.

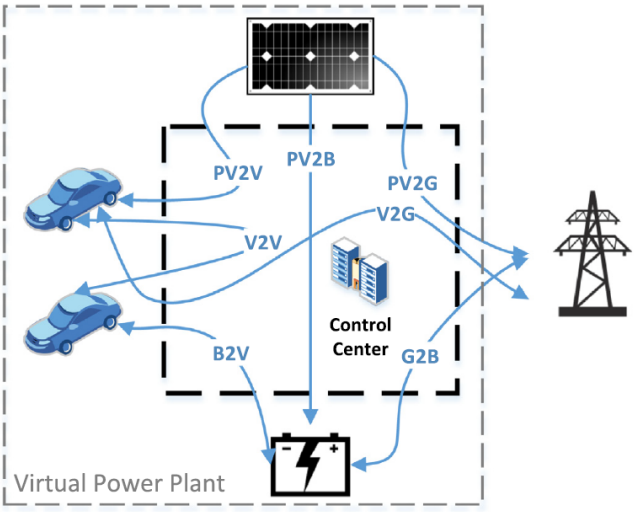

Fig. 3: The energy fluxes in an EVSPL are shown (Nunes et al., 2016). The energy fluxes are named according to the following configuration: 'PV2V', which stands for the energy flux from the PV array to the (Electric) Vehicle. The same accounts for the other fluxes where B is used to describe the BESS, and G stands for the utility grid.

There are unidirectional and bidirectional energy flows in an EVSPL, as shown in Figure 3. The PV arrays generate energy which must be distributed along unidirectional energy fluxes towards the EVs, BESS, or the utility grid. The other flows within the EVSPL are often bidirectional, which entails that electricity is able to flow in both directions. Vehicle-2-Grid (V2G) implies that EVs share their energy with the utility grid which is often accompanied with financial compensations for the EV owners. Vehicle-2-Vehicle (V2V) fluxes are explained by vehicles which donate part of their stored energy to other vehicles. This might occur in the situation that a specific EV needs to leave in a short time frame, while other EVs have enough time to (re)charge and can therefore decide to donate part of their energy. In general often pricing is a key element to establish which way energy should flow.

There are several parties involved in an EVSPL which are associated with decision-making. The **operator of the EVSPL** often pursues the goal of maximising profit by creating revenues from parking fees, charging fees and fees to stabilise the utility grid and minimising operational costs (Babic et al., 2017), (Nunes et al., 2016). The **owners of the EVs** have their own charging strategies and will be able to make decisions regarding maximum charging price, regarding length of charging time, whether discharging is an option, and the maximal energy which may be discharged. Also, the EVs will be full of constraints in the field of charging (max. power flows, max voltages, etc.). Lastly, the **system operators of the utility grid** will determine the electricity pricing and the capacity of the utility grid. The Distribution System Operators (DSO) will account for the day-ahead-market and local power distribution. Transmission System Operators (TSO) will determine power supply on regional or national level, including the pricing. Especially DSOs will be in contact with EVSPL operators as it will be mainly focused on the day-ahead market and local grid stabilisation in short time frames (Nunes et al., 2016).

2.2 Benefits & Challenges

Nunes et al. (2016) provides an overview of the benefits which EVSPLs will bring, as well as challenges which must be overcome in the short future. They are categorised in the usage of renewable energy, balance of energy, infrastructure, awareness of electric driving, and the stimulation of local economies.

First of all, EVSPLs use mostly RESs for charging instead of home charging. A challenge which arises here, is the actual coordination between the production of the renewable energy and the charger demand of the EVs as the RESs come with lower predictability.

Secondly, EVSPLs can be used to balance peaks in the utility grid as it has an extensive buffer system, consisting of EVs and a BESS to its decision. On the contrary, EVs also create loads which are difficult to schedule due to human behaviour (Mwasilu et al., 2014). How this energy should be distributed efficiently is still a challenge which must be overcome. Also, as charging and discharging has impact on the battery life of the EVs (Nazri and Pistoia, 2008). An agreement must be established with the EV owners implying constraints of charging and discharging and the financial compensations.

Moreover, construction of EVSPLs leads to an improved charging infrastructure which will stimulate the electric driving sector. Although space in densely populated urban areas is scarce, parking spaces have always been available. Rearranging them to smart-parking areas, will improve charging infrastructure without competing for land use. In rural areas EVSPLs could be helpfull as well. Research of Robinson et al. (2014) has shown that people add value to shaded parking, as it reduces the temperature in the vehicle and protects the vehicle from weather circumstances as intense sunlight or precipitation.

Next to that, an increased infrastructure will increase awareness of the electric driving sector which has a positive feedback on the adoption of EVs and vice-verse (Robinson et al., 2014). Furthermore, trends can be closely watched and reacted upon, as EVSPL will have access to a lot of data regarding charging of EVs.

Lastly, the local economy is stimulated when EVSPLs are present. Next to the construction and maintenance of the car park, an EVSPL will always be associated with a business model. How the exact business models will look like is still a challenge which must be overcome.

Benefits	**Challenges**
Usage of renewable energy	Coordination of RES production and EV demand
Balancing of peaks in the utility grid	Control of energy distribution
Improvement in the charging infrastructure	Agreement on battery life conditions
No competition for land usage	Creation of business models
Protection of EVs from weather circumstances	
Increased awareness for electric driving	
Insights in trends of EVs	
Stimulation of local economies	

Tab. 1: A summmary of the benefits and challenges of an EVSPL are shown here.

2.3 Charging Strategies

In Yilmaz and Krein (2013) different EV charger typologies have been reviewed. First of all, a separation is made between on-board charging and off-board charging with unidirectional or bidirectional energy flows. Yilmaz and Krein (2013) distinguishes three charging levels from slow (1) to fast (3) as shown in Table 2. All EVs have an on-board charger, which is able to change Alternating Current (AC) to the required Direct Current (DC) for the battery. Due to this configuration, the EV can be charged at most regular power sockets. If a higher charging level is required, the electricity is converted beforehand, using off-board converters to create DC which can directly be used by the battery of the EV. Due to the high costs, large space occupation and high weight of these converters, they are found in charging station instead of in the EVs.

Level	Voltage	Charger Type	Power Supply	Typical Use	Typical Location
Level 1	230	On-Board	1.4 kW (at 12 A)	PHEVs	Home
	AC	1-Phase	1.9 kW (at 20 A)	EVs	Office
Level 2	400	On-Board	4 kW (at 17 A)	PHEVs	Private Outlets
	AC	1-Phase or	8 kW (at 32 A)	EVs	Public Outlets
		3-Phase	19.2 kW (at 80 A)		
Level 3	200-600	Off-Board	50 kW	EVs	Commercial Stations
	DC	3-Phase	100 kW		EVSPL

Tab. 2: Different charging levels in Europe for typical locations, based on Yilmaz and Krein (2013). PHEV stands for Plug-in-Hybrid Electric Vehicle.

A review of García-Villalobos et al. (2014) clearly makes a distinction between *uncontrolled* and *controlled* charging which is categorised in off-peak charging, and two types of smart-charging (valley filling and peak saving). From the lowest level of control (*Uncontrolled Charging*) to the highest level of control (*Smart Charging: Peak Saving*) the implementation will become more and more complex. This encompasses complicated algorithms and high computation power which is often related to high costs. Also, the user friendliness of charging will decrease when the level of control increases, due to focus on grid information, instead of solely taking into account EV owners' charging behaviour. Another aspect which should be taken into account is the battery life of the EVs, as constantly charging and discharging will degrade the battery more quickly, as described by Nazri and Pistoia (2008).

On the other hand, smart charging creates huge opportunities for the utility grid. It will be able to reduce peaks in power fluctuations, which provides a higher stability and is accompanied with lower investment and maintenance costs for the grid operators. Next to that, optimal integration with unpredictable RES power will provide a stable network ready for the future. Also, anticipating on electricity prices will save energy costs and can generate new business models.

Within controlled charging, a distinction is made between *centralised*, *decentralised* and *distributed* control. A typical centralised control architecture consists of an aggregator which communicates with the utility grid, distributes the energy fluxes and will make sure the network is safely operated. All decisions are made by a central control centre. Decentralised control is also known as indirect or local control and entails that control inputs can be generated without the knowledge of the states of other EVs. Distributed control however, takes into account the states of EVs and the computations are spread over the different chargers.

It is noted that optimisation algorithms of centralised control are relatively easy to compose, but require a large amount of data which is not always simply available in advance (due to e.g. privacy issues). This asks for high computation power at the central location, resulting in difficult scalable models as an increase of EVs will directly result in higher computation power. However, the renewable energy is generated centrally, which can easily be implemented in centralised control but back-up systems should also be taken into account when all decisions are made centrally. Distributed charging also requires a lot of data, but the computation can be spread over multiple EVs.

In decentralised control, the EVs will determine the power flows, and an optimum energy distribution

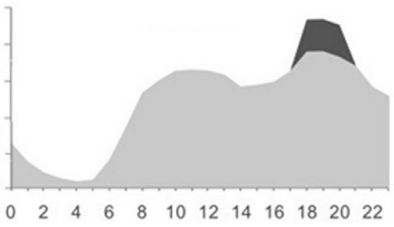

(a) Uncontrolled Charging

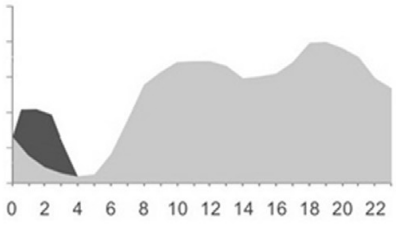

(b) Off-Peak Charging

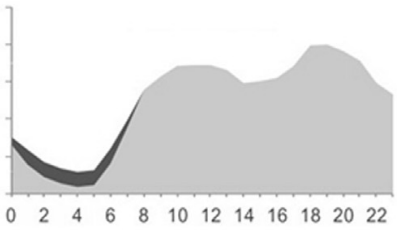

(c) Smart Charging: Valley Filling

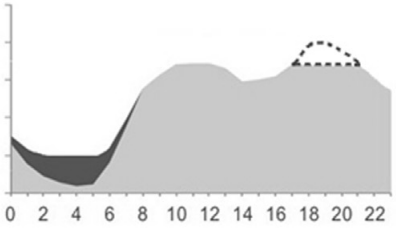

(d) Smart Charging: Peak Saving

Fig. 4: In the figure, different charging types according to (García-Villalobos et al., 2014) are shown. Uncontrolled charging will lead to higher peaks at the moment people are already using a lot of electricity. This situation refers to people which arrive at home around 18:00 PM and immediately start charging as shown by the dark-grey area in 4a. Off-peak charging postpones charging to an off-peak moment in the regular electricity usage e.g. 02:00 AM (4b). Smart charging will allow the electricity to be balanced more evenly in either valley filling mode (4c) or peak saving mode (4d). The difference between these two options is the fact that the peak saving mode will also reduce the peaks of the regular electricity usage by storing energy in, or withdrawing energy from the EVs.

is often found due to pricing mechanisms. This requires fewer computation power and easier scalable models. As the market is not regulated by centralised or distributed control, the market possibilities seem higher for decentralised control compared to the other options. To summarise, the mentioned aspects related to the level of control are graded in five terms (++, +, +−, −, −−) based on the positive and negative value of the aspects. This is shown in Table 3.

Level of Control → Aspects ↓	**Low**	**High Centralised**	**High Decentralised**	**High Distributed**
Communication Infrastructure	+ +	+ -	-	-
Complexity Data Processing	+ +	- -	-	- -
Data Availability	+ +	- -	+ -	+ -
Forecasting Difficulty	- -	+ +	-	- -
Grid Maint. Costs	- -	+ +	+	+
Grid Stability	- -	+ +	+ -	+ +
Integration of RESs	- -	+ +	+	+
Market Possibilities	- -	+	+ +	+
User Friendliness	+ +	- -	-	-
Privacy	+ +	- -	+	-
Scalability	+ +	- -	+	+ -
Service and Maintenance	- -	+ +	+ -	+ -
Utilisation Network Capacity	- -	+ +	+	+ +

Tab. 3: The positive and negative aspects regarding the different levels of control.

2.4 Case Studies

In literature, many case studies have been executed, which will be explored in this section. The case studies will be subdivided into categories based on Richardson (2013), Nunes et al. (2016) and García-Villalobos et al. (2014). The studies will be categorised in terms of their objectives, which can be subdivided into either economical analysis (focusing on costs savings or profitability) or environmental analysis (focusing on reduction of environmental impact in terms of CO_2). Regarding these analyses multiple perspectives are chosen; an EV owner's, the EVSPL owner's or the utility grid operator's (DSO) perspective. There are studies which combine an EV/EVSPL perspective or an EVSPL/DSO perspective, yet no combination of an EV/DSO perspective was found in literature. This results in the structure as described by Figure 5.

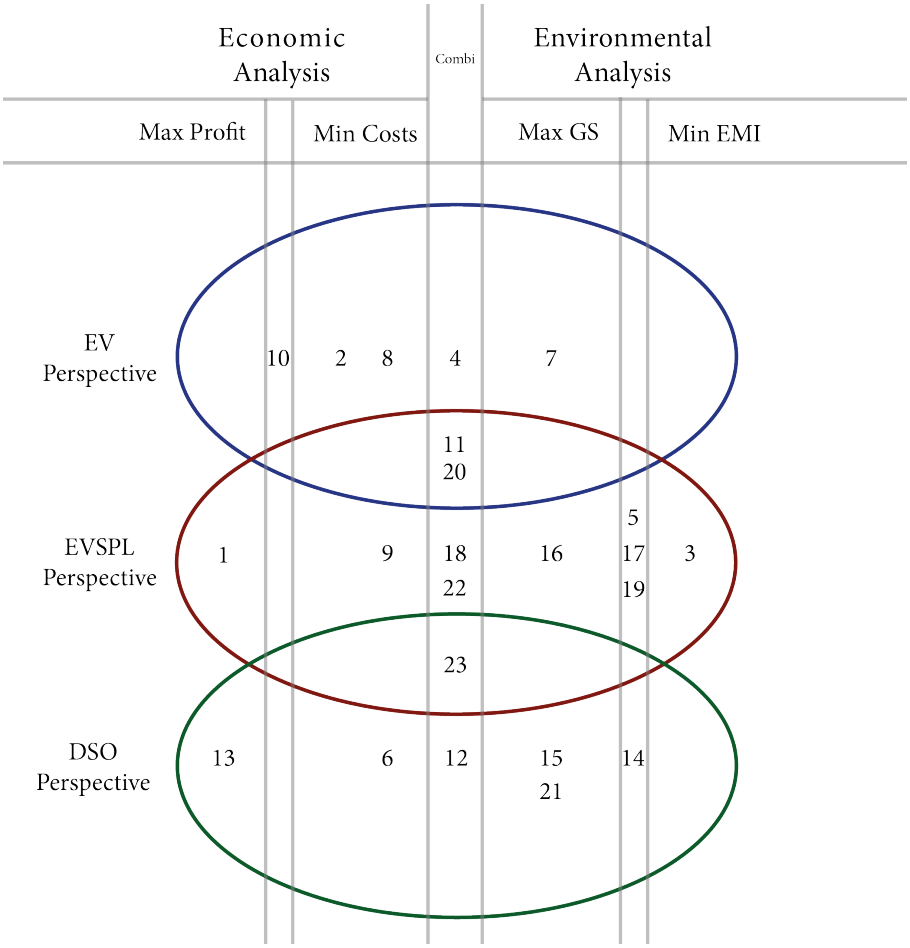

Fig. 5: This figure illustrates the chosen structure for the case studies by goal. The goal 'Max GS' implies maximum grid stability and 'Min EMI' implies minimising the emissions of GHGs. The goal 'Max Profit', solely enhances financial issues, while the 'Min Costs' is often connected to the 'Max GS'. The same numbers as Table 5, and Table 7 are used.

A separation is also made within the control structure in terms of uncontrolled, centralised and distributed control with associated approaches like: Agent-Based Control, Model Predictive Control (MPC), Mixed Integer Linear Programming (MILP) Control, Mixed Integer Non-Linear Programming Control (MILNP) and Genetic Algorithms.

The analysed case studies are summarised using two tables; Table 5 summarises the objective(s) and the control strategies of different case studies and Table 7 elaborates on the components of these case studies.

2.4.1 Types of Analysis

In this thesis, three categories will be reflected upon; **economical**, **environmental** or a **combination of both**. In Tulpule et al. (2013), the economic and environmental aspects of a solar powered parking station are discussed from multiple perspectives. It concludes with an advice that future carbon tax will increase the attractiveness of the charging facilities. Babic et al. (2017), however solely focuses on the economic benefits of an EVSPL and compares parking time revenues to profits of energy distribution. An impression of investment costs are shown in different EVSPL sizes when the utilisation of the parking lot is calculated by an agent-based simulation approach using real-life data. Fazelpour et al. (2014) and Rahbari et al. (2017) on the contrary, are not interested in profitability or pricing around an EVSPL. These papers focus on designing a controller to stabilise the MG and make optimal use of RESs.

2.4.2 Perspectives

Next to the different types of analyses, a distinction is made from what perspective the case studies are performed. A study is either investigated from the perspective of the **EVSPL owner**, the **EV owner**, the **utility grid operator** (DSO) or a **combination** of these. In the case of the EVSPL, the focus is often on saving costs or improving profitability, regularly in combination with maximising the usage of RES energy. From the perspective of the DSO, the interaction between the EVSPL and the utility grid is often the central topic as shown in an economically oriented case study of Moradijoz et al. (2013). It concludes that a DSO will end up with an economical profit as well as an improved voltage profile when EVs would be implemented in the local utility grid. On the other hand, human aspects must be taken into account when (dis)charging EVs as shown in a study of Babic et al. (2016). Related to profitability, Jurica Babic configures a model, by means of a Bayesian Network, entailing an EV owner's willingness to pay for charging the EV. Honarmand et al. (2015) combines multiple perspectives in his aim to maximise the total benefits of an EVSPL and an EV in terms of profitability using a a MILP solver.

2.4.3 Objective Functions

As all case studies have different objectives, a selection has been made according to optimisation functions within the economical and environmental analyses. From an economic perspective a difference is seen at **maximising profit** (MaxPROF) and **minimising costs** (MinCOST) due to the fact that profitability is often related with the EVSPL, leaving no room for an EV or DSO perspective. Also, maximising a profit includes revenue streams while cost reduction is just an element of profitability. From the sustainable point of view, two objective functions arise; **maximising grid stability** (MaxGS) and **minimising emissions** (MinEMI). In Figure 5, the middle column shows a combination of economical and environmental analyses, which also gives rise to a combination of objective functions.

An example of such a combination function is found in Pahasa and Ngamroo (2015) which focuses on coordinating the utility grid with disturbances due to PHEVs and RES. The environmental impact is kept as low as possible while trying to make profit in balancing the network. Mohamed et al. (2014) uses a similar objective, yet optimising stochastic models in terms of different charging priority levels. Traube et al. (2012) investigates different operating modes and the effect on the utility grid using a laboratory experimental setup. The conclusion is that the system facilitates efficient and fast EV charging without requiring communication between the utility grid. Preetham and Shireen (2012) executes a similar objective but uses simulation tools to come to the conclusion that a unique control strategy, based on DC voltage sensing, decreases the fluctuations in the utility grid in different charging modes.

2.4.4 Controller

Within control strategies, the categories in subsection 2.3 are used. Most of the analysed studies, use a centralised controller. However, distributed charging was described in e.g. Gan et al. (2013) and Pahasa and Ngamroo (2016). The first paper introduces a distributed algorithm which controls the energy flow, and accurately describes the mathematical descriptions of these algorithms. Pahasa and Ngamroo (2016) uses distributed MPC to combine smoothing wind power by changing the pitch angle, and PHEV charging in most efficient way.

2.4.5 Approach

A **Model Predictive Control** (MPC) approach is often used in the renewable energy sector as it features the ability to multitask, by addressing the different control objectives in a single cost function of the algorithm (Sultana et al., 2017). More information regarding MPC can be found in section 6. In Su et al. (2014) a multi-level control approach, with MPC and power tools software, a optimisation on power losses and pricing is investigated. It concludes that MPC is able to accommodate uncertainties and variability in EV charging. This is confirmed by Di Giorgio et al. (2014) which summarises the effect of an MPC controller in terms of sustainability and cost efficiency. Halvgaard et al. (2012) uses a specific type of MPC, referred to as economic MPC which is completely driven by pricing.

Genetic algorithms are often used as optimisation technique (Fazelpour et al., 2014),(Moradijoz et al., 2013) and (Rahbari et al., 2017), as well as **Multi-Integer-Linear-Programming Tools** (Su et al., 2014), (Zakariazadeh et al., 2015) and (Honarmand et al., 2015). When control on lower level is executed, often case studies use **Proportional-Integral-Derivative (PID) Control within converters** (Goli and Shireen, 2014) and (Traube et al., 2012). Yet, **multi-level control** is not as much used, as expected. As most case studies focus on either the energy distribution, or converter control a multi-level approach is only described by a few case studies like Mohamed et al. (2014) and Su et al. (2014). It seems interesting to investigate opportunities around multi-level control.

2.4.6 Components

In this literature review, a separation is made between the different components and their description. First of all, the EVs are specified by amount, type, arrival rate, pricing strategy and whether depletion is taken into account. The grid is characterised by the option of V2G and whether is pricing is fixed, variable or not part of the research. Lastly, Table 7 clearly shows whether PV Cells, Wind Generation, Storage Capacity or Generators are taken into account. The last column in the table determines whether a stochastic or deterministic model is used by the authors.

Honarmand et al. (2014a) gives a great overview when all components are involved in optimal charging to minimise the operation costs of an EVSPL. Zakariazadeh et al. (2015) focuses more on the integration of the RES energy in reserve scheduling of the EVs. As the most promising RES for an EVSPL is solar energy, many papers are using this combination; Birnie (2009), Goli and Shireen (2014), Tulpule et al. (2013) and Honarmand et al. (2015). The amount of EVs differs hugely throughout different case studies. Situations with more than 1000 EV are analysed ((Pahasa and Ngamroo, 2015) and (Pahasa and Ngamroo, 2016), while other studies only focus on one battery and its impact ((Yan et al., 2011) and (Goli and Shireen, 2014)).

Case Studies

No.	Described by	Objective	Analysis	Perspective	Obj. Function	Controller	Approach	Remarks
1.	Babic et al. (2017)	Economic benefits of EVSPL	Eco	EVSPL	MaxPROF	Centr	Agent-Based	Focuses on different sizes of EVSPLs and their profits due to electricity trading and extended parking.
2.	Babic et al. (2016)	Willingness to pay for charging services	Eco	EV	MaxPROF	Unctrl	Bayesian	Establishes willingness to pay in terms of EV capacity, EV SOC, charging speed and reference price.
3.	Birnie (2009)	Analyse impact on daytime charging during work hours	Env	EVSPL	MinEMI	Unctrl	-	Establishes clear models of PV irradiance and its possibilities.
4.	Di Giorgio et al. (2014)	Test an event-driven MPC strategy at saving costs within proper power profiles	Eco/Env	EV	MinCOST / MaxGS	Centr	Event-driven MPC / MILP	Simulates 3 cases: 1) normal operation; 2) reaction to DSM signals; 3) sensitivity analysis.
5.	Fazelpour et al. (2014)	Optimum size, site and charge allocation of EVSPL	Env	EVSPL	MaxGS / MinEMI	Centr	GEN	Optimisation on power and voltage profiles for charge allocation.
6.	Gan et al. (2013)	Uses decentralised charging technique	Eco	DSO	MinCOST	Distr	New Algorithm	Two cases, homogeneous and non-homogenous charging pattern of EVs. Clear mathematical description of algorithms.

Table Continues on Next Page

Case Studies

No.	Described by	Objective	Analysis	Perspective	Obj. Function	Controller	Approach	Remarks
7.	Goli and Shireen (2014)	Charge PHEV using minimal energy from utility grid	Env	EVSPL	MaxGS	Centr	PID Voltage	Uses real experimental setup with variable solar irradiance.
8.	Halvgaard et al. (2012)	Tests working of economic MPC in charging costs and driving pattern	Eco	EV	MinCOST	Centr	Economic MPC / MILP	Compares uncontrolled/controlled takes into accountn driving patterns.
9.	Honarmand et al. (2014a)	Minimize microgrid total operation costs.	Eco	EVSPL	MinCOST	Centr	MILP / LP	Simulates scenarios: 1) EVs variable load; 2) V2G, no reserve scheduling; 3) V2G, incl. reserve scheduling
10.	Honarmand et al. (2014b)	Maximise profit for EV by charge scheduling	Eco	EV	maxPROF / minCOST	Centr	NP	Simulation of 2 scenarios: 1) infinite switching charging/discharging 2) older battery relates to lower amount of switching
11.	Honarmand et al. (2015)	Maximise benefits of EVSPL and EV	Eco/Env	EV/EVSPL	MaxPROF / MinEMI	Centr	MILP/LP	Multiple perspectives approach using a clear description of solver technique.
12.	Mohamed et al. (2014)	Develop energy management algorithm using statistical data.	Eco/Env	DSO	MinCOST / MaxGS	Centr	Multi-Level / Fuzzy Control	Uses 5 priority levels with different charging rates. Combination MATLAB/SIMULINK and PowerFactory program.

Table Continues on Next Page

Case Studies

No.	Described by	Objective	Analysis	Perspective	Obj. Function	Controller	Approach	Remarks
13.	Moradijoz et al. (2013)	Optimum size of EVSPL for supplying loads to the utility grid	Eco	DSO	MaxPROF	Centr	GEN	Economical profit for DSO and improved voltage profile.
14.	Pahasa and Ngamroo (2015)	Real-time optimal control by MMPC algorithm	Env	DSO	MaxGS / MinEMI	Distr	MMPC / MPC / PID	Investigates 4 studies where all EVs have different initial states of charge.
15.	Pahasa and Ngamroo (2016)	Coordinate control of wind and PHEV load for charging by means of MPC	Env	DSO	MaxGS	Distr	MPC / PID	Summarises three cases of different wind speed.
16.	Preetham and Shireen (2012)	Charge PHEV using minimal energy from the utility which is validated by a simulation in Simulink	Env	EVSPL	MaxGS	Centr	PID Voltage	Validates converter control in four different modes.
17.	Rahbari et al. (2017)	Location EVSPL, size HRES and distribute energy	Env	EVSPL	MaxGS / MinEMI	Centr	GEN/PSO	Optimisation on power losses and minimum voltage deviation.
18.	Su et al. (2014)	Test whether MPC works for charging PHEVs under various charging schemes	Eco / Env	EVSPL	MinCOST / MaxGS	Centr	Multilevel MPC / Power Systems Tools	Compares MPC to non-MPC with a constant EV load which acts upon the grid. Focuses on charging costs and power loses.

Table Continues on Next Page

Case Studies

No.	Described by	Objective	Analysis	Perspective	Obj. Function	Controller	Approach	Remarks
19.	Traube et al. (2012)	Present operating modes, charging and grid support in real experimental setup	Env	EVSPL	MaxGS / MinEMI	Centr	PI Voltage	Shows different charging modes in real life setup.
20.	Tulpule et al. (2013)	Impact of optimal charge scheduling on economics and emission	Eco/Env	EV/EVSPL	MaxPROF / MinEMI	Unctrl/Centr	DP	Compares uncontrolled charging with smart algorithm in terms of emission and reserve scheduling.
21.	Yan et al. (2011)	Test a MPC controller in a single battery attached to the utility grid	Env	DSO	MaxGS	Centr	MPC / Genetic Algorithm	Focuses on charging duration and the temperature of the battery.
22.	Zakariazadeh et al. (2014)	Test multi-objective scheduling method	Eco/Env	EVSPL	MinCOST / MinEMI	Centr	MINLP/NLP/ MILP	Balances costs and emission in three case studies, separate and combined.
23.	Zakariazadeh et al. (2015)	Examine potential of Evs in two types of reserve scheduling to integrate RES	Eco/Env	EVSPL / DSO	MinCOST / MinEMI	Centr	MILP	Focuses on reserve scheduling using the integration of RES.

End of Table

Tab. 5: Overview Case Studies by Goals

Component Structure

No.	Article	EVs					Grid		PV	Wind	Storage	Generator	
		Amount	Types	Arrival	Pricing	Depletion	V2G	Pricing					Model
1.	Babic et al. (2017)	30-90	1	Stoch	Var	Y	Y	Fix	N	N	N	N	-
2.	Babic et al. (2016)	1	2	Stoch	Fix	N	N	Fix	N	N	N	N	-
3.	Birnie (2009)	1	1	-	-	N	Y	-	Y	N	N	N	Det
4.	Di Giorgio et al. (2014)	1	1	-	Var	Y	Y	Var	N	N	N	N	-
5.	Fazelpour et al. (2014)	1000	1	Stoch	-	-	Y	-	Y	Y	N	Y	Stoch
6.	Gan et al. (2013)	20	1	Stoch	Var	N	N	Var	N	N	N	N	-
7.	Goli and Shireen (2014)	1	1	-	-	N	Y	-	Y	N	N	N	Det
8.	Halvgaard et al. (2012)	1	1	-	Var	N	Y	Var	N	N	N	N	-
9.	Honarmand et al. (2014a)	500	1	Stoch	Var	N	Y	Var	Y	Y	Y	Y	Stoch
10.	Honarmand et al. (2014b)	500	1	Det	Var	Y	Y	Var	N	N	Y	N	-
11.	Honarmand et al. (2015)	500	1	Stoch	Var	N	Y	Var	Y	N	N	Y	Stoch
12.	Mohamed et al. (2014)	900	3	Stoch	Var	N	Y	Var	Y	N	N	N	Stoch
13.	Moradijoz et al. (2013)	25-150	1	Stoch	Var	N	Y	Var	N	N	N	N	-
14.	Pahasa and Ngamroo (2015)	100,000	1	Stoch	-	N	Y	-	N	Y	N	Y	Det
15.	Pahasa and Ngamroo (2016)	400,000	1	Stoch	-	N	Y	-	N	Y	N	N	Det
16.	Preetham and Shireen (2012)	1	1	-	-	N	Y	-	Y	N	N	N	Det
17.	Rahbari et al. (2017)	1-300	1	Stoch	-	N	Y	-	Y	Y	N	N	Det
18.	Su et al. (2014)	1	1	-	Var	N	N	Var	Y	Y	Y	Y	Det
19.	Traube et al. (2012)	1	1	-	-	Y	Y	-	Y	N	N	N	Det
20.	Tulpule et al. (2013)	50	3	Stoch	Fix	N	Y	Fix	Y	N	N	N	Stoch
21.	Yan et al. (2011)	1	1	-	-	N	N	-	N	N	N	N	-
22.	Zakariazadeh et al. (2014)	50-200	3	Det	Var	-	Y	Var	N	N	Y	Y	Det
23.	Zakariazadeh et al. (2015)	120-200	1	Det	Var	N	Y	Var	Y	Y	N	N	Det

End of Table

Tab. 7: Overview Case Studies by Components

2.5 Open Issues

According to García-Villalobos et al. (2014) and Nunes et al. (2016), there are still a lot of obstacles and open issues which deserve more attention in future research. Research topics like;

- Battery Characteristics,
- Field Testing,
- Human Behaviour,
- Integration in MGs,
- New Mobility Concepts,
- Policies for Trading,
- Power Systems Analysis Tools, and
- V1G instead of V2G Systems.

First of all, often battery fading is not taken into account in the case studies. Although it requires more complex battery modelling, it is still a major issue, especially in V2G processes. Assuming infinite charging and discharging, without affecting battery life is not recommended, but often done in literature. This creates too optimistic scenarios. Though a lot of research is devoted to V2G systems, in the near future Grid-to-Vehicle (V1G) seems at least as interesting due to major battery issues which must be solved before actually implementing V2G systems on a large scale.

Secondly, field testing is still in early stages of development for EVs and their infrastructure, as described by (Knezović et al., 2017). (Nunes et al., 2016) confirms this by stating that field testing would be the next step which need to be addressed more in literature.

Trading policies must be established as there is a high chance that pricing will establish control within MGs and EVSPLs in the future. How these trading policies will be designed is an interesting subject which needs more attention (Nunes et al., 2016).

In the analysed literature reviews, human behaviour is only described by (Babic et al., 2016), which is addressing a willingness to pay model from the perspective of EV owners. Trade-offs of EV owners' impact in terms of response to pricing, battery life, and new mobility concepts are barely reviewed in literature (Nunes et al., 2016). New mobility trends like automatic driving and vehicle sharing, will hugely affect the operations of an EVSPL as well as EV owners' behaviour. Research on these topics is seen as a next step, which should be taken.

Following Table 7 often research is done one a particular limited MG, excluding many components (e.g. storage). In most case studies, the relation between the different components are not taken into account. The combination of multiple components and their response to EV charging seems an interesting direction for future studies.

Lastly, one of the major drawbacks of most current studies is the fact that power systems analysis software is not used often. The energy losses and voltage fluctuations in a MG are not taken into account, providing unrealistic scenarios. Although field testing will provide more accurate results, power analysis software tools like MATLAB/Simulink or OrCAD/Pspice will already improve the results extensively (Preetham and Shireen, 2012).

3 Research Focus

As described insubsection 2.5, many open issues are present regarding EVSPLs. As not all issues can be explored due to time limitations, this thesis will focus on the following open issues:

- the integration in Micro-Grids,
- the implementation of power systems analysis tools, and
- a V1G configuration instead of V2G systems.

The integration of different components within a MG will be the central theme which will be investigated using the power systems analysis tools MATLAB/Simulink. This will be investigated by establishing a simulation model of the EVSPL including its components. Important to take into account is the control scheme of an EVSPL, which is key to understanding and designing a realistic simulation model. Control methods will be established to control the power flows within the EVSPL. When the model is constructed, case studies will be designed to test the different control methods. Moreover, the simulation model should be easily adaptable, as further research at the University of Groningen can use the model to test newly designed case studies. The current and future scenarios will be able to create insight in the operational issues of EVSPLs and their control, as stated in the introduction.

> ***Research Goal:*** *To design a control strategy for an EVSPL which is tested for different scenarios using a realistic simulation model of an EVSPL. The simulation model should be easily adaptable and should make use of power systems tools. Also, case scenarios should be designed to generate insight in the operational issues of EVSPLs.*

3.1 Research Questions

To attain the research goal and provide structure to this thesis, research questions are designed. According to Wieringa (2014), these questions can be subdivided into research and design questions. Knowledge questions will be seen as questions which solely asks for knowledge about the world without any aim to improve it. Design questions aim for information towards a specific goal, in a specific situation.

1. How will the set-up of the EVSPL be configured?
   This design question will determine how set-up of the EVSPL will be configured in 'basic conditions'.
2. How will the configuration of the control strategy be designed?
   This design question will determine how the EVSPL will be controlled.
3. How will the simulation model of the EVSPL be designed to resemble a real EVSPL, while making use of power systems analysis tools?
   This design question will determine how the simulation model of the EVSPL will be configured, and the design choices will be explained carefully.
4. Which control methods are applicable to stabilise the energy fluxes of an EVSPL, and how do these work?
   This knowledge question will summarise different Lower-Level Control techniques.
5. How will the EVSPL be controlled, taking into account future time steps?
   This design question will determine how the Higher-Level Control strategy will be designed to create the setpoints for the Lower-Level Controller.
6. How will the case scenarios be constructed?
   This design question will construct case scenarios to test which add value to the current knowledge base found in literature.
7. What will result from the case scenarios?
   This knowledge question will answer what conclusions can be drawn from the results of the case studies to add knowledge to existing literature.

The research questions will be answered in chronological order during the next sections.

3.2 The Configuration of the EVSPL

In this section, the first research questions: "*How will the set-up of the EVSPL be configured?*" will be answered. It will provide a brief overview of the different components and explain the design choices of the MG.

Based on literature, it is chosen to construct the EVSPL as a DC network, consisting of PV cells, a BESS, a connection to the Utility Grid, multiple EVs and a central controller, as shown in Figure 6. A PV array is regularly chosen as RES due to the convenience of daytime charging (Birnie, 2009), the convenience in space occupation in urban areas (Fazelpour et al., 2014), and the future prospect of solar energy (EIA, 2014). Due to the absence of integrated buffer systems described in subsection 2.5, a BESS is included in the configuration of the EVSPL. Lastly, the connection to the utility grid will provide a stable power source as well as a flexible load to make sure that all energy can be balanced.

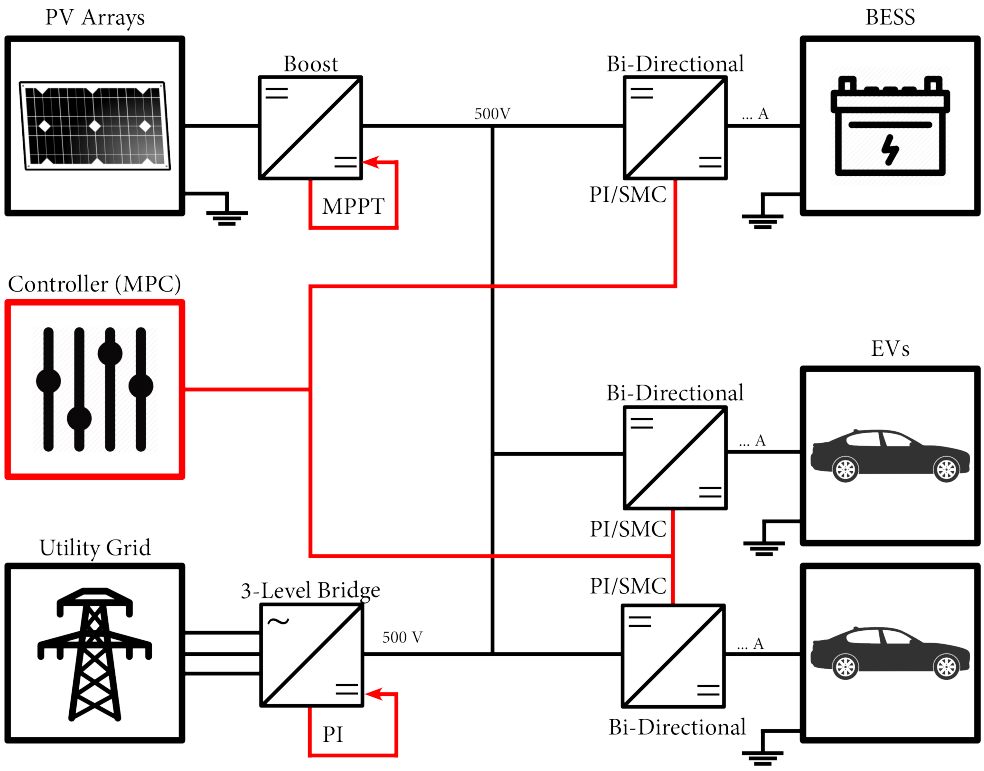

Fig. 6: The configuration of the EVSPL as a DC microgrid is shown.

A DC network was chosen over an AC network, due to multiple reasons. First of all DC infrastructures are easier controllable due to the absence of reactive power, frequency monitoring and electromagnetic interferences (Justo et al., 2013). Also, DC distribution lines have lower line resistance, which is related to a lower amount of power loss. Moreover, converting energy is always accompanied with power losses, making it more efficient to keep the DC generated power from the PV cells and BESS instead of transforming it. Lastly, as explained in subsection 2.3, a DC network offers advantages for fast-charging (Hamilton et al., 2010). As high voltage lines are accompanied with lower power losses, and the nominal voltage of most EVs is around 365V (Mwasilu et al., 2014), it was chosen to keep the voltage of the MG at 500V DC.

The 'basic conditions' of the EVSPL is designed as 10 parking places in the configuration shown in section 10. The roof is completely filled with PV cells, to generate as much energy as possible for charging the EVs. When the amount of EVs is increased, the area of the PV array will increase proportionally.

3.3 The Configuration of the Control Strategy.

This section will answer the second research questions: " *How will the configuration of the control strategy be designed?*", by explaining the MLC strategy.

The DC microgrid is stabilised using converters at different positions, as shown in Figure 6. The 3-Level-Bridge will keep the voltage at 500V DC by either feeding 3-phase AC power to the MG, or taking DC power from the MG. Simultaneously, the PV Arrays will generate power which is maximised using a Maximum Power Point Tracking (MPPT) algorithm, and converted to 500V DC.

After considering the positive and negative aspects in subsection 2.3, a combination of centralised and decentralised control is proposed. As all information regarding the RES and EVs will be generated at a central location, a high grid stability is demanded and forecasting will be taken into account, a centralised HLCer is designed. This HLC strategy is based on the MPC methodology and determines the desired current for the EVSPL. The desired current is stablished with help of the voltage V(t) and State-Of-Charge Q(t) of the BESS and the EVs, hich provided by the EVSPL.

The LLCer uses Pulse-Width Modulation techniques to control the Bi-Directional Converters which results in the power flow from and towards the BESS and the EVs. To keep the power flows of the BESS and the EVs constant, the objective of the LLCer is to keep the current at the desired reference value which is generated by the HLCer. This will be done using Proportional-Integral (PI) Control or Sliding Mode Control (SMC). The overall control scheme is shown in Figure 7. The next sections (5, 6) will go more in-depth on the two different control strategies.

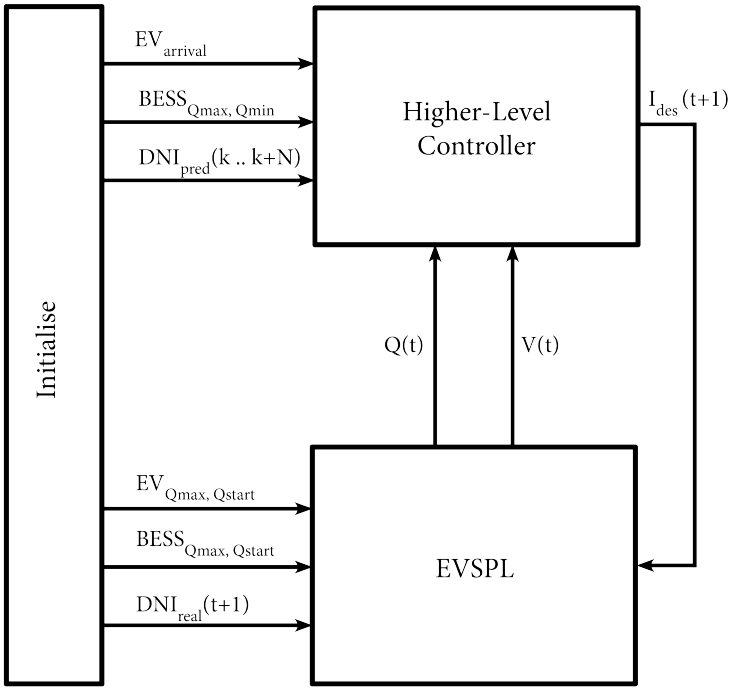

Fig. 7: The MLC scheme of the EVSPL is shown. First the HLCer is initialised using the arrival data, BESS initialising values and the predicted direct normal irradiance DNI as input signals. In the meantime, the EVSPL simulation model is initialised using the EVs' and BESS' battery conditions and their initial SOC Q_{start}. For every time step, the current Voltage V(t) and SOC Q(t) are provided to the HLCer which in return sends to desired current for the next time step for the BESS and the EVs. It should be noted that the LLCer can be found within the EVSPL in this figure.

4 Simulation Model of the EVSPL

In this section, the research question: "*How will the simulation model of the EVSPL be designed to resemble a real EVSPL, while making use of Power Systems Tools?*", will be answered. The simulation model of the EVSPL, will resemble a real EVSPL, and will be used to the multi-level control strategy. First, the used Power Analysis Tools is described. Secondly, the components are described in 'basic' conditions, which is referred to later during the case studies in subsection 2.4. The section is finalised by carefully explaining how the simulation model is integrated in Simulink.

4.1 Power Analysis Software

As described in subsection 2.5, more attention should be spent on simulation using power systems tools. In this thesis, *MATLAB & Simulink's Simscape Power Systems Toolbox* will be used to simulate the behaviour of power flows within the DC network. The choice for MATLAB/Simulink was made because the software is widely available at the University of Groningen, has easy access to convex optimisation solvers, and has a large variety of pre-programmed objects for renewable energy research (Mathworks, 2017c). With help of the existing models of Pierre Giroux (Pierre Giroux, 2012) relating to PV arrays and Mahmoud Saleh's bi-directional converter model (Saleh et al., 2016), the simulation model of the EVSPL was established.

4.2 Photovoltaic Array

On the roof of the EVSPL, photovoltaic array will be placed which will generate power for the charging of the EVs. According to Top10Reviews (2017), the best reviewed solar panel at the moment, is the *Kyocera KD315GX-LPB*. Therefore, this panel is chosen for the simulation model resulting in the details shown in Table 8 which are loaded in Simulink's PV Array Block (Mathworks, 2017b). The circuit diagram of the PV cell is shown in Figure 8 and for a single module the following equations arise;

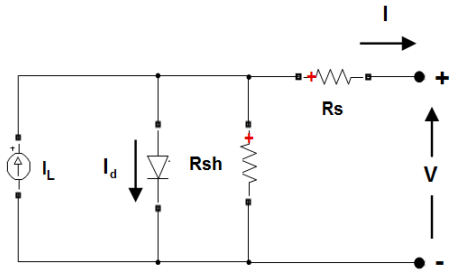

Fig. 8: Circuit Diagram of PV Cell

$$\begin{aligned} \mathrm{I}(t) &= \mathrm{I_L} - \mathrm{I_D}(t) - \mathrm{I}_{sh}(t) \\ \mathrm{I_D}(t) &= \mathrm{I_0}\left(exp\left(\frac{\mathrm{V}_d}{\frac{\eta k \mathrm{T}(t)}{q}\mathrm{N}_{cells}}\right) - 1\right) \\ \mathrm{I}_{sh}(t) &= \frac{\mathrm{V}_d(t)}{\mathrm{R}_{sh}} \end{aligned} \tag{1}$$

$$\begin{aligned} \mathrm{I}(t) &= \mathrm{I_L} - \mathrm{I_0}\left(exp\left(\frac{\mathrm{V}_d}{\frac{\eta k \mathrm{T}(t)}{q}\mathrm{N}_{cells}}\right) - 1\right) - \frac{\mathrm{V}_d(t)}{\mathrm{R}_{sh}} \\ \mathrm{V}(t) &= \mathrm{V}_d(t) - \mathrm{R}_s\mathrm{I}. \end{aligned} \tag{2}$$

where

$\mathrm{I_D}$	= Diode Current		[A]
$\mathrm{I_L}$	= Light-Generated Current (based on irradiance & temp)	8.5131	[A]
$\mathrm{I_0}$	= Diode Saturation Current	$3.9265 * 10^{-10}$	[A]
η	= Diode Ideality Factor	1.0066	
k	= Boltzmann Constant	$1.3806 * 10^{-23}$	$[\frac{\mathrm{J}}{\mathrm{K}}]$
q	= Electron Charge	$1.6022 * 10^{-19}$	[C]
T	= Cell Temperature		[K]
N_{cells}	= Number of Cells Connected in Series in a Module.	80	
R_{sh}	= Shunt Resistance	$2.8434 * 10^{2}$	[Ω]
R_s	= Series Resistance	0.4194	[Ω]
V_d	= Diode Voltage		[V]

In section 10, the total area of the parking lot is calculated using (MUTCD, 2009), resulting in 247.5m^2 in 'basic conditions'. The configuration of the solar panels can be chosen in terms of parallel and series-connected modules. Kirchoff's voltage and current laws can be applied to calculate the voltage and current in the modules. In this way the PV array's voltage can be chosen such that it will be close to the desired 500V of the DC network, resulting in lower stresses for the MPPT-Boost converter. Also keeping in mind the maximal surface area, the PV array was designed such that:

Parallel Strings	10
Series-Connected Modules	10

Resulting in the following configuration;

KyoceraKD315GX-LPB	**Module**	**Array**	**Unit**
Maximum Power	315.2	31520	W
Open Circuit Voltage	49.2	492	V
Short Circuit Current	8.5	85	A
Maximum Power Point Voltage	39.8	398	V
Maximum Power Point Current	7.9	79	A
Number of Cells	80	8000	
Average Solar Efficiency	16	16	%
Dimensions	1.65 x 1.32	16.5 x 13.2	m

Tab. 8: The details of the PV Array.

Figure 9, shows the current and power dynamics for the PV array. The maximum power point is shown by the red dots for two irradiances, 500W/m^2 in blue, and 1000W/m^2 in red. The PV array will work with a Maximum Power Point Tracking technique, which enables a PV array to generate as much energy as possible.

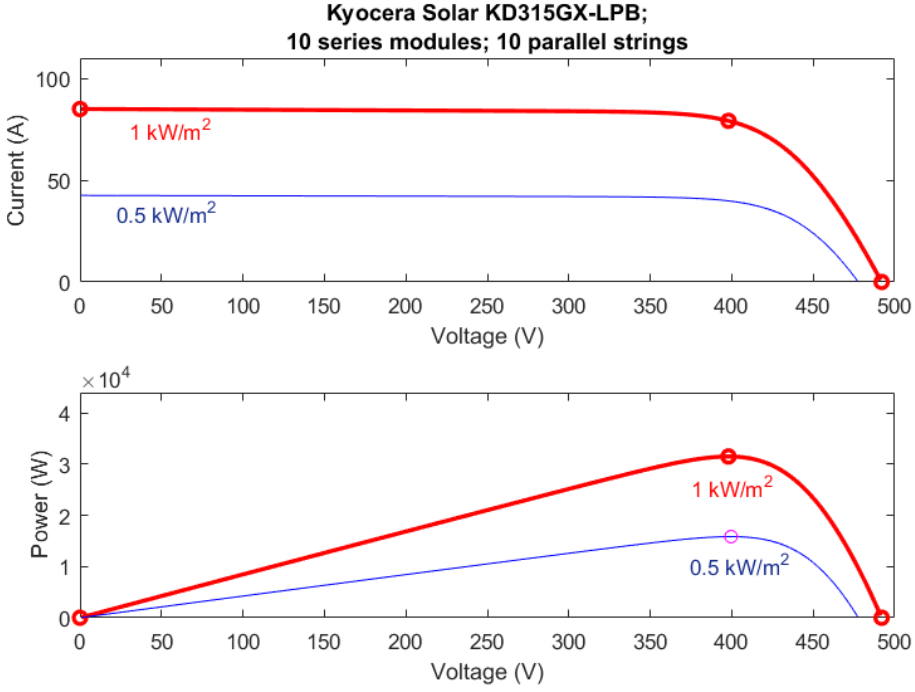

Fig. 9: The current and power dynamics for the Kycocera Solar PV Array.

4.3 Battery Energy Storage System

A Battery Energy Storage System (BESS) will be incorporated in the simulation model, as energy storage is recognised as a valuable tool for alleviating a temporary difference between the supply and demand of energy, especially when unpredictable RES power generation is responsible for the power supply (Chakraborty et al., 2013). The DC network will be able to operate less dependently from the utility grid as well as having the ability to process high loads within a short time frame. An example why this might be useful in an EVPSL, is the arrival of a electric bus, which must be charged immediately. A more detailed description of the components will follow in the next sections.

The BESS will be simulated using the characteristics of a Lithium-Ion Battery Pack due to its high energy density (Chakraborty et al., 2013). The Battery Simscape Power Systems Block of Mathworks' Simulink will be used to simulate the Battery Pack (Mathworks, 2017a). The battery dynamics are given by the following equations; for **charging**

$$\mathrm{V_{BESS}}(t) = \mathrm{V_0} - \mathrm{K}\frac{\mathrm{Q}_{max}}{\mathrm{Q}(t) + 0.1\mathrm{Q}_{max}} i_{lf}(t) - \mathrm{K}\frac{\mathrm{Q}_{max}}{\mathrm{Q}_{max} - \mathrm{Q}(t)}\mathrm{Q}(t) + \mathrm{A}e^{-\mathrm{BQ}(t)} \tag{3}$$

and for **discharging**

$$\mathrm{V_{BESS}}(t) = \mathrm{V_0} - \mathrm{K}\frac{\mathrm{Q}_{max}}{\mathrm{Q}_{max} - \mathrm{Q}(t)} i_{lf}(t) - \mathrm{K}\frac{\mathrm{Q}_{max}}{\mathrm{Q}_{max} - \mathrm{Q}(t)}\mathrm{Q}(t) + \mathrm{A}e^{-\mathrm{BQ}(t)} \tag{4}$$

where

$\mathrm{V_{BESS}}(t)$	= nonlinear voltage		[V]
$\mathrm{V_0}$	= constant voltage	395.791	[V]
K	= polarisation constant	$4.9905 * 10^{-3}$	$[\mathrm{A}h^{-1}]$
$i(t)$	= current through the battery		[Ah]
$i_{lf}(t)$	= low frequency current (after low-pass filter)		[A]
$\mathrm{Q}(t)$	= extracted capacity (integrated current)		[Ah]
Q_{max}	= capacity	547.945	[Ah]
R	= internal resistance of battery	$6.6612 * 10^{-3}$	[Ω]
A	= exponential voltage	30.6512	[V]
B	= exponential capacity	$1.1144 * 10^{-1}$	[Ah]
t	= time		[s]

The capacity (Q_{max}) of the buffer is set at 200 kWh (548 Ah, at the nominal voltage), which is based on charging two 2 EVs without any help of the utility grid. The dynamics, given by the equations above, are shown in means of a discharge curve in Figure 10.

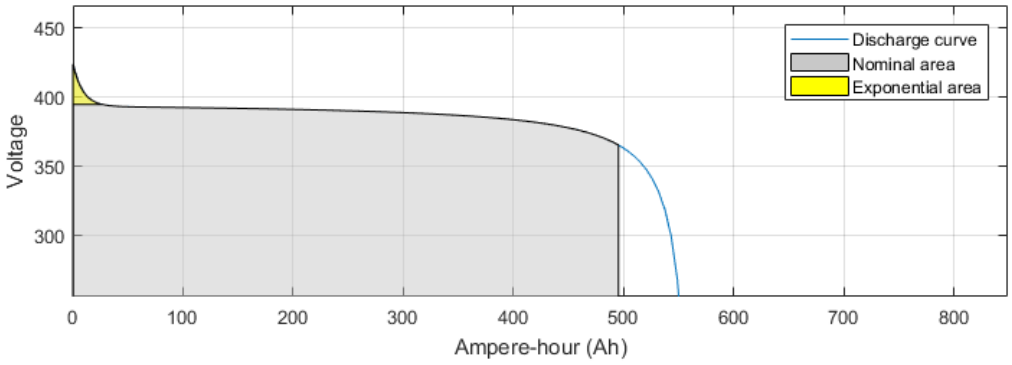

Fig. 10: The discharge curve of the BESS.

For the Lithium-Ion battery pack, a constant load will show an immediately voltage drop when fully charged. After leaving the exponential area, the discharge curve is nearly constant until the nominal voltage (V_n = 365V) is reached. Ideally, the BESS will only be charged as far as 90% and discharged as far as 20% of the capacity.

4.4 Electric Vehicles

Electric Vehicles (EVs) are defined as vehicles using electric energy, partly or completely, to create motion (Dhameja, 2001). A signal from the driver (using the accelerator) applies a current from the battery system to the electric motor, which translates this current at a certain voltage, into torque to the wheels. These vehicles can either be classified as fully Electric Vehicles (EV) or Hybrid Electric Vehicles (HEV), which combine an electric motor with another source of motion. HEV are categorised in Plug-in-Hybrid Electric Vehicles (PHEV), or Fuel Cell Hybrid Electric Vehicles (FCHV). PHEVs combine battery power with an internal combustion engine and FCHVs combine fuel cells and battery power to convert energy into motion. This thesis will solely focus on fully EVs which means that the internal combustion engines and fuel cells will be beyond scope of the research.

4.4.1 Types

The three most-sold Evs in 2017 are the Chevrolet Volt, Nissan Leaf and Tesla Model S (Ma and Horie, 2017), (Gearheads, 2017). With an eye on the future, the most advanced versions the aforementioned EVs were chosen and they are shown in Table 9. The specifications are found using the companies' websites (Chevrolet, 2017), (Nissan, 2017), (Tesla, 2017), Sahan (2017), Arcus (2016) and confirmed in literature by Mwasilu et al. (2014).

Types of EV → / **Specifications ↓**	**Chevrolet Volt**	**Nissan Leaf**	**Tesla Model S**
Battery Capacity (kWh)	18.4	24.0	100.0
Maximal AC Charging (kW)	3.3	6.6	10.0
Maximal DC Charging (kW)	3.3	16.0	120.0
Nominal Voltage (V)	365	365	365
Fully Charged Voltage (V)	403	403	403
Amount of Modules (in series)	96	48	16
Cell Structure per Module (series x parallel)	1 x 2	2 x 2	1 x 86
Amount of Cells Total	192	192	8256
Capacity per Cell (Wh)	95.8	125.8	12.6
Nominal Voltage per Cell (V)	3.8	3.8	3.8
Max Voltage per Cell (V)	4.2	4.2	4.2

Tab. 9: The specifications of the three most sold EVs in 2017.

4.4.2 Battery Characteristics

The car will be modelled using the battery characteristics explained in subsection 4.3 as confirmed by Tremblay et al. (2007). In all chosen EVs, the batteries use Lithium-Ion as main component. The reasons for using Li-Ion cells are described by Dhameja (2001) and entail the highest negative potential per weight, the quick reversibility and the potential's long-life time compared to e.g. Pb-Acid or NiMH. The chemical reactions of charging is shown by the arrow to the right, and the discharging process is shown by the arrow to the left and confirmed by;

$$\begin{aligned} \textit{Anode:} \quad & \mathrm{Li}_x\mathrm{C}_6 + x\mathrm{Li}^+ + xe^- \longleftrightarrow \mathrm{Li}C_6 \\ \textit{Cathode:} \quad & \mathrm{LiCoO}_2 \longleftrightarrow x\mathrm{Li}^+ + xe^- + \mathrm{Li}_{(1-x)}\mathrm{CoO}_2 \end{aligned} \tag{5}$$

All EVs have an on-board charger, as explained in subsection 2.3, yet applying direct DC voltage has great advantages (Hamilton et al., 2010). In this way the energy is directly applied to the battery of the EV, instead of first being converted. In this thesis, it is assumed that there will be no power losses when the currents are directly applied to the EV's battery. As shown in Table 9, all cars have the same nominal voltage, and the EVs solely differ in terms of their capacity. This is shown by the general formula of

(dis)charging the battery,

$$\begin{aligned} \textit{Charge:} \quad & V_{EV}(t) = V_0 - K\frac{Q_{max}}{Q(t)+0.1Q_{max}} i_{lf}(t) - K\frac{Q_{max}}{Q_{max}-Q(t)}Q(t) + Ae^{-BQ(t)} \\ \textit{Discharge:} \quad & V_{EV}(t) = V_0 - K\frac{Q_{max}}{Q_{max}-Q(t)} i_{lf}(t) - K\frac{Q_{max}}{Q_{max}-Q(t)}Q(t) + Ae^{-BQ(t)} \end{aligned} \tag{6}$$

and using the parameters below for the different EVs:

Car Type	V_0	Q_{max}	R	K	A	B
Chevrolet Volt	397.0	50.4	0.0724	0.0569	7.580	1.212
Nissan Leaf	397.0	65.8	0.0555	0.0436	7.580	0.928
Tesla Model S	397.0	274.0	0.0133	0.0105	7.580	0.223

Lithium-ion batteries are charged according to the following pattern; First a constant current is applied until a certain percentage of the capacity is reached. From that moment, the charging behaviour is switched from constant current charging, to constant voltage charging. This is due to safety issues as the voltage of the battery is not linear in the last part of the charging curve, which is shown in Figure 10. In this way, the battery is never overcharged, as voltage is constant and the current will slowly degrade to zero.

Discharging the EV's battery is beyond scope of this thesis. It could be useful in future research as it provides a large buffer of energy in the EVSPL. An example of a situation is that an EV has arrived at short notice and needs to be charged as quickly as possible, while other EVs have spare energy and still enough time before they will leave to be fully charged. One should be careful using these options, as switching between charging and discharging can lead to faster battery degradation (Nitta et al., 2015).

4.4.3 Arrival & Departure

In 'basic' conditions, the following arrival and departure distributions were chosen. The arrival and departure time are random distribution between 07:00 - 09:00, and 16:00 - 18:00 respectively. The real departure time is calculated by creating a random offset with the planned departure time with 20% chance of leaving earlier than expected, and 80% chance of leaving later than expected. The initial State-of-Charge (SOC) and the desired SOC are determined using random percentages between 10% and 75% , and random values between 75% and 100% for the desired SOC.

Parameter	**Distribution**	**Probability**	**Between**	
Arrival Time	Random		07:00	09:00
Departure Time Planned	Random		16:00	18:00
Departure Time Real	Random	20%	17:00	18:00
	& Probability	80%	18:00	19:00
SOC at Arrival Time	Random		10% of Q_{max}	65% of Q_{max}
Desired SOC at Departure Time	Random		70% of Q_{max}	100% of Q_{max}

Tab. 10: The arrival and departure distributions.

4.5 Utility Grid

There are many studies which analysed the impact of huge numbers of EVs on the utility grid. As EVs can be regarded as hard-to-schedule dynamic loads, it may result in voltage deviations, an increase in fault currents, an increase in power loss, overheating of power transformers and overloading of lines (García-Villalobos et al., 2014). Yet, EVs can also act as buffer, adding value to the utility grid in terms of performance, efficiency and power quality (Mwasilu et al., 2014). Taking into account the open issues, solely charging vehicles (V1G) needs more attention and therefore the case studies will be not focused on balancing the utility grid with help of EVs. In 'basic' conditions, the utility grid capacity 100 kW with a three-phase voltage frequency of 60Hz.

4.6 Simulink Model

As explained before with the help of Pierre Giroux (2012) and Saleh et al. (2016) it was possible to create the simulation model of the EVSPL using MATLAB's Simulink. The simulation model, shown in Figure 14 including the more in depth description of the converters in the simulation model. Control of all converters is executed using the Pulse-Width-Modulation-technique which will be explained in subsubsection 5.2.1. The exact parameters can be found in appendix 11.

PV Array & MPPT Boost Converter

The PV Array will generate a power flow, based on the DNI and the temperature, which will be the input for the MPPT Boost converter. To achieve the highest power flow, the MPPT Boost Converter is able to create an optimal power configuration by tracking the maximum power point of the PV array. This is done by constantly checking the voltage and current of the PV array according to the incremental conductance method in combination with an integral regulator, as described by Pierre Giroux (2012). The output voltage of the Boost converter will be 500V.

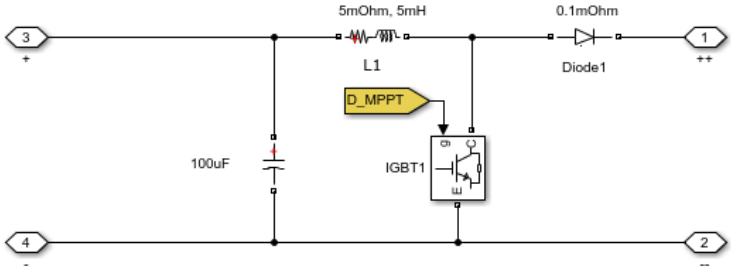

Fig. 11: The MPPT Boost converter at the PV Array.

Utility Grid & 3-Level Bridge

The utility grid can function as a power load or power source. The voltage is kept at 500V by converting the surplus energy to three-phase power and vice verse in means of a 3-Level-Bridge. Voltage control is established using a PI controller with sinusoidal reference signals.

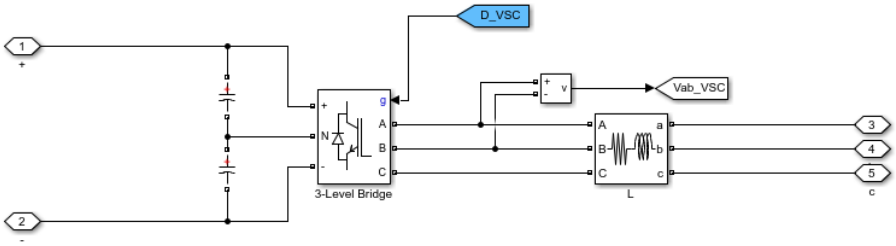

Fig. 12: The VSC converter at the Utility Grid.

BESS/EVs & Bi-Directional Converter

The BESS and EVs are designed parallel to each other, and the power flow is controlled by changing the desired current. The bi-directional converter has two switching devices which are implemented using an ideal Insulated-Gate Bipolar Transistor (IGBT) and anti-parallel diode. These switching devices work asynchronous. When the converter is in Buck mode, the electricity will flow from left to right in Figure 13, controlling the current through the inductor. In Boost mode, the current will flow in opposite direction and discharge the EVs' batter or BESS.

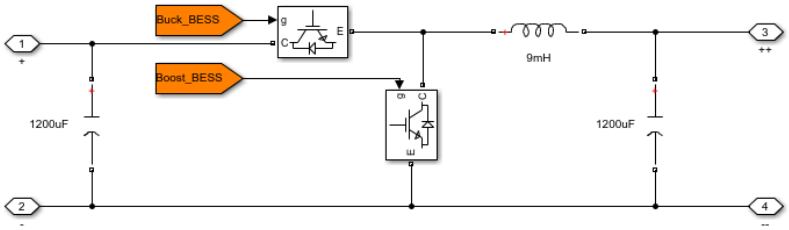

Fig. 13: The bi-directional converter, at the EVs and BESS.

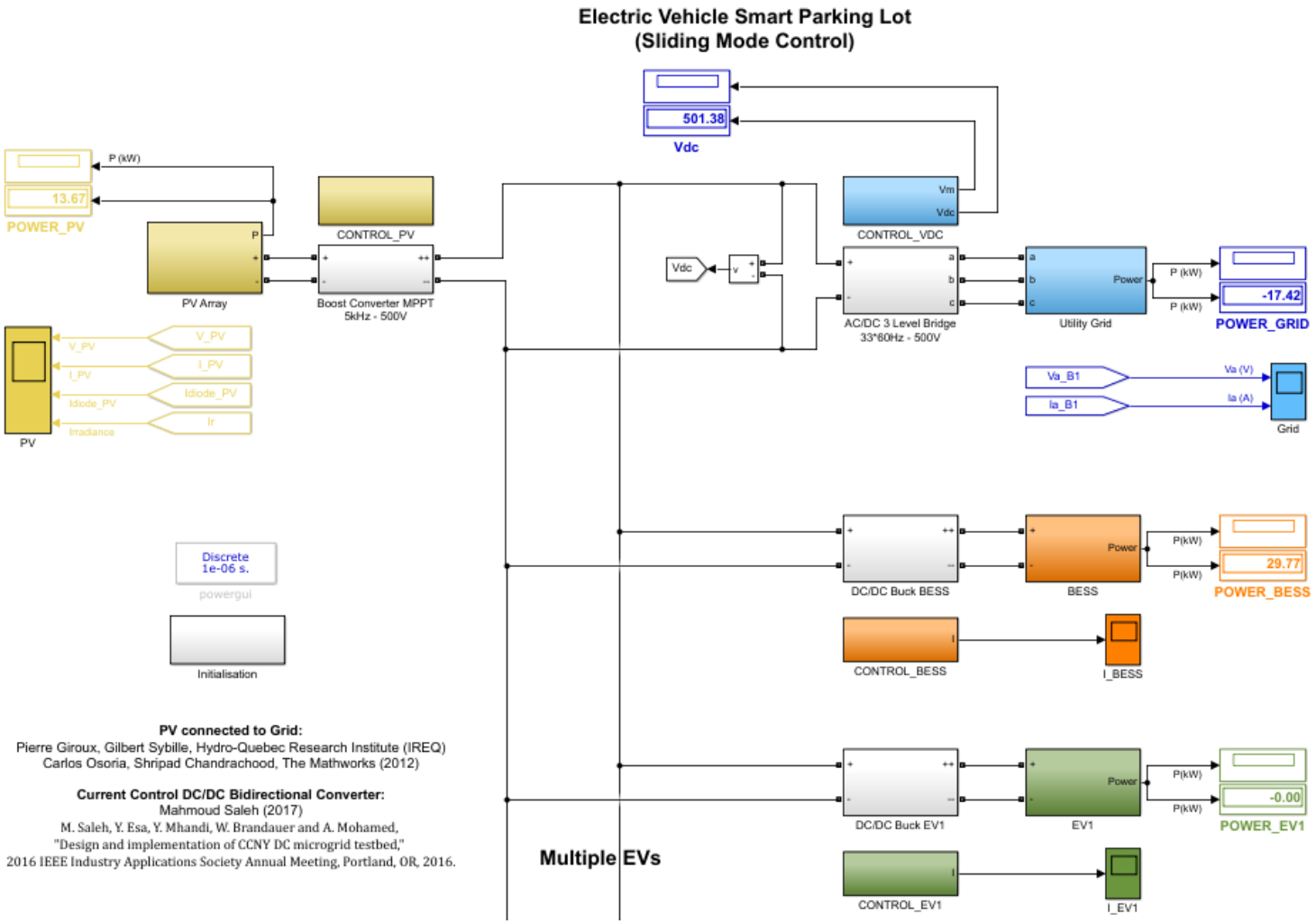

Fig. 14: The simulation model in Simulink as explained in subsection 4.6. The yellow blocks resemble the PV array and its control, the blue blocks represent the utility grid, the orange blocks the BESS and the green blocks the EVs.

5 Lower-Level Control

Within the EVSPL, Lower-Level Control (LLC) will be used to stabilise the power in the DC microgrid. In this section, the research question: "*Which control methods are applicable to stabilise the energy fluxes of an EVSPL, and how do these work?*", will be answered. The power flows which cause the charging and discharging of the BESS and EVs, are controlled using DC/DC Bi-Directional converters, as explained in subsection 3.3.

The LLCer receives setpoints from the Higher-Level Controller (HCL), and provides the HLCer with the state-of-charge Q(t) and the voltage V(t) of the BESS and EVs. This is shown in the control scheme in Figure 15.

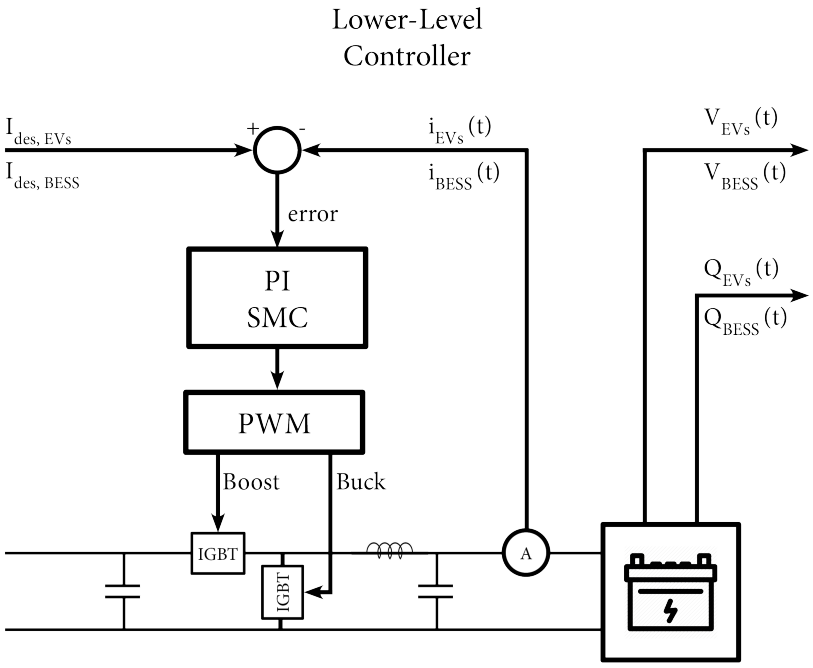

Fig. 15: The control scheme of the LLCer. The setpoints I_{des}, provided by the HLCer, are constant in terms of the time scale at LLC. For every time step, this constant signal is compared to the current $i(t)$ of the BESS or the EV. A Proportional-Integral controller (PI) or Sliding Mode Controller (SMC) will try to converge the error signal to zero. The output of the PI or SMC controller will be changed to a binary signal in means of Pulse-Width-Modulation described in subsubsection 5.2.1. This binary signal is sent to the switching devices (IGBTs) of the converters. The voltages V(t) and SOC Q(t) are sent to the HLCer.

This section is structured as follows. First the basic principles of converters will be explained in detail for the Buck and Boost converter. This is followed by an accurate description of different control methods and techniques which can be applied to regulate the converters. In this thesis the considered methods are limited to Proportional-Integral Control (PI) and Sliding Mode Control (SMC), of which the latter will be investigated in terms of first- and second-order methods.

5.1 Basics Principles of Converters

In the field of electrical engineering, a converter is a collective noun for all devices which are able to convert electric energy from one form to another. Converters are able to change alternating current (AC) to direct current (DC), the power composition of voltage and current, or a combination of the aforementioned. Converters are found in all devices nowadays in a vast variety of forms and functions. In this subsection the DC/DC Buck converter and DC/DC Boost converter are discussed. The configuration and figures used are explained in the book '*Control Design Techniques in Power Electronics Devices*' of Sira-Ramirez and Silva-Ortigoza (2006).

5.1.1 Buck Converter

The goal of a Buck converter is to lower the input voltage to a regulated output voltage. The circuit topology of the Buck converter is shown in Figure 16. By changing the switching frequency of the switching element Q, the output voltage v can be regulated in terms of the input voltage E. The in-series inductor, parallel capacitor, and parallel diode ascertain that a more constant power flow is assured, as the inductor and capacitor are able to store energy in their magnetic and electric fields, respectively. The control input (u) is binary valued ($u \in \{0,1\}$), and it determines whether the circuit is closed (at $u = 1$) or opened (at $u = 0$). A closed circuit allows current to flow to the resistor R, until the switch is opened again which allows the power to slowly dissipate.

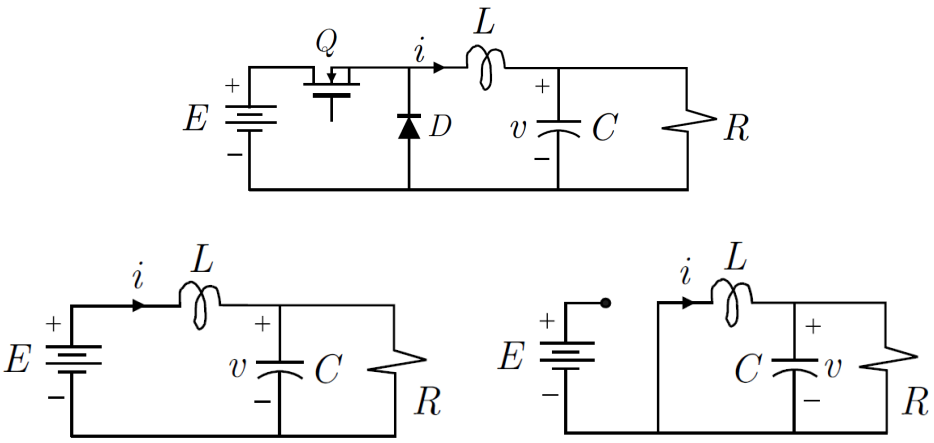

(a) Switch at $u = 1$.

(b) Switch at $u = 0$.

Fig. 16: Schematic circuit diagram of a Buck converter

The system dynamics are described according to the following set of equations

$$\begin{aligned} \mathrm{L}\frac{di(t)}{dt} &= -v(t) + u(t)\mathrm{E} \\ \mathrm{C}\frac{dv(t)}{dt} &= i(t) - \frac{v(t)}{\mathrm{R}}, \end{aligned} \tag{7}$$

where L is the inductance, C the capacitance, $i(t)$ the current, $v(t)$ the output voltage, R the resistance, E the constant input voltage, and $u(t) \in [0,1]$ the control input. Choosing

$$\begin{bmatrix} x_1 & x_2 \end{bmatrix}^{\mathrm{T}} = \begin{bmatrix} i & v \end{bmatrix}^{\mathrm{T}} \tag{8}$$

to describe the dynamics in state space yields

$$\frac{d}{dt}\begin{bmatrix} x_1 \\ x_2 \end{bmatrix} = \begin{bmatrix} 0 & -\frac{1}{\mathrm{L}} \\ \frac{1}{\mathrm{C}} & -\frac{1}{\mathrm{RC}} \end{bmatrix}\begin{bmatrix} x_1 \\ x_2 \end{bmatrix} + \begin{bmatrix} \frac{\mathrm{E}}{\mathrm{L}} \\ 0 \end{bmatrix} u. \tag{9}$$

To find the steady-state solution, the time derivatives of x_1 and x_2 will be set to zero, resulting in the solution $\bar{x}_1$ and $\bar{x}_2$ for a given input signal $\bar{u}$:

$$\begin{aligned} -\frac{1}{\mathrm{L}}\bar{x}_2 + \frac{\mathrm{E}}{\mathrm{L}}\bar{u} = 0 \quad &\rightarrow \quad \bar{x}_2 = \mathrm{E}\bar{u} \\ \frac{1}{\mathrm{C}}\bar{x}_1 - \frac{1}{\mathrm{RC}}\bar{x}_2 = 0 \quad &\rightarrow \quad \bar{x}_1 = \frac{\bar{x}_2}{\mathrm{R}} \end{aligned} \tag{10}$$

or equivalentely

$$\bar{i} = \frac{\bar{v}}{\mathrm{R}}, \qquad \bar{v} = \mathrm{E}\bar{u}. \tag{11}$$

Dividing the steady state output voltage ($\bar{v}$) by the input voltage (E) yields the *static transfer function* of the converter,

$$\mathscr{H}(\mathrm{U}) = \frac{\bar{v}}{\mathrm{E}} = \frac{\bar{u}\mathrm{E}}{\mathrm{E}} = \bar{u}. \tag{12}$$

The output voltage is multiplied by a control input between zero and one, making sure the output voltage will always be lower than the input voltage. This linear static transfer function is plot in Figure 17, where U = $\bar{u}$ and also often referred to as the Duty Cycle D. The Duty Cycle is a continuous signal which yields the fraction of one time period in which the signal is active.

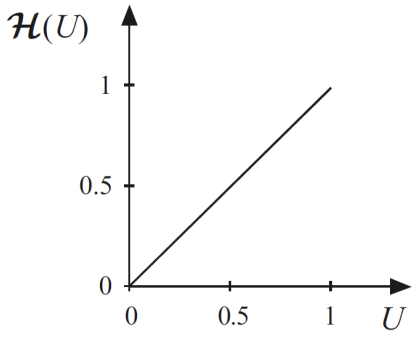

Fig. 17: Static transfer function of the Buck converter.

5.1.2 Boost Converter

The Boost converter will create a higher output voltage v compared to the input voltage E. The system is short-circuited when the switch is closed (at $u = 0$) which creates a high current, resulting in 'stored' energy in the inductor's magnetic field. When the right side of the circuit is connected (at $u = 1$), the built-up energy flows through the diode to the right side allowing a higher voltage to arise on the right side. A schematic diagram of the Boost converter is shown in Figure 18 and the system dynamics are written as

$$\begin{aligned} \mathrm{L}\frac{di(t)}{dt} &= -\Big(1-u(t)\Big)v(t) + \mathrm{E} \\ \mathrm{C}\frac{dv(t)}{dt} &= \Big(1-u(t)\Big)i(t) - \frac{v(t)}{\mathrm{R}}. \end{aligned} \tag{13}$$

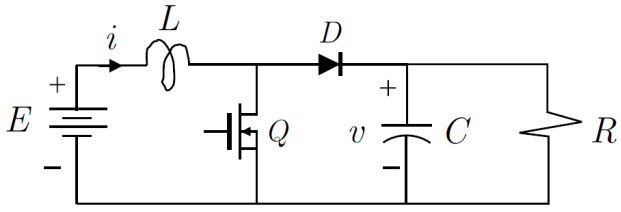

Fig. 18: Schematic circuit diagram of a Boost converter

While choosing the same coordinates as applied to the Buck converter, the dynamics in state space yields,

$$\frac{d}{dt}\begin{bmatrix} x_1 \\ x_2 \end{bmatrix} = \begin{bmatrix} 0 & -\frac{(1-u)}{\mathrm{L}} \\ \frac{(1-u)}{\mathrm{C}} & -\frac{1}{\mathrm{RC}} \end{bmatrix}\begin{bmatrix} x_1 \\ x_2 \end{bmatrix} + \frac{\mathrm{E}}{\mathrm{L}}. \tag{14}$$

To find the steady-state solution, the time derivatives of x_1 and x_2 will be equal to zero, resulting in the solution $\bar{x}_1$ and $\bar{x}_2$ for the input signal $\bar{u}$:

$$\begin{aligned} -\frac{(1-\bar{u})}{\mathrm{L}}\bar{x}_2 + \frac{\mathrm{E}}{\mathrm{L}} = 0 \quad &\rightarrow \quad \bar{x}_2 = \frac{\mathrm{E}}{(1-\bar{u})} \\ \frac{(1-\bar{u})}{\mathrm{C}}\bar{x}_1 - \frac{1}{\mathrm{RC}}\bar{x}_2 = 0 \quad &\rightarrow \quad \bar{x}_1 = \frac{\mathrm{CE}}{(1-\bar{u})^2\mathrm{RC}} = \frac{\bar{x_2}^2}{\mathrm{RE}} \end{aligned} \tag{15}$$

which are given by

$$\bar{i} = \frac{\bar{v}^2}{\mathrm{RE}}, \qquad \bar{v} = \frac{\mathrm{E}}{1-\bar{u}}. \tag{16}$$

The *static transfer function* of the Boost converter is given by

$$\mathscr{H}(\mathrm{U}) = \frac{\bar{v}}{\mathrm{E}} = \frac{\frac{\mathrm{E}}{1-\bar{u}}}{\mathrm{E}} = \frac{1}{1-\bar{u}}, \tag{17}$$

implying that the output voltage v rises exponentially when the input $\bar{u}$ is increased. When the system is short-circuited, the voltage will keep increasing as shown in the static transfer function, in Figure 19.

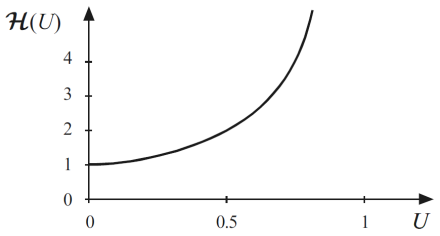

Fig. 19: Static transfer function of the boost converter.

5.2 Current Control in Power Systems

In order to regulate the power flows in the DC network, current control will be applied to the switches of the converters. The output $y(t)$ of the process P is regulated by means of a control algorithm in C. The control algorithm compares a reference signal $r(t)$ to the current output signal creating the error function $e(t)$. A simple control scheme is shown in Figure 20. The error signal is shown by e, the input of the process (which is the output of the controller) is given by $u(t)$ and the output of the process is given by $y(t)$. Disturbances (d) and a measurement noise signal (n) will effect the process and disturb the optimal functioning of the controller.

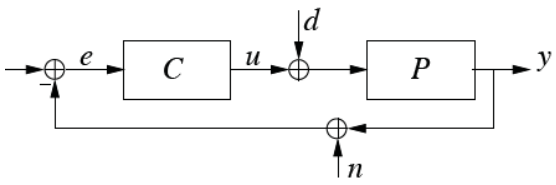

Fig. 20: Control Scheme of a Process (Visioli, 2006)

5.2.1 Pulse Width Modulation

As the converters are controlled using binary signals, a continuous control signal should be translated to a binary signal (or a pulse). As the process of switching the electronic devices in a power electronic converter from one state to another is called modulation (Holmes and Lipo, 2003), the term Pulse Width Modulation (PWM) arises. One of the simplest form of PWM is to compare the continuous control signal to a sawtooth (a triangular waveform). When the continuous control signal is greater than the modulation waveform (the sawtooth), the output signal is in the 'on' state, and otherwise the result is the 'off' state. The average value is given by;

$$\bar{y}(t) = \frac{1}{\mathrm{T}}\left(\int_0^{\mathrm{DT}} y_{max}\,dt + \int_{\mathrm{DT}}^{\mathrm{T}} y_{min}\,dt\right), \tag{18}$$

where, $\bar{y}(t)$ is the discrete output value, D the Duty Cycle, and T the period of the signal. In power electronics often y_{max} is 1 and $y_{min} = 0$, resulting in the direct relation $\bar{y} = \mathrm{D}$. In Figure 21 the translation of the sine wave to a discrete output signal y(t) is shown.

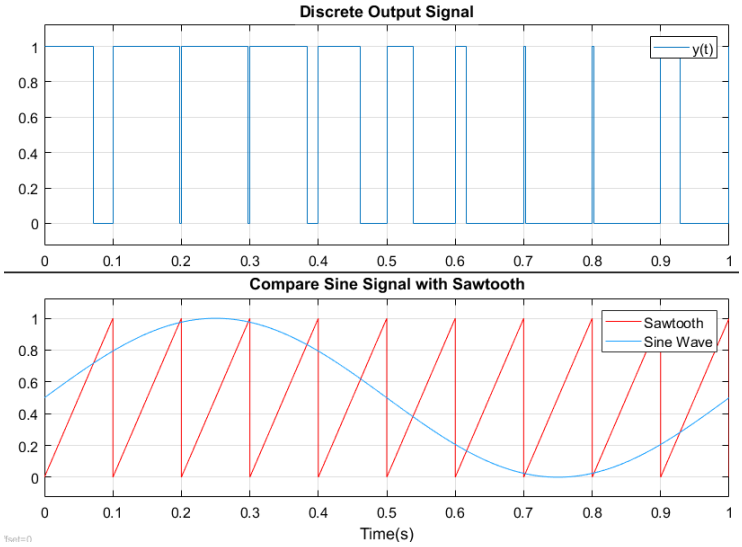

Fig. 21: Pulse Width Modulation of a Sine Signal

5.2.2 Conduction Modes

Power systems can either function in **Continuous Conduction Mode (CCM)** or in **Discontinuous Conduction Mode (DCM)**, as described by Chan (2010). CCM implies a constant current flow, as the stored current in the inductor is sufficient to bridge the gap between two pulses. In Figure 22 both modes are shown where k is the Duty Cycle (D).

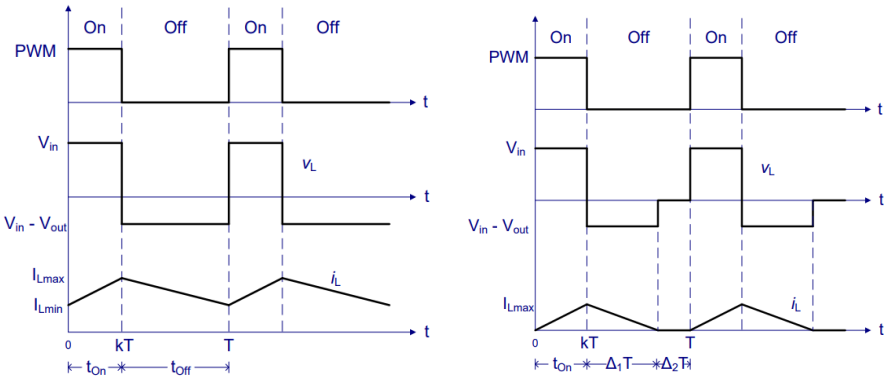

(a) Continuous (b) Discontinuous

Fig. 22: Conduction Modes of Boost Converter

The advantages of CCM over DCM are described by Kazimierczuk (2015), and entail that the input current is continuous and not pulsating (which is easier for computation), the voltage gain is not dependent of the load and a higher efficiency can be achieved compared to DCM. A high efficiency is preferred, and the load of the EVSPL are nonlinear EV batteries, making it more convenient to be independent of these loads. This resulted in the converters described in subsection 4.6 which are designed to function in CCM.

5.2.3 PI Control

A widely used control control loop feedback mechanism in a wide range of industries, is the Proportional-Integral-Derivative (PID) controller (Visioli, 2006). It is an easily comprehensible and implementable controller which converges to the desired value in most scenarios (when tuned well). In power systems, more often PI control is applied, due to the oscillatory behaviour of converters. A PI controller is more capable of creating a steady state with high fluctuations as noise compared to PID control, due to the Derivative term which is more sensible to higher frequency terms in the error signal. For that reason, PI Control is investigated in this thesis.

A PI controller works in the following way; First the system computes the error signal by calculating the difference between the actual signal (i), and the desired signal (I_d);

$$e(t) = y(t) - r(t) = i(t) - \mathrm{I}_d = x_1 - \bar{x}_1, \tag{19}$$

where, $x_1 = i(t)$, $e(t)$ is the error signal, $r(t)$ the reference signal, and $y(t)$ the output signal. This error signal is multiplied by a proportional action K_p and an integral action resulting in the input for the overall system:

$$\begin{aligned} u(t) &= \theta(t) - \mathrm{K}_p\big(x_1 - \bar{x}_1\big) \\ \dot{\theta}(t) &= -\mathrm{K}_i\big(x_1 - \bar{x}_1\big). \end{aligned} \tag{20}$$

If the error is positive, the input will be negative to counteract the error, and vice verse. The proportional gain will create an equilibrium between the error and the desired state of the system, referred to as the *steady-state error*. By summing up the error with help of the integral term the steady-state error will dissolve. For current control, this implies

$$\lim_{x\to\infty} i(t) = \mathrm{I}_{des}.$$

5.2.4 Sliding Mode Control

Sliding Mode Control (SMC) is a method that alters the dynamics of the system by applying a discontinuous signal that makes sure that a system slides along a a cross-section of the normal behaviour (referred to as the sliding surface) (Shtessel et al., 2014). A sliding function is designed, which is often related to the error signal e(t). When the sliding function is positive, SMC will make sure that the derivative of the sliding function will be negative and vice verse.

Using, Cucuzzella et al. (2018) definitions which are essential to SMC are stated; consider a system

$$\dot{x} = \xi(x, u), \tag{21}$$

with $x \in \mathbb{R}$, $u \in \mathbb{R}$.

Definition 1 (Sliding Function): the sliding function $\sigma(x) : \mathbb{R}^{\mathrm{n}} \to \mathbb{R}^{\mathrm{m}}$. is a sufficiently smooth output function of Equation 21.

Definition 2 (Sliding Manifold): The r-sliding manifold is given by

$$\Big\{x \in \mathbb{R}^{\mathrm{n}}, \mathrm{u} \in \mathbb{R}^{\mathrm{m}} : \sigma = \mathrm{L}_\xi \sigma = \mathrm{L}_\xi^{(\mathrm{r}-1)} \sigma\Big\}, \tag{22}$$

where, $\mathrm{L}_x i^{(r-1)}\sigma$ is the (r-1)th Lie derivative of $\sigma(x)$ along the vector field of the system $\xi(x, u)$.

Definition 3 (Sliding Mode Order): A r-order sliding mode is enforced from $t = \mathrm{T}_r \geq 0$, when the state of Equation 21 reaches the r-sliding manifold, and remains there $\forall\, t \geq \mathrm{T}_r$

Definition 4 The relative degree of the system is defined as the minimum order ρ of the time derivative $\sigma^{(p)}$, of the sliding function in which the control input u explicitly appears.

First Order SMC

The system of the Boost converter is derived in subsubsection 5.1.2 and described by,

$$\begin{aligned} \mathrm{L}\dot{x}_1 &= -\mathbf{u}x_2 + \mathrm{E} \\ \mathrm{C}\dot{x}_2 &= \mathbf{u}x_1 - \frac{x_2}{\mathrm{R}}, \end{aligned} \tag{23}$$

with $\begin{bmatrix} x_1 & x_2 \end{bmatrix}^{\mathrm{T}} = \begin{bmatrix} i(t) & v(t) \end{bmatrix}^{\mathrm{T}}$ and $\mathbf{u}$ is equal to the $(1-u)$ defined before and implies the non-average control input. This can also be written in the non-linear form;

$$\begin{aligned} \dot{x} &= f(x) + g(x)u \\ y &= \sigma(x) \end{aligned} \tag{24}$$

where $x \in \mathbb{R}^{\mathrm{n}}, \mathrm{u} \in \{0,1\}$, and $y \in \mathbb{R}^{\mathrm{n}}$.

$$f(x) = \begin{bmatrix} \mathrm{E} \\ -\frac{x_2}{\mathrm{RC}} \end{bmatrix}, \qquad g(x) = \begin{bmatrix} -\frac{x_2}{\mathrm{L}} \\ \frac{x_1}{\mathrm{C}} \end{bmatrix}. \tag{25}$$

The sliding function is chosen as the error function $e(t)$, which was determined before, resulting in the sliding function $\sigma \in \mathbb{R}^{\mathrm{n}}$ on the sliding manifold $\{(x_1) : \sigma = 0\}$,

$$\sigma(x) = i - \mathrm{I}_d = x_1 - \bar{x}_1, \tag{26}$$

which results in the following Lie derivatives

$$\begin{aligned} \mathrm{L}_f\sigma &= \frac{\partial\sigma}{\partial x^{\mathrm{T}}} f(x) = \mathrm{E} \\ \mathrm{L}_g\sigma &= \frac{\partial\sigma}{\partial x^{\mathrm{T}}} g(x) = -\frac{x_2}{\mathrm{L}}, \end{aligned} \tag{27}$$

and the control input:

$$\mathbf{u}(x) = -\frac{\mathrm{L}_f\sigma}{\mathrm{L}_g\sigma} = \frac{\mathrm{EL}}{x_2}. \tag{28}$$

The time-derivative of the sliding function entails

$$\dot{\sigma}(x) = \frac{\partial\sigma}{\partial x}\Big(f(x) + g(x)\mathbf{u}\Big) = \mathrm{L}_f\sigma(x) + \big[\mathrm{L}_g\sigma(x)\big]u = \mathrm{E} - \frac{x_2}{\mathrm{L}}\mathbf{u}. \tag{29}$$

To translate the dynamics into a control input, the system must make sure that the sliding function $(\sigma(x))$ fluctuates around zero, implying that the derivative should be smaller than zero, when the function is bigger than zero and vice verse. This results in the following controlled input $u(x)$

$$\begin{aligned} u(x) &= \begin{cases} 1 & if \quad \sigma(x) > 0 \quad \& \quad \dot{\sigma}(x) < 0 \\ 0 & if \quad \sigma(x) \leq 0 \quad \& \quad \dot{\sigma}(x) \geq 0 \end{cases} \\ u(x) &= \frac{1}{2}\Big[1 + sgn(x_1 - \bar{x}_1)\Big] \\ u(t) &= \frac{1}{2}\Big[1 + sgn\big(\mathrm{I}(t) - \mathrm{I}_{des}\big)\Big]. \end{aligned} \tag{30}$$

Stability:
Following Sira-Ramirez and Silva-Ortigoza (2006), the system is normalised using $\hat{x}_1 \in \mathbb{R}$ and $\hat{x}_2 \in \mathbb{R}$ according to the below mentioned set

$$\begin{bmatrix} \hat{x}_1 \\ \hat{x}_2 \end{bmatrix} = \begin{bmatrix} \frac{1}{E}\sqrt{\frac{L}{C}} & 0 \\ 0 & \frac{1}{E} \end{bmatrix} \begin{bmatrix} i \\ v \end{bmatrix}, \qquad \tau = \frac{t}{\sqrt{LC}}, \tag{31}$$

resulting in the following system

$$\begin{aligned} \dot{\hat{x}}_1 &= -\mathbf{u} + 1 \\ \dot{\hat{x}}_2 &= \mathbf{u}\hat{x}_1 - \frac{\hat{x}_2}{R\sqrt{\frac{C}{L}}}. \end{aligned} \tag{32}$$

with the following normalised steady-state solution:

$$\tilde{x}_1 = \frac{\tilde{x}_2^2}{R\sqrt{\frac{C}{L}}}, \quad \tilde{x}_2 = \frac{E}{1-\mathbf{u}}, \quad \mathbf{u}_{norm} = \frac{1}{\hat{x}_2}. \tag{33}$$

To find out whether first-order SMC is stable in terms of the voltage, Lyapunov's second method for stability is used on the output voltage $v(t)$ with help of the candidate Lyapunov function of Sira-Ramirez and Silva-Ortigoza (2006) given by;

$$\begin{aligned} V(\hat{x}_2) &= \frac{1}{2}(\hat{x}_2 - \tilde{x}_2)^2 \\ \dot{V}(\hat{x}_2) &= (\hat{x}_2 - \tilde{x}_2)\dot{\hat{x}}_2. \end{aligned} \tag{34}$$

Making use of the normalised steady-state solution, the normalised input ($\mathbf{u}_{norm}$)and the reaching of the sliding manifold, $\sigma(x) = 0$, $\dot{\hat{x}}_2$ can be derived;

$$\dot{\hat{x}}_2 = \mathbf{u}\hat{x}_1 - \frac{\hat{x}_2}{R\sqrt{\frac{C}{L}}} = \left(\frac{1}{\hat{x}_2}\right)\left(\frac{\tilde{x}_2^2}{R\sqrt{\frac{C}{L}}}\right) - \frac{\hat{x}_2}{R\sqrt{\frac{C}{L}}} = \frac{\tilde{x}_2^2 - \hat{x}_2^2}{\hat{x}_2 R\sqrt{\frac{C}{L}}}. \tag{35}$$

Pursuing the Lyapunov analysis, $\dot{V}(\hat{x}_2)$ is calculated;

$$\begin{aligned} \dot{V}(\hat{x}_2) &= \frac{1}{\hat{x}_2\ R\sqrt{\frac{C}{L}}}(\hat{x}_2 - \tilde{x}_2)(\tilde{x}_2^2 - \hat{x}_2^2) \\ \dot{V}(\hat{x}_2) &= \frac{1}{\hat{x}_2\ R\sqrt{\frac{C}{L}}}(\hat{x}_2\tilde{x}_2^2 - \hat{x}_2^3 - \tilde{x}_2^3 + \hat{x}_2^2\tilde{x}_2) \\ \dot{V}(\hat{x}_2) &= -\frac{1}{\hat{x}_2\ R\sqrt{\frac{C}{L}}}\ (\hat{x}_2^2 + \tilde{x}_2^2 - 2\hat{x}_2\tilde{x}_2)(\hat{x}_2 + \tilde{x}_2) \\ \dot{V}(\hat{x}_2) &= -\frac{1}{\hat{x}_2\ R\sqrt{\frac{C}{L}}}(\hat{x}_2 - \tilde{x}_2)^2(\hat{x}_2 + \tilde{x}_2) < 0. \end{aligned} \tag{36}$$

These equations show a negative definite equilibrium point $\tilde{x}_2$ for $x_2 > 0$, which means that the dynamics are asymptotically stable at the desired voltage ($\tilde{x}_2$). As the following Lyapunov conditions of asymptotic stability are met: $V(x) = 0 \iff x = 0$; $V(x) > 0 \quad \forall x > 0$, and $\dot{V} < 0 \quad \forall x \neq 0$. This implies that applying direct current control will stabilise the system.

Although the first order sliding mode control law can be directly applied open en close the switching devices and show fast convergence, the Insulated Gate Bipolar Transistors (IGBTs) switching frequency cannot be a-priori fixed, due to high power losses (Lai and Chen, 1993) and (Cucuzzella et al., 2018). The IGBTs require a constant frequency, which is usually overcome by implementing the Pulse-Width-Modulation technique described in subsubsection 5.2.1. To make use of this technique, a continuous control signal is required.

Second-Order Sliding Mode Control

Establishing a continuous signal by integrating the discontinuous signal, is suggested by (Bartolini et al., 1998a). Is the output will be integrated, the following adaption to Equation 23 arises,

$$\begin{aligned} \mathrm{L}\dot{x}_1 &= -\mathbf{u}x_2 + \mathrm{E} \\ \mathrm{C}\dot{x}_2 &= \mathbf{u}x_1 - \frac{x_2}{\mathrm{R}} \\ \dot{u} &= h, \end{aligned} \tag{37}$$

where $h \in \mathbb{R}^{\mathrm{n}}$ is the new sliding mode control input. This changes the relative degree of the system to two. In this way it is possible to implement a second-order sliding method. The *'Suboptimal Second Order Sliding Mode'* controller is proposed in Cucuzzella et al. (2018) and Cucuzzella et al. (2017) and carefully explained in Bartolini et al. (1998a).

An auxiliary system, where $\xi_1 = \sigma$ and $\xi_2 = \mathrm{L}_\xi\sigma$ is developed, with $\{(x_1, u) : \sigma = \mathrm{L}_\xi\sigma = 0\}$ as sliding manifold.

$$\begin{aligned} \dot{\xi}_1 &= \xi_2 \\ \dot{\xi}_2 &= \phi(\dot{x}_1, \dot{x}_2, u) - \gamma(x_1, x_2)h \\ \dot{u} &= h, \end{aligned} \tag{38}$$

where ϕ and γ can be calculated by taking the second order Lie derivative of $\sigma(x)$. This will result in the following variables;

$$\begin{aligned} \phi(\dot{x}_1, \dot{x}_2, u) &= -\frac{1}{\mathrm{L}}\dot{x}_2\mathbf{u} \\ \gamma(x_1, x_2) &= -\frac{1}{\mathrm{L}}x_2, \end{aligned} \tag{39}$$

which are assumed to be bounded with the known bounds:

$$\begin{aligned} &|\phi(\dot{x}_1, \dot{x}_2, u)| \leq \Phi \\ &0 < \Gamma_{min} \leq \gamma(x_1, x_2) \leq \Gamma_{max}, \end{aligned} \tag{40}$$

and constants $\Phi, \Gamma_{min}, \Gamma_{max} \geq 0$. If it is difficult or impossible to estimate these bounds a-priori, a solution can be found in adaptive SOSMC, as described in Incremona et al. (2016), yet this will be beyond scope of this thesis.

System 37 results in the following control law which is able to steer ξ_1 and ξ_2, to zero in a finite time:

$$h(x) = \alpha \mathrm{H}_{max} sgn\left(\xi_1, -\frac{1}{2}\xi_1, max\right), \tag{41}$$

with

$$\mathrm{H}_{max} > max\left(\frac{\Phi}{\alpha^*\Gamma_{min}} \frac{4\Phi}{3\Gamma_{min} - \alpha^*\Gamma_{max}}\right) \tag{42}$$

$$\alpha^* \in (0, 1] \cap \left(0, \frac{3\Gamma_{min}}{\Gamma_{max}}\right), \tag{43}$$

with $\alpha \in \{\alpha^*, 1\}$ and $\xi_{1,max}$ as the extreme value of ξ_1 which is identified with a peak detector, introduced in Bartolini et al. (1998b).

The convergence of second-order SMC in an EVSPL is investigated in case study I in subsection 2.4 in means of an extensive comparison study between second-order SMC and PI control.

6 Higher-Level Control

As explained in subsection 3.3, Multi-Level Control (MLC) will be applied in the EVSPL. This section will elaborate on Higher-Level Control (HLC) and will answer the research question: *"How will the distribution of power in the EVSPL be controlled, taking into account future time steps?"*. The HLCer will generate setpoints for (dis)charging the BESS and the EVs for the Lower-Level Controller (LLCer). It will make use of a Model-Predictive-Control (MPC) methodology which takes into account optimality criteria and future time steps. The control scheme is shown in Figure 23. To show how the time steps are defined between the MPC Model and the EVSPL, Figure 24 gives an overview.

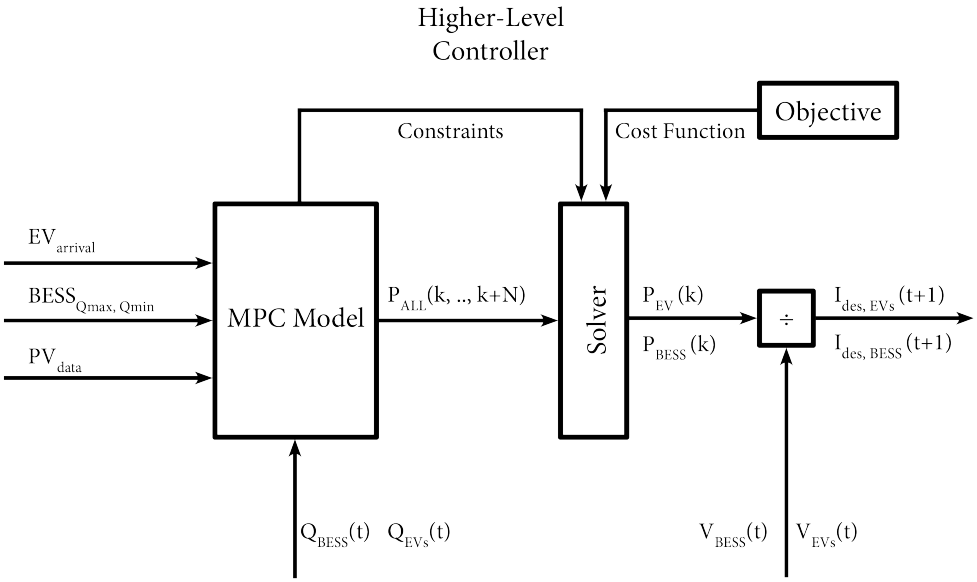

Fig. 23: The control scheme of the HLCer is shown. The arrival data of the EVs, the initial values of the BESS, and the direct normal irradiance (DNI) arrive from the initialisation block. From the EVSPL the current SOC Q(t) of the EVs and the BESS are input values for the MPC Model. The MPC Model provides constraints and equips the solver with an overview of all possible power flows from time steps [$k+1$,.., $k+$N], where N is the prediction horizon. The solver determines the optimal solution for the power flows and solely provides the first value to the EVs and to the BESS. The last step is dividing the desired power, by the real-time voltage of the EVs and BESS, creating the desired setpoint I_{des} for the next time step ($t+1$) for the LLCer.

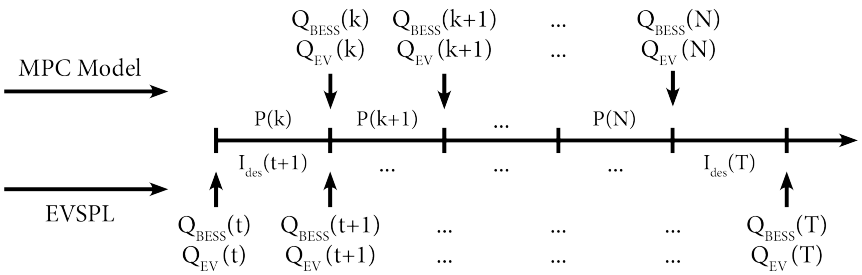

Fig. 24: An overview of the time steps of the EVSPL (t = [1..T]) and the prediction values of the MPC Model at prediction time steps (k = [1,..,N]). The first prediction time step k will provide the setpoint for next step in time, $t+1$, for the LLCer.

The parameters used in this section are explained in Table 12. First the background of MPC including its advantages and disadvantages will be investigated. Secondly, the MPC Model which forecasts the behaviour of the system in future time instants will be introduced. The objective function which will be minimised, and the solver which determines the optimal values for the power flow is illustrated next. The section is finalised by describing the interaction between MATLAB and Simulink.

6.1 Model Predictive Control

Model Predictive Control is a range of control methods which make explicit use of a model of a process, to predict the process output at future time instants. This is done by calculating a control sequence minimising an objective function with a receding strategy which only implements the first control signal at each time instant (Camacho and Alba, 2013). The strategy can be summarised in the following steps;

1. At each time instant t, the process model predicts future output signals $\hat{y}(t+k \mid t)$ for predicted time instants $k = 1,..,\mathrm{N}$, where N is the prediction horizon. The notation implies that the value $\hat{y}$ at instant $t+k$ is calculated at instant t. Using the known past input, the known past output signals, and the future control input, the predicted outputs are calculated.
2. The future control input signals $u(t+k \mid t)$ for $t = 1..(\mathrm{N}-1)$ are determined by optimising a cost function with constraints, to keep the process as close as possible to a reference signal $r(t+k)$.
3. The control input signal of the current time instant $u(t \mid t)$ is sent to the process, leaving the signals for other time instant. The new $u(t+1 \mid t+1)$ is calculated by repeating step 1 and 2 while new information of $y(t+1)$ is available. This is referred to as the receding horizon concept.

MPC is a methodology which is a popular methodology due to its totally open methodology, its easy extension to multivariable cases and the ease of implementation (Camacho and Alba, 2013). As the model can be adjusted easily, the methodology is open for extension as the model can be designed to the desired extensiveness. Especially in the case pre-known future references (e.g. the desired state of a robot) MPC is very useful.

A large drawback is the need for an accurate model, which is required to implement MPC. Designing an accurate model can be complex, consequently time consuming and costly. Also, for every time step t, the computation can be very heavy if many constraints are involved. This can be a bottleneck for industrial processes as these control computers are not always at their best in terms of computation power, and most of the available time is needed for other purposes than the control algorithm (Camacho and Alba, 2013).

Still, MPC is used often in industries, and more and more often in the renewable energy sector (Sultana et al., 2017). This shows that the current knowledge on MPC is gradually rising.

Advantages	**Disadvantages**
Open methodology, open for extension	Accurate model is required
Resulting control law easily implementable	Derivation of control law is complex
Multivariable case can easily be dealt with	
Widely used in industries and RES sector	

Tab. 11: The advantages and disadvantages of MPC.

Parameter		Explanation
Indices		
t	$\in \{1,..T\}$	Index of time instants
k	$\in \{1,..N\}$	Index of prediction time instants
m	$\in \{1,..M\}$	Index of EVs
Variables		
$Q_{EV}(t,m)$	$\in \mathbb{R}^{T+1,M}$	State of charge of EV m, at instant t
$Q_{EV,plan}(t,m)$	$\in \mathbb{R}^{T+1,M}$	Planned state of charge of EV m, at instant t
$Q_{EV,max}(m)$	$\in \mathbb{R}^{M}$	Capacity of EV m
$Q_{EV,0}(m)$	$\in \mathbb{R}^{M}$	Starting state of charge of EV m, at t_arrive
$Q_{EV,des}(m)$	$\in \mathbb{R}^{M}$	Desired state of charge of EV m, at t_plan
$EV_{maxin}(m)$	$\in \mathbb{R}^{M}$	Maximal power which can be stored per time instant, in EV m
$EV_{maxout}(m)$	$\in \mathbb{R}^{M}$	Maximal power which can be withdrawn per time instant from EV m
$t_{arrive}(m)$	$\in \mathbb{R}^{M}$	The arrival time of EV m
$t_{des}(m)$	$\in \mathbb{R}^{M}$	The desired departure time of EV m
$t_{depart}(m)$	$\in \mathbb{R}^{M}$	The real departure time of EV m
$\lambda(m)$	$\in \mathbb{R}^{M}$	Variable which shortens the prediction horizon, per EV
$\Delta(m)$	$\in \mathbb{R}^{M}$	Linear charge step, per EV m
$Q_{BESS}(t)$	$\in \mathbb{R}^{T+1}$	State of charge of the BESS, at instant t
$Q_{BESS,0}$	$\in \mathbb{R}^{1}$	Starting state of charge of the BESS, at $t=0$
$Q_{BESS,min}$	$\in \mathbb{R}^{1}$	Critical buffer level of the BESS
$Q_{BESS,min}$	$\in \mathbb{R}^{1}$	Capacity of the BESS
B_{maxin}	$\in \mathbb{R}^{1}$	Maximal power which can be stored per time instant in the BESS
B_{maxout}	$\in \mathbb{R}^{1}$	Maximal power which can be withdrawn per time instant from the BESS
$DNI_{pred}(t)$	$\in \mathbb{R}^{T}$	Irradiance according to yearly prediction for all time instants
A	$\in \mathbb{R}^{1}$	Surface area of the PV array
η	$\in \mathbb{R}^{1}$	Efficiency of the PV array
Solver Variables		
$\hat{P}_{PV}(k)$	$\in \mathbb{R}^{N}$	Predicted power, generated by the PV array, in instant k
$\hat{P}_{GRID}(k)$	$\in \mathbb{R}^{N}$	Predicted power, consumed/generated by the Utility Grid, in instant k
$\hat{Q}_{EV}(k,m)$	$\in \mathbb{R}^{N+1,M}$	Predicted state of charge EV m, at instant k
$\hat{Q}_{BESS}(k)$	$\in \mathbb{R}^{N+1}$	Predicted state of charge of the BESS, at instant k
$\hat{P}_{EV}(k,m)$	$\in \mathbb{R}^{N,M}$	Predicted power, consumed by EV m, in instant k
$\hat{P}_{BESS}(k)$	$\in \mathbb{R}^{N}$	Predicted power, consumed/generated by the BESS, in instant k
$\hat{P}_{PV\to B}(k)$	$\in \mathbb{R}^{N}$	Predicted power flow from PV array to the BESS, in instant k
$\hat{P}_{PV\to G}(k)$	$\in \mathbb{R}^{N}$	Predicted power flow from PV array to the Utility Grid, in instant k
$\hat{P}_{PV\to C}(k)$	$\in \mathbb{R}^{N}$	Predicted power flow from PV array to the Charger, in instant k
$\hat{P}_{B\to C}(k)$	$\in \mathbb{R}^{N}$	Predicted power flow from BESS to Charger, in instant k
$\hat{P}_{G\to C}(k)$	$\in \mathbb{R}^{N}$	Predicted power flow from Utility Grid to Charger, in instant k
$\hat{P}_{C\to EV}(k,m)$	$\in \mathbb{R}^{N,M}$	Power from the Charger to the EV, per EV m, in instant k
β	$\in \mathbb{R}^{N}$	Priority array, to counteract postponed charging.
Outputs		
$\hat{P}_{EV}(k,m)$	$\in \mathbb{R}^{1,M}$	First value of the predicted power flow to EV m, at $k=1$
$\hat{P}_{BESS}(k)$	$\in \mathbb{R}^{M}$	First value of the predicted power flow to for the BESS, at $k=1$

Tab. 12: The parameters of the MPC Algorithm.

6.2 The MPC Model

As explained in subsection 6.1 a MPC control methodology always consists of a model of the process. This model is used to forecast future time inputs for the real process, referred to as the EVSPL, described in section 4. The higher-level controller will derive a simplified model of the EVSPL, from now on referred to as *the MPC Model*.

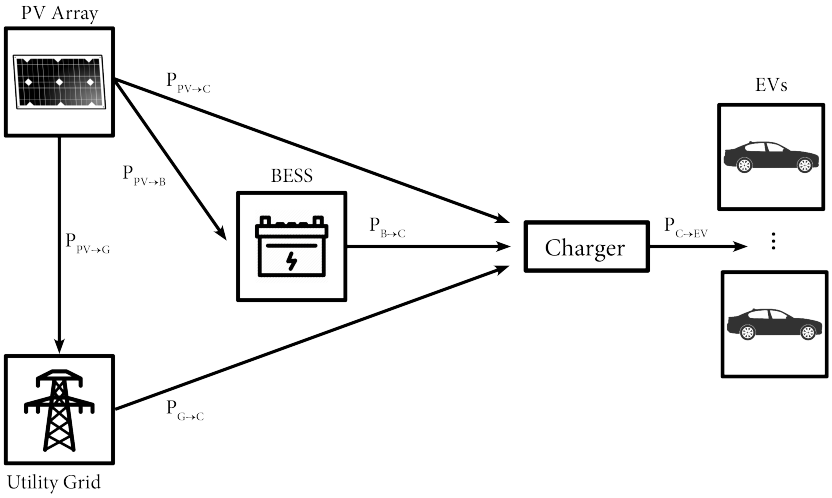

Fig. 25: The possible power flows in the MPC Model.

The MPC model is initialised using the following variables;

	W/m^2	m^2	%	kWh	%	%	kW	kW	$hh:mm:ss$		
EV	-	-	-	Q_{max}	Q_0	Q_{des}	EV_{maxin}	EV_{maxout}	t_{arrive}	t_{plan}	t_{depart}
BESS	-	-	-	Q_{max}	Q_0	-	-	-	-	-	
PV	DNI_{pred}	A	η	-	-	-	-	-	-		

Tab. 13: The initialisation data of the MPC model.

The generated power of the PV array $\hat{P}_{PV}$ is modelled using a prediction of the direct normal irradiance and an efficiency, according to the following formula:

$$\hat{P}_{PV}(k) = DNI_{pred}(t) * A * \eta, \tag{44}$$

where DNI_{pred} is the predicted direct normal solar irradiance in W/m^2, A the surface area of the solar array in m^2, and η the efficiency of the solar array. The predicted DNI is derived from the solar data of National Solar Radiation Database of 2010 in Los Angeles (NREL, 2010) as shown in the appendix [1].

The grid power will be generated according to the shortage of surplus of power according to the following formula;

$$\hat{P}_{GRID}(k) = \sum_{m=1}^{M} \left(\hat{P}_{EV}(k,m)\right) - \hat{P}_{BESS}(k) - \hat{P}_{PV}(k). \tag{45}$$

When P_{GRID} is negative, it implies that the grid will have an intake of power as the solar power added to the power of the BESS, is higher than the charger demand. When the charger demand is higher, the P_{GRID} value will become positive, implying a generation of power by the grid.

The BESS is assumed to be (dis)charging linearly by adding the flow of power to the SOC of the previous time instant. In the case of the first prediction time instant ($k = 1$), $Q_{BESS}(k)$ is calculated with the

[1] The solar irradiance of 2010 was used as benchmark due to the availability of data of Los Angeles.

$Q_{BESS}(t)$, provided by the EVSPL, and the predicted flow of power. This is shown by the following set of equations;

$$\begin{aligned} \hat{Q}_{BESS}(k,m) &= Q_{BESS}(t,m) + \hat{P}_{BESS}(k,m) \quad if \quad k=1 \\ \hat{Q}_{BESS}(k+1,m) &= \hat{Q}_{BESS}(k,m) + \hat{P}_{BESS}(k,m). \end{aligned} \tag{46}$$

The EVs are assumed to be charging similar to the BESS, according to the following set of equations;

$$\begin{aligned} \hat{Q}_{EV}(k,m) &= Q_{EV}(t,m) + \hat{P}_{EV}(k,m) \quad if \quad k=1 \\ \hat{Q}_{EV}(k+1,m) &= \hat{Q}_{EV}(k,m) + \hat{P}_{EV}(k,m), \end{aligned} \tag{47}$$

where $m = \in \{1,2,..M\}$ is the index of the EVs.

When the EVs arrive, first it is calculated whether the charging demand is feasible. The demand is feasible if the linear charge step

$$\Delta(m) = \frac{Q_{EV,des}(m) - Q_{EV,start}(m)}{t_{des}(m) - t_{arrival}(m)}, \tag{48}$$

is smaller is the maximum inflow of EV m:

$$\Delta(m) \leq EV_{maxin}(m) \quad \forall m. \tag{49}$$

Also a linear charging plan is established, which is referred to as the $Q_{EV,plan}$. This implies that for every time instant t, a planned SOC is introduced. This will later be used as a constraint in the solver, see subsection 6.4.

$$\begin{aligned} \hat{Q}_{EV,plan}(t,m) &= Q_{EV,0} && if \quad t=1 \\ \hat{Q}_{EV,plan}(t+1,m) &= Q_{EV,plan}(t,m) + \Delta(m) && if \quad t <= t_{depart} \\ \hat{Q}_{EV,plan}(t+1,m) &= Q_{EV,plan}(t,m) && if \quad t > t_{depart} \end{aligned} \tag{50}$$

6.3 The Objective

The objective of the HLCer is to charge the EVs as efficiently as possible. This implies using all the power generated by the PV array while minimising the power taken from the utility grid. In this way the EVSPL, can operate as independently of the utility grid as possible while charging the EVs with maximum usage of the RES. The purposes of the BESS are to store energy in case of overproduction of the PV array, and having the ability to process high loads within a short time frame. Due to these design decisions, the following optimisation function arises;

$$\min_{\hat{P}^*} \quad 4\beta^T\left(\hat{P}_{G\to C}\right)^2 + 2\beta\left(\hat{P}_{B\to C}\right)^2 + \beta\left(\hat{P}_{PV\to C}\right)^2 + 3\beta\left(\hat{P}_{PV\to G}\right)^2 + \beta\left(\hat{P}_{PV\to B}\right)^2, \tag{51}$$

where $\hat{P}^*$ implies the variables: $\hat{P}_{G\to C}$, $\hat{P}_{B\to C}$, $\hat{P}_{PV\to C}$, $\hat{P}_{PV\to G}$, and $\hat{P}_{PV\to B}$. Also,

$$\beta = [1, \quad (1+\frac{1}{N}) \quad ... \quad 2], \tag{52}$$

is the prioritising array, which is creating a penalty for postponing charging. In this way, the charging is brought to earlier time instants which has more effect on the MPC strategy, as the output of the higher-level controller solely consists of the first prediction time step.

To distribute the power more evenly over the time steps, the values are quadratised before they are multiplied with the prioritising array. Furthermore, penalties are added to the objective function, according to the design choices explained before. When the charger demand is met but a surplus of PV power is still available, this is seen as overproduction.

In case of overproduction, the penalty for sending energy to the utility grid is three times as severe compared to storing the energy in the BESS or providing the EVs with more energy than demanded. In case of underproduction, using energy from the BESS results in a four times as mild penalty compared to buying energy from the utility grid. The constraints will make sure that the EVs are charged according to the EVs desired SOC at a certain time instant and the restrictions from the EVSPL are taken into account.

6.4 The Solver

To solve the objective function, the following constraints will arise. First of all, the predicted power flow variables must be positive,

$$\begin{array}{lll} \hat{\mathrm{P}}_{\mathrm{PV}\to\mathrm{B}}(k) & \geq 0 & \forall k \\ \hat{\mathrm{P}}_{\mathrm{PV}\to\mathrm{G}}(k) & \geq 0 & \forall k \\ \hat{\mathrm{P}}_{\mathrm{PV}\to\mathrm{C}}(k) & \geq 0 & \forall k \\ \hat{\mathrm{P}}_{\mathrm{B}\to\mathrm{C}}(k) & \geq 0 & \forall k \\ \hat{\mathrm{P}}_{\mathrm{G}\to\mathrm{C}}(k) & \geq 0 & \forall k \\ \hat{\mathrm{P}}_{\mathrm{C}\to\mathrm{EV}}(k,m) & \geq 0 & \forall k,m, \end{array} \tag{53}$$

and the total power flow must be conserved:

$$\begin{array}{lcll} \hat{\mathrm{P}}_{\mathrm{PV}\to\mathrm{C}}(k,m)+\hat{\mathrm{P}}_{\mathrm{PV}\to\mathrm{B}}(k)+\hat{\mathrm{P}}_{\mathrm{PV}\to\mathrm{G}}(k) & = & \hat{\mathrm{P}}_{\mathrm{PV}}(k+t) & \forall k,m,t \\ \hat{\mathrm{P}}_{\mathrm{PV}\to\mathrm{C}}(k,m)+\hat{\mathrm{P}}_{\mathrm{B}\to\mathrm{C}}(k,m)+\hat{\mathrm{P}}_{\mathrm{G}\to\mathrm{C}}(k,m) & = & \sum_{m=1}^{\mathrm{M}}\left(\hat{\mathrm{P}}_{\mathrm{C}\to\mathrm{EV}}(k,m)\right) & \forall k,m. \end{array} \tag{54}$$

Constraints regarding the BESS imply not exceeding the capacity, the critical buffer level or the maximum in- or outflow of the BESS

$$\begin{array}{lcll} \hat{\mathrm{Q}}_{\mathrm{BESS}}(k) & \leq & \mathrm{Q}_{\mathrm{BESS},max} & \forall k \\ \hat{\mathrm{Q}}_{\mathrm{BESS}}(k) & \geq & \mathrm{Q}_{\mathrm{BESS},min} & \forall k \\ \hat{\mathrm{P}}_{\mathrm{PV}\to\mathrm{B}}(k) & \leq & \mathrm{B}_{maxin} & \forall k \\ \hat{\mathrm{P}}_{\mathrm{B}\to\mathrm{C}}(k) & \leq & \mathrm{B}_{maxout} & \forall k, \end{array} \tag{55}$$

Constraints regarding the EVs are similar;

$$\begin{array}{lcll} \hat{\mathrm{Q}}_{\mathrm{EV}}(k,m) & \leq & \mathrm{Q}_{\mathrm{EV},max} & \forall k,m \\ \hat{\mathrm{P}}_{\mathrm{C}\to\mathrm{EV}}(k,m) & \leq & \mathrm{EV}_{maxin} & \forall k,m \\ \hat{\mathrm{P}}_{\mathrm{C}\to\mathrm{EV}}(k,m) & \leq & \mathrm{EV}_{maxout} & \forall k,m, \end{array} \tag{56}$$

with the exception of the charging demand not being feasible as described in the MPC model. In this case, the EV will be charged with maximal capacity:

$$\hat{\mathrm{P}}_{\mathrm{C}\to\mathrm{EV}}(k,m)=\mathrm{EV}_{maxin} \quad \forall k,m. \tag{57}$$

If charging demand is regarded as feasible, the predicted SOC of the EVs, must be equal to the planned SOC at the prediction horizon N, which is established by an estimation of a linear model of charging the battery;

$$\hat{\mathrm{Q}}_{\mathrm{EV}}\Big(\big(\mathrm{N}-\lambda(m)\big),m\Big)=\mathrm{Q}_{\mathrm{EV},plan}\Big(\big(\mathrm{N}-\lambda(m)\big)+t,m\Big) \quad \forall m,t, \tag{58}$$

where $\lambda(m)$ is a variable which shortens the length of the prediction horizon per EV. This variable makes sure that the prediction horizon of a specific EV will become shorter when the $\mathrm{Q}_{\mathrm{EV},des}(t,m)$ is within the prediction horizon.

The first value of the predicted battery level is equal to the established SOC of previous iteration. The same entails for the SOC of the EVs according to the MPC Model;

$$\begin{array}{lcll} \hat{\mathrm{Q}}_{\mathrm{EV}}(k,m) & = & \mathrm{Q}_{\mathrm{EV}}(t,m)+\hat{\mathrm{P}}_{\mathrm{C}\to\mathrm{EV}}(k,m) & \forall(k=1),m \\ \hat{\mathrm{Q}}_{\mathrm{EV}}(k+1,m) & = & \hat{\mathrm{Q}}_{\mathrm{EV}}(k,m)+\hat{\mathrm{P}}_{\mathrm{C}\to\mathrm{EV}}(k,m) & \forall k,m. \\ & & & \\ \hat{\mathrm{Q}}_{\mathrm{BESS}}(k) & = & \mathrm{Q}_{\mathrm{BESS}}(t)+\hat{\mathrm{P}}_{\mathrm{PV}\to\mathrm{B}}(k)-\hat{\mathrm{P}}_{\mathrm{B}\to\mathrm{C}}(k,m) & \forall(k=1),m \\ \hat{\mathrm{Q}}_{\mathrm{BESS}}(k+1) & = & \hat{\mathrm{Q}}_{\mathrm{BESS}}(k)+\hat{\mathrm{P}}_{\mathrm{PV}\to\mathrm{B}}(k)-\hat{\mathrm{P}}_{\mathrm{B}\to\mathrm{C}}(k,m) & \forall k,m. \end{array} \tag{59}$$

The last step is to update the current level of the BESS and the batteries of the EVs by only using the first predicted value.

$$\begin{array}{lcll} \mathrm{P}_{\mathrm{EV}}(k,m) & = & \hat{\mathrm{P}}_{\mathrm{C}\to\mathrm{EV}}(1,m) & \forall k,m \\ \mathrm{P}_{\mathrm{BESS}}(k) & = & \hat{\mathrm{P}}_{\mathrm{PV}\to\mathrm{B}}(1)-\hat{\mathrm{P}}_{\mathrm{B}\to\mathrm{C}}(1,m) & \forall k,m. \end{array} \tag{60}$$

6.5 Interaction MATLAB/Simulink

The output of the MPC Model is used to generate the desired current with help of the power law;

$$\begin{aligned} \mathrm{I}_{des,\mathrm{EV}}(t+1,m) &= \frac{\mathrm{P}_{\mathrm{EV}}(1,m)}{\mathrm{V}_{\mathrm{EV}}(t,m)} \quad \forall m,t \\ \mathrm{I}_{des,\mathrm{BESS}}(t+1) &= \frac{\mathrm{P}_{\mathrm{BESS}}(1)}{\mathrm{V}_{\mathrm{BESS}}(t)} \quad \forall t. \end{aligned} \tag{61}$$

It should be noted that the voltage of the EVs and BESS of previous time step are used to determine $\mathrm{I}_{des}(t+1)$. As the SOC is only changing slightly during one time step, it is assumed that $\mathrm{V}_{\mathrm{EV}}(t,m)$ will be approximately equal to $\mathrm{V}_{\mathrm{EV}}(t+1,m)$.

The EVSPL, which is modelled using SIMULINK as described in Figure 14, is paused after every iteration k. While pausing the simulation, the HLC is run which results in the values for for the I_{des} and DNI_{real}. These setpoints are updated and the simulation is continued. The LLC method is described in section 5 will keep the power flows constant, while the setpoints are changed.

Lastly, the safety issue described in subsection 4.4 is implemented in the Simulink model. When the $\mathrm{Q}_{\mathrm{EV}}(t)$ or the $\mathrm{Q}_{\mathrm{BESS}}(t)$ will become larger than the following Q_{crit}

Car Type	$\mathrm{Q}_{max}(k\mathrm{W}h)$	$\mathrm{Q}_{crit}(\%)$
BESS	200	96.3
TESL	100	95.7
NISS	24	85.3
CHEV	18.4	85.0

Tab. 14: The critical safety values for different EVs and the BESS.

the chargers will switch to constant voltage control at 400V. These values were obtained by using trial and error in designing a maximal power flow of $10k$W at 400V. The current will be around 25A, and will generally drop to zero.

In subsection 7.2 the MPC model is tested with reference to different prediction horizons and different disturbances.

7 Scenarios

In this section, different scenarios are be designed and evaluated to generate insight in EVSPLs. The research questions, "*How will the case studies be constructed?*", and "*What will result from the case scenarios?*" will be answered. As the construction of the EVSPL, and the different control methods have been described, the next step is to test the these control methods. This is done using three different scenarios, with the main goal being;

- determining the stability in the power flows of the EVSPL,
- testing the performance in the creation of charging setpoints, and
- checking whether both control methods combined work appropriately on the EVSPL.

Scenario I will elaborate on the stability of the power flows within the EVSPL, as stability must be guaranteed. Especially in the charging and discharging of batteries. Here it is important to minimise power fluctuations in order to decrease the rate of degradation of the battery (Nazri and Pistoia, 2008). Unstable power flows generate high peaks which can damage the cable structures within the EVSPL and leads to high maintenance costs. Charging and discharging results in bi-directional power flows, which are controlled using Bi-Directional DC/DC converters. Controlling the power in bi-directional flows is a difficult process due to the differences of the converter modes which are accompanied to a specific direction, as described in subsection 4.6. In the EVSPL, the Buck mode is active when the battery is charged, which results in a linear conversion of power. When the battery is discharged, the Boost mode is active which is accompanied with its nonlinear nature. To test this process, scenario I will compare PI and second-order Sliding Mode control in the charging and discharging modes of a battery.

Secondly, scenario II elaborates on the HLC strategy which is introduced in section 6. As the MPC model will generate the charging setpoints for the LLC method, it should be extensively tested. If unrealistic setpoints are introduced, the LLCer will not be able to keep the power flows constant, resulting in the issues described above. The HLCer is tested on a perfect match of the MPC model, to clearly see the reaction to disturbances in the environment for different prediction horizons. Lastly, the scalability of the MPC model is investigated.

The last scenario explores the performance of combining both control methods, resulting in the MLC strategy. The HLC method is tested on a real EVSPL, which is represented by the Simulink model, as described in subsection 4.6. The overall grid stability is investigated, as well as the performance of the HLCer to translate the charging setpoints to the LLCer.

This section is structured according in the following way: every case scenario (which is labelled using roman numerals) consists of multiple simulations (which are labelled alphabetically) which will be executed. These simulations are introduced in the beginning of each case scenario, together with the general starting conditions and input values. After this introduction, the different simulations are described in the following way: first, the changing parameters are described , which is followed by an extensive interpretation of the generated results. Figures and tables are used to illustrate the results and provide more transparency in the data. Lastly, a general conclusions and recommendations are made for each scenario based on the executed simulations.

To refer back to the analysed case studies in the literature review in subsection 2.4, the scenarios are summarised using the table Table 15 and Table 16. The same abbreviations are used to describe to scenarios in the tables.

Scenario	**Objective**	**Analysis**	**Perspective**	**Obj. Function**	**Controller**	**Approach**
I	Test the performance of a PI controller and Sliding Mode controller in an EVSPL.	MaxGS	EVSPL	MaxGS	Decentr.	PI & SMC
II	Test MPC controller in terms of different prediction horizons and the response to external disturbances.	Eco/Env	EVSPL	MinCOST	Centr.	MPC
III	Test the performance of the Multi-Level controller.	MaxGS	EVSPL	MaxGS	Centr. / Decentr.	Multi-Level (MPC & SMC)

Tab. 15: The three case studies which will be explored during this section.

Scenario	**EVs**					**Grid**		**Components**				
	Amount	Types	Arrival	Pricing	Depletion	V2G	Pricing	PV Cells	Wind	Storage	Generators	Model
I	0	0	-	-	-	-	-	Y	N	Y	N	-
II	5-50	3	Stoch	-	N	N	-	Y	N	Y	N	-
III	3	2	Det	-	N	N	-	N	N	Y	N	-

Tab. 16: The components of the three case studies which will be explored during this section.

7.1 Scenario I : PI Control vs. Second Order Sliding Mode Control

In this scenario, LLC in the EVSPL will be the central topic. It is important that the power flow is stable when different EVs are charging at the same time. If the charging network is unstable high maintenance costs will arise, battery degradation will speed up, and the batteries might be overcharged which leads to battery damage (Nazri and Pistoia, 2008). Furthermore, an unstable MG will provide unpredictable charging results which will lead to inaccurate charging setpoints by HLCer. This will create a chain effect, and leads to even lower stability in the network. The two explained control methods of section 5; second-order SMC vs PI control, will be tested according to their performance with reference to;

- the reaction to different starting error signals,
- the reaction to a disturbance signal, and
- the performance when the step function is changed to a ramp function.

This leads to the objective;

> *The objective of this scenario is to decide whether PI control or SMC will perform better for the power flows within an EVSPL, keeping in mind charging and discharging.*

The simulation will occur in 'basic' conditions, as defined in section 4 and subsection 4.6. This scenario will be restricted to only one battery component (BESS) charged at 50%, connected to a PV array and the utility grid. After tuning the controllers, the simulation was initialised using the values shown in section 11. The Direct Normal Irradiance (DNI_{real}) = 1000W/m_2 and the Temperature is constant at 25.

A: Changing the Desired Current

The simulation is started at $t = 0$, and after $t = 1$ seconds, the value of the desired current of the BESS is changed. In Buck mode, the value is changed from 10 A, to a higher value, which implies an increase in the charging speed. In Boost mode, the current is changed from −10 A, to a more negative value, implying an increase in discharging speed. The desired current values are updated as a step function. The SMC and PI controllers will be investigated with help of the error signal $e(t) = (\mathrm{I}_d - i)$.

Name Scenario	$\mathrm{I}_d(t)$	$\mathrm{I}_d(t+1)$	$e(0)$	Mode
5A	10	15	5	Buck
25A	10	35	25	Buck
125A	10	135	125	Buck
-5	-10	-15	-5	Boost
-25A	-10	-35	-25	Boost
-125A	-10	-135	-125	Boost

Tab. 17: The difference in the desired currents and their error functions.

Interpretation

The results are shown in Figure 26, and Table 18. The convergence time is described as the time it will take for the controller to reduce the error between −1 and 1 Ampere and is determined using Figure 26.

First of all it should be noted that both controllers are able to converge very quickly (at least within 0.04 seconds) for the control of a DC Powergrid systems compared to experiments done in Sira-Ramirez and Silva-Ortigoza (2006). Although both convergences seems within the desired boundaries, in both modes (Buck/Boost), PI control is converging faster with a small starting error, yet SMC is able to converge faster with bigger starting errors. For the over- and undershoot, comparable results as the convergence time are noticed. With a relatively small starting error, PI control is able to provide stability with a smaller undershoot compared to SMC, however when the starting error is increased SMC immediately shows improved results. This is confirmed by the Root-Mean Squared Error, which shows similar behaviour.

In terms of computation time seems PI control a little faster, compared to SMC. SMC takes around 9% longer than PI control.

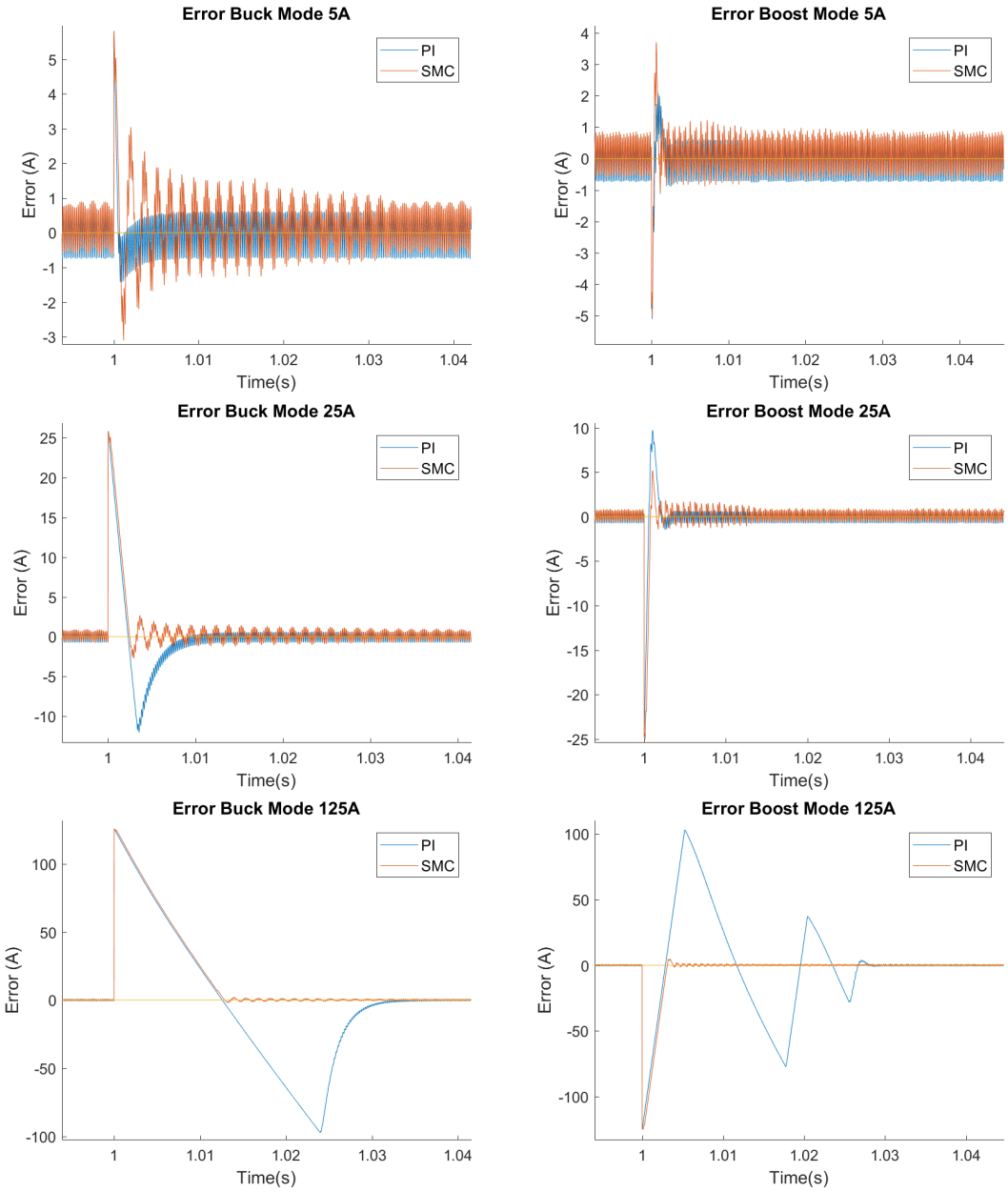

Fig. 26: This figure shows the convergence of $e(t)$ for different I_d in, Buck and Boost mode.

Also it is interesting, however not surprising, to see that SMC is able to provide better results in Boost mode compared to PI control. The nonlinear behaviour of the Boost converter is easier controllable using a nonlinear control method. Especially with high starting errors this is clearly visible as PI control shows multiple over- and undershoots while SMC converges quickly with only one minor overshoot.

The desired currents in the simulation model will be able to differ much, resulting in high starting errors. For the overall stability of the system, SMC seems able to perform with higher robustness compared to PI control in terms of the starting error. Also, the difference in computation time seems negligible in the simulation which confirms the choice for SMC in terms of the starting error.

Mode	**Buck**					
Method	PI			SMC		
Name Scenario	5A	25A	125A	5A	25A	125A
Convergence Time (s)	0.006	0.006	0.037	0.032	0.017	0.026
Undershoot (A)	-1.429	-12.04	-97.42	-3.108	-2.730	-1.985
Root-Mean Squared Error (A)	0.493	2.291	27.87	0.641	2.177	21.47
Average Computation Time(s)	26.21			28.45		

Mode	**Boost**					
Method	PI			SMC		
Name	5A	25A	125A	5A	25A	125A
Convergence Time (s)	0.005	0.016	0.037	0.007	0.017	0.026
Overshoot (A)	2.095	9.727	103.2	3.707	5.199	4.839
Root-Mean Squared Error (A)	0.479	1.190	21.89	0.534	1.410	11.39
Average Computation Time(s)	26.15			28.47		

Tab. 18: The results of simulation I A.

B: Introducing a Disturbance Signal

In the next simulation, the following disturbance signal is added to the duty cycle, before it is converted to a discontinuous signal with help of the PWM technique;

$$d(t) = \mathrm{A} * sin\big(f * t + \varphi\big), \tag{62}$$

where;

$$\begin{array}{lll} \mathrm{A} & = \text{Amplitude} & \\ f & = \text{Frequency} & (\mathrm{H}z) \\ \varphi & = \text{Phase} & (rad) \\ t & = \text{Time} & (\mathrm{s}). \end{array}$$

This will provide insight in the robustness of both control methods. An example in the EVSPL which may lead to a disturbance signal is an EV with a damaged battery, or an internal problem with the BESS.

Again, the simulation is started at $t = 0$, and after $t = 1$ seconds, the value of the desired current of the BESS is changed. In Buck mode, the value is changed from 10 A, to 25 A, and in Boost mode, the current is changed from -10 A, -23 A. The reason for choosing a starting error of 15 A in Buck mode, and -13 A in Boost mode, is the fact that the both PI control and SMC are performing similar in terms of their error convergence with these starting values. In this way the reaction on the disturbance signal can be better established. The desired current values are updated as a step function. The SMC and PI controllers will be investigated with help of the error signal $e(t) = (\mathrm{I}_d - i)$.

Name Scenario	A	f	φ	$e(0)$	Mode
Basic	0.05	100π	0	15	Buck
Amplitude	0.2	100π	0	15	Buck
Frequency	0.05	1000π	0	15	Buck
Basic	0.05	100π	0	-13	Boost
Amplitude	0.2	100π	0	-13	Boost
Frequency	0.05	1000π	0	-13	Boost

Tab. 19: The parameters of the disturbance signal $d(t)$.

Interpretation

The results are shown in Figure 27.

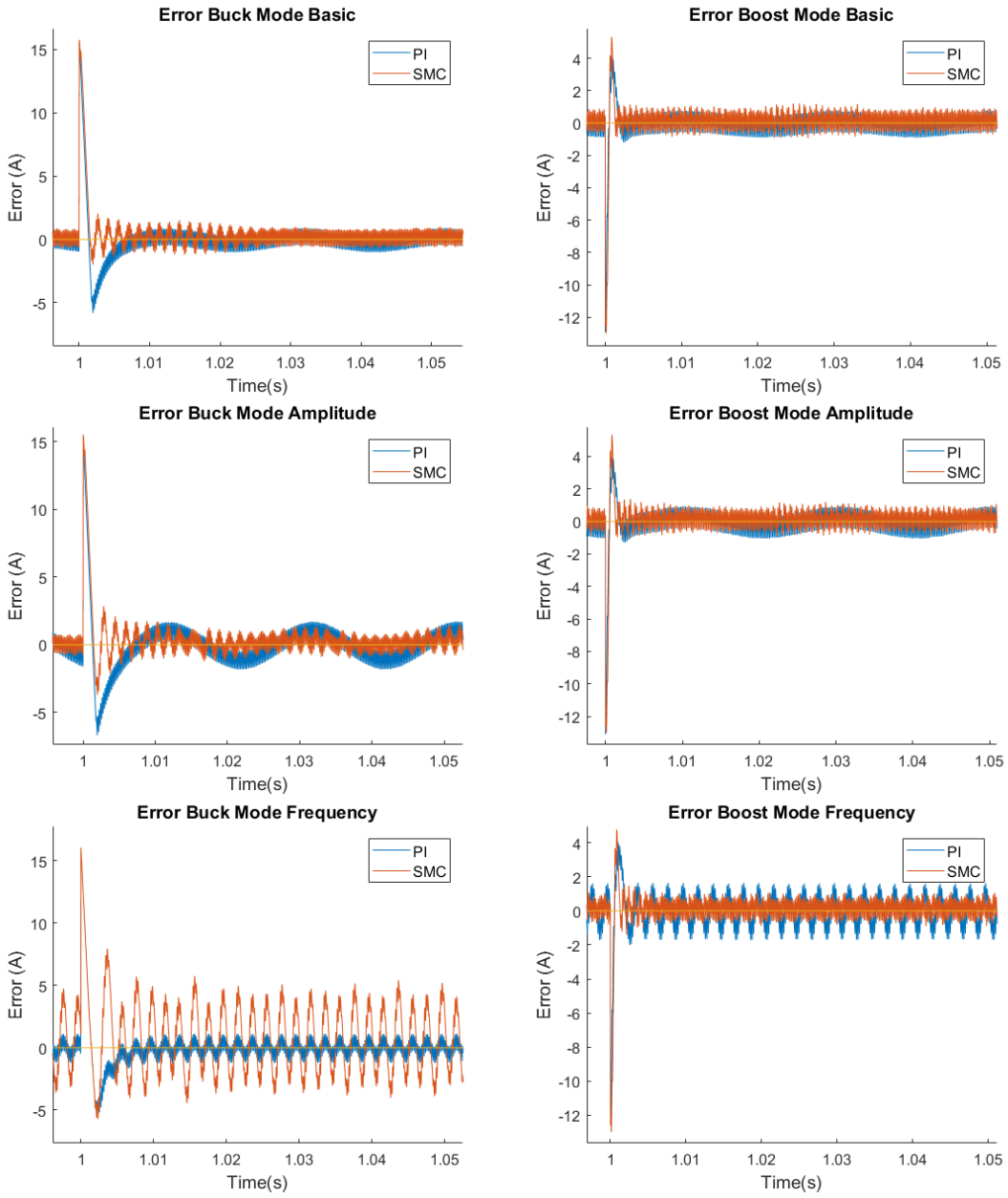

Fig. 27: The convergence of $e(t)$ for different disturbance signals, in Buck and Boost mode.

Both control methods are able to stabilise the network despite of the disturbance signal. Both methods are able to converge quickly and the steady-state error of both signals is comparable. It is noticed that the convergence time of SMC in Buck mode is slightly faster compared to PI control.

When the amplitude of the disturbance signal is increased, the PI error signal is effected more than the SMC error signal implying that SMC is more capable of reacting upon high disturbances. Especially in Buck mode, PI control clearly holds a steady-state error comparable to the behaviour of the disturbance signal.

An increase in the frequency provides different results. In Buck mode, PI control establishes a small steady-state-error while SMC shows chattering behaviour. A possible explanation for this might be the discrete behaviour of SMC as this results in high overshoots when the disturbance signal is quickly

changing polarity (and thus not allowing the controller to stay near the manifold), whereas PI control has the ability to use a continuous signal. However, in Boost mode SMC is providing improved results, which even transcend the behaviour of PI control in spite of the high frequency of the disturbance signal. This is probably due to the nonlinear nature of the SMC.

C: Changing the Step Function to a Ramp Function

The last simulation will introduce the new reference value as a ramp function instead of a step function. This will lead to a less gradient transition which generates insight whether the convergence time for both control methods will improve. During the ramp function, the controller has multiple reference points before actually reaching the desired value. The ramp function is created from the starting time $T_{start} = 0$ to the desired value in the settling time T_{set}. A step function was created by choosing the settling time smaller than the discrete steps of the simulation.

Name Scenario	T_{set}	$e(0)$	Mode
Step Function	$1 * 10^{-7}$	15	Buck
Ramp Function	$1 * 10^{-3}$	15	Buck
Step Function	$1 * 10^{-7}$	-13	Buck
Ramp Function	$1 * 10^{-3}$	-13	Buck

Tab. 20: The parameters for the ramp function.

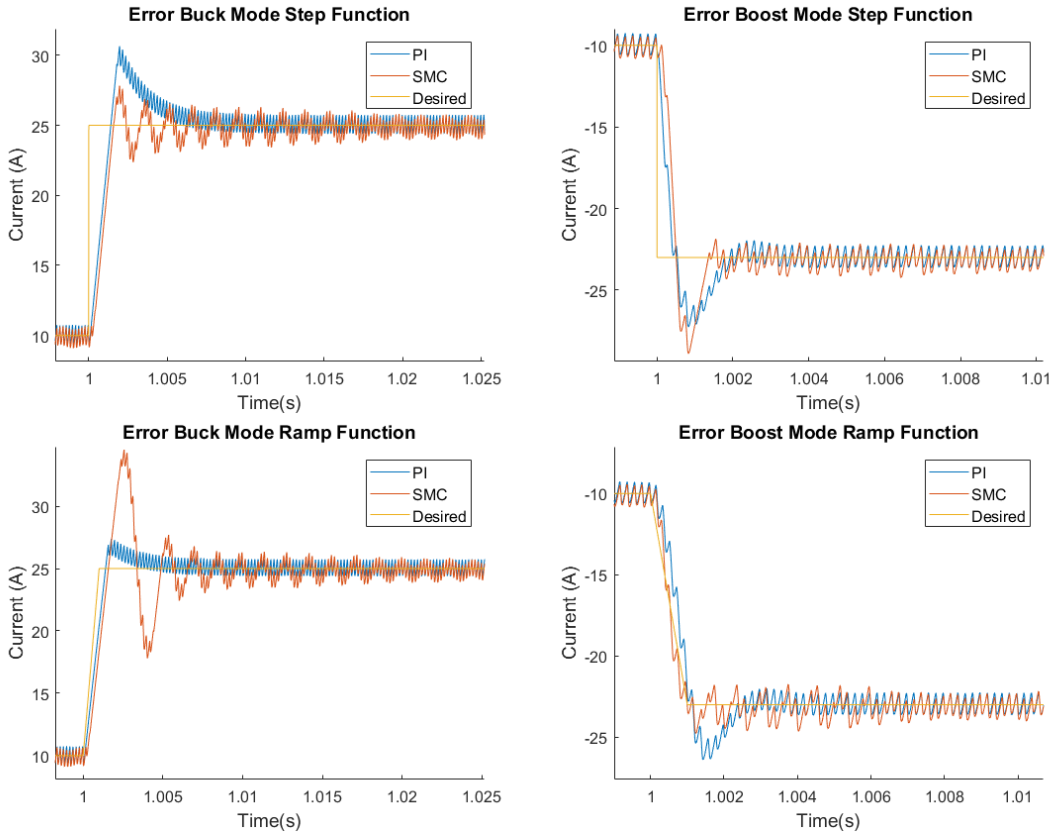

Fig. 28: The convergence of $e(t)$ for the step and ramp function, in Buck and Boost mode.

Interpretation
The results are shown in Figure 28. During Buck mode a ramp function seems to oppose the convergence of the error signal with SMC, and PI seems to benefit from the ramp function by reducing the error to a third of the original value. Yet, in Boost mode the SMC seems to gain advantage from the ramp function compared to the step function while PI control does not. Especially in the bottom right figure of Figure 28, it is clearly shown that SMC will keep close to its manifold, while PI control has more difficulty in keeping the $e(t)$ zero.

It is clear that SMC performs better at a step function while PI control seems the perform similar to SMC at a ramp function. As it is easier to update values using step functions, SMC will receive preference over PI control in terms of the way values are updated.

7.1.1 Discussion & Conclusion

Different simulations have been executed regarding PI control and SMC on the network of the EVSPL, with the objective of determining which control method would perform best.

First of all, the error convergences of both SMC and PI control, are performing outstanding. In all scenarios a steady-state equilibrium was reached within 0.05 seconds, and the error stayed within a limit of +/- 1 Ampere of the desired current. Yet, SMC showed improved results compared to PI control, when high starting errors were given as input signal. This was shown by large overshoots in the results PI control, while SMC converged quicker and more stable. Although SMC is accompanied with a little higher computation time (around 9%), it performs better than PI control.

Also, a clear difference is seen in Buck and Boost mode. In every simulation, the nonlinear behaviour of SMC is performing better compared to the linear behaviour of PI control. In Buck mode, occasionally PI control is performing slightly better, yet in most cases SMC is still outperforming PI control.

When disturbance signals were added to the network, SMC showed superior results compared to PI control in most situations. One exception was found in Buck mode, where the frequency of the added disturbances signal was exceptionally high. Still, SMC is able to keep the lowest steady-state error as long is the frequency is not exceptionally high.

Changing the updating value from a step function to a ramp function increased the performance of especially PI control. Even the improved results of PI control outperformed SMC only in one situation. Also, updating in terms of step functions is easier to establish as it only requires one update value.

It should be noted that the results were obtained during a short time frame. When the time frame is increased, the SOC of the battery will increase or decrease resulting in different conditions. In scenario III, these effects will be discussed.

To conclude, SMC performs better for the control of power in a EVSPL, due to the high robustness, quick converge rate and steady-state error. It responds better to a disturbance signal and is able to converge more quickly when the values are updated using a step function. Especially in Boost mode, the nonlinear SMC is able to respond to the nonlinearities of this particular mode.

7.2 Scenario II: Model Predictive Control

Although the EVSPL is stabilised using the LLCer, the HLCer must still provide the right charging set-points to create this stability. Therefore, the HLCer should be tested extensively, which will happen in this scenario according to;

- differences in prediction horizons N,
- the reaction to an unexpected change in solar irradiance, and
- the scalability of the MPC model.

This leads to the following objective;

> *The objective of scenario II is to test the performance of the Higher-Level-Controller keeping in mind disturbances in the environment.*

During this scenario, simulations will be executed apart from the Simulink model. As it requires high computational loads to balance the Simulink model, it is not possible to examine the results carefully. Therefore, the HLCer is tested on a perfect match of the MPC model, to clearly see the reaction to disturbances in the environment for different prediction horizons. Differences in the prediction horizon, and differences regarding the real irradiance (DNI_{real}) and predicted irradiance (DNI_{pred}) will test the response of the controller. In case of underproduction ($DNI_{real} < DNI_{pred}$), the EVs are still charged as predicted, yet the shortage of energy is taken from the utility grid. In case of overproduction ($DNI_{real} >= DNI_{pred}$) , the surplus of energy is delivered to the utility grid.

The time instants imply a time slot of 5 min and the total simulation time is a full day (T = 288). The data in Table 21 is used for the arriving EVs and the yearly average DNI_{pred} can be found in section 12.

Name	Brand	Q (kWh)	Q_0 (%)	Q_{des} (%)	EV_{maxin} (kW)	t_{arr} ($hh:mm:ss$)	$t_{dep,planned}$ ($hh:mm:ss$)	$t_{dep,real}$ ($hh:mm:ss$)
EV1	TESL	100	43	96	145	08:06:00	17:47:51	18:03:09
EV2	CHEV	18.4	43	86	3.3	07:05:13	16:00:52	16:53:07
EV3	NISS	24	31	70	16	08:07:41	17:27:45	17:35:39
EV4	CHEV	18.4	15	97	3.3	07:09:39	16:20:02	17:29:31
EV5	TESL	100	20	72	145	07:45:54	16:30:21	17:53:20

Tab. 21: The arrival data of the EVs in scenario II.

A: Changing the Prediction Horizon

In this simulation the influence of the prediction horizon on the HLCer will be measured. The prediction horizon N is explained in subsection 6.1 and will change according to the values stated in Table 22. The different horizons will be assessed in terms of the net result of power to the grid.

N	1	12	24
Time	5 min	1 hrs	2 hrs

Tab. 22: The different prediction horizons, and their representation in time for Scenario II A

Interpretation

The results are shown in Figure 29. First of all, it should be noted that the smoothness of all charging curves in the sub-figures increase when N increases. The peaks in the power flows are gradually reduced, resulting in a higher grid stability, and thus a longer life time of the battery, as described in Nazri and Pistoia (2008). This is clearly shown in the 'Power to Charger' figure, where the high peaks of N = 1 between 07:00 and 09:00, disappear when the prediction horizon is increased. Moreover, the net result to the utility grid does not show any huge differences for the three different prediction horizons. The only value worth of mentioning is the peak for N = 1 at 18:00, which is caused by a fully charged BESS. In the case of a higher prediction horizon, the charging of the BESS is spread more evenly, which omits the aforementioned peak.

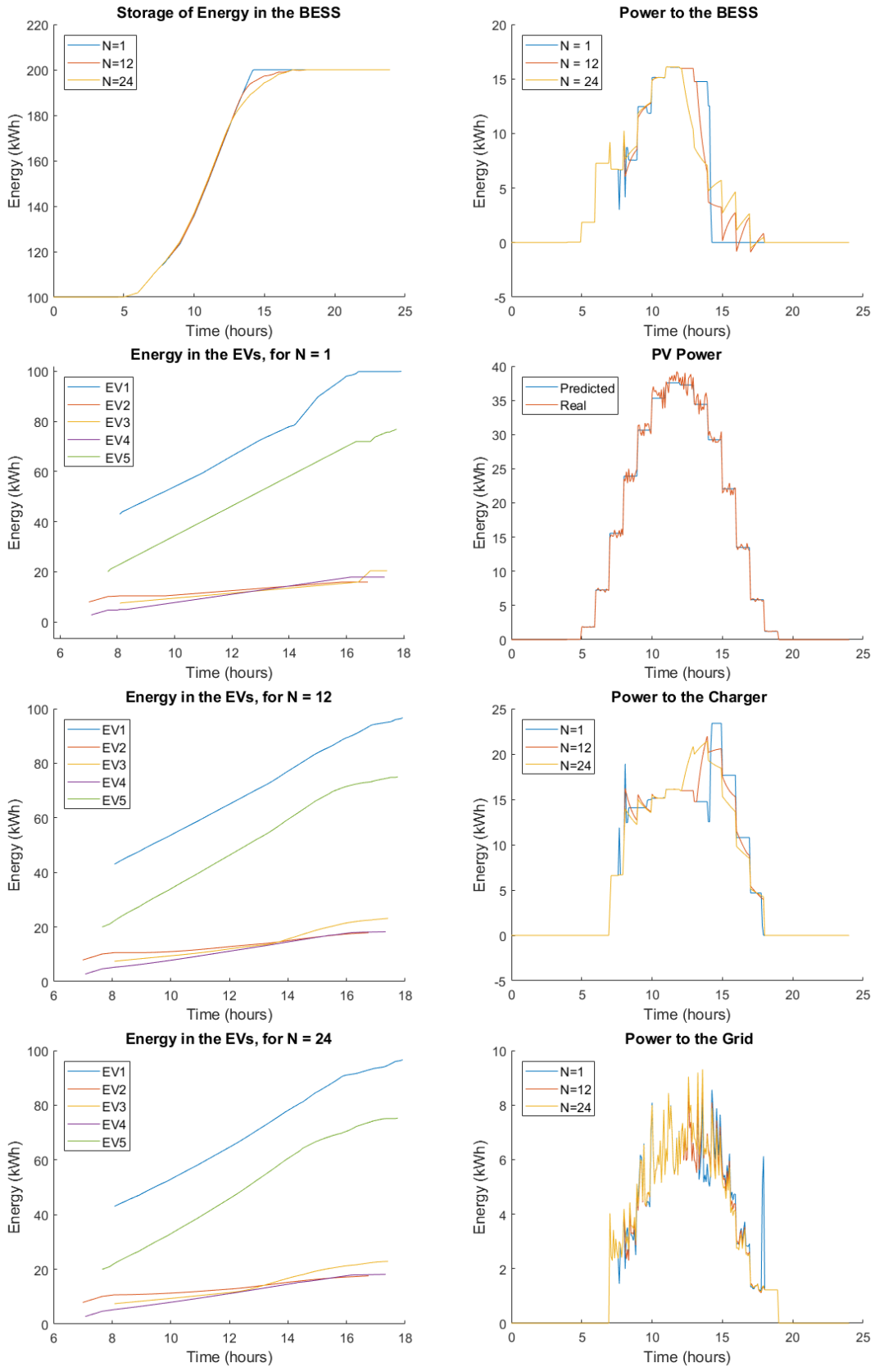

Fig. 29: The results of changing the prediction horizon for N = 1, N = 12, and N = 24. The figures on the left show the storage of energy in the BESS and the EVs over time. The figures on the right side entail multiple prediction horizons in one figure, and illustrate the flows of power.

The last observations made is that increasing the prediction horizon is not always accompanied with improved charging behaviour. Although the 'prioritising array' of subsection 6.4 is introduced, still the MPC strategy is postponing charging, which is shown by the more shapely end of the charge curve. As the constraint in Equation 50 only states that the end value of the prediction horizon should be met, a larger prediction horizon will generate more freedom for the solver to create charging setpoint. As charging results in a penalty for the solver, the HLCer would like to postpone charging. Near the end of the simulation, the prediction horizon becomes smaller, which results in the change of the curve for N = 12 at one hour before $t_{dep,planned}$ and for N = 24 at two hours before before the $t_{dep,planned}$.

N	1	12	24
Average Computation Time	0.1882	0.4963	0.8456
PV Power Real	3567,426	3567.426	3567.426
Power taken from the Grid	-554.069	-551.844	-556.457
Energy stored in the BESS	1200.000	1199,838	1199,926
Energy stored in the EVs	1797.856	1801.400	1796.699

Tab. 23: The results of the simulations of different prediction horizons. The average computation time is the total computation time divided by the complete number of time instants T = 288.

B: Changing the Solar Irradiance

In the next simulation study, difference irradiances are given as input to the HLCer. The same irradiance as previous simulation study is used, with the alterations shown in Table 24 and the top two subfigures of Figure 30. In alterations one, the real DNI changes, while the MPC model still estimates the PV power by using the DNI_{pred} of previous scenario. In alterations two, the drop in PV power is predicted by the HCLer and the solver takes these values into account.

	Variable	Change Value to	Between t = ..	
Alteration 1	DNI_{pred}	-	-	-
	DNI_{real}	0	140	145
Alteration 2	DNI_{pred}	0	140	145
	DNI_{real}	0	140	145

Tab. 24: The two alterations in the solar irradiance data, retrieved from section 12.

Interpretation

The results are shown in Figure 30. After alteration 1, the charging behaviour is exactly the same as the simulations described in subsection 7.2. The differences in the results are found in the power flows to the utility grid. At t = 140 the drop in solar irradiance is not corrected by the HCLer, resulting in high demands of power from the utility grid. This is confirmed by the more negative value in Table 25.

Alteration 2 however, shows promising results in the charging behaviour due to its prediction of the drop in solar irradiance. When N = 1, the peak of the grid power around noontime, is significantly lower (from 33 kW to 5 kW). The HLCer has decided to withdraw energy from the BESS to provide the EVs with power. Also, a minor dip in the power to the charger is shown, resulting in a higher charging duration. Still all EVs are charged within the desired boundaries.

An increase in the prediction horizon improves the results of the charging behaviour. Firstly, the power from the grid has almost completely dissolved resulting in a more independently operating EVSPL. Secondly, the HLCer forecasts the drop of solar irradiance and translates this into increasing the charging power just before noontime. Due to this, the conditions of linear charging are still satisfied without extracting power from the grid, nor the BESS.

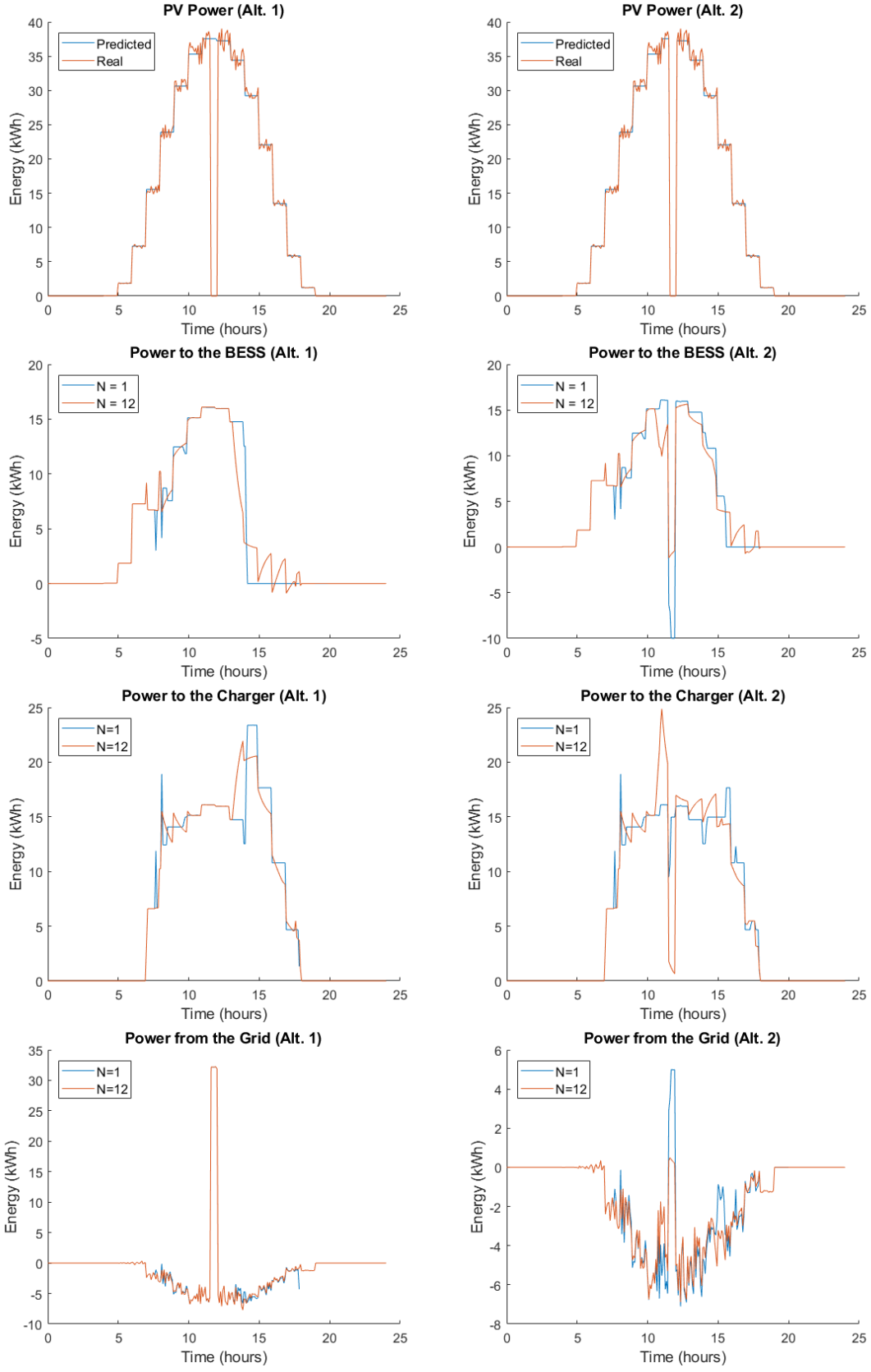

Fig. 30: The power flows of the simulation II B. The figures on the left represent the unpredicted change in DNI_{real} and the reaction of the HLCer. In the figures on the left, the change of solar irradiance is expected, and the HLCer responds accordingly.

Alteration	1		2	
N	1	12	1	12
Power taken from the Grid	-323.452	-321.228	-437.276	-448.763
Energy stored in the EVs	1797.856	1801.4	1685.19	1673.978
Energy stored in the BESS	1200	1199.838	1200	1199.726
PV Power	101798.3	101798.3	95341.9	95341.9

Tab. 25: The results of simulation II B. The average computation time is the total computation time divided by the complete number of time instants T = 288.

C: Changing the Amount of EVs

The last simulations will be done to test whether the HCL is easily scalable. The arrival pattern of section 13 is used for 50 EVs. The yearly average PV irradiance of section 12 is used, and the prediction horizons N = 1 and N = 12 are taken into account. The surface area of the PV power is increased linearly relative to the number of EVs, as described in subsection 3.2.

Interpretation

The HLCer is clearly scalable, as it has no difficulty in assembling the values for 50 EV while taking into account higher prediction horizons. As the HLCer will be configured centrally, the computing load can easily be obtained for the central controller, as described in subsection 2.3. No issues will arise as long as the average computation time is smaller than the length of a time instant in which new charging setpoints must be provided. Taking a safety margin within these boundaries is advised.

Amount of EVs	5	25	50
N = 1	0.189	0.261	0.338
N = 12	.481	1.3567	2.501

Tab. 26: The average computation times of scenario II C. The average computation time is taken by dividing the total computation time over the amount of time instants T = 288.

Discussion & Conclusion

Multiple simulations have been executed to test the performance of the HLC strategy on a simplification of the EVSPL. Disturbances in the environment were added to illustrate the reaction of the HLCer.

An increase in the prediction horizon clearly provides improved results in terms of grid stability. The power flows are smoother compared to lower prediction horizons, which results in a more linear charging curve. Yet, an increase in the prediction horizon also increases the issue of postponed charging. The priority array, described in subsection 6.3 is apparently not significant when the prediction horizon is increased. Further research could imply an adapting priority array which will counteract the postponing charging behaviour more satisfyingly.

The HLCer is able to anticipate on changes in the environment, if predicted correctly. It correctly reduces the power taken from the grid, while satisfying the charging constraints. When the prediction horizon is increased, the model responds appropriately by changing the power flows in advance to eliminate peaks when the disturbance of the environment is present. It should be noted that a correct model for external factors in the environment is a prerequisite to make use of the opportunities of the HLC strategy. The forecasting of external disturbances is beyond scope of this thesis, but can easily be implemented in the HLCer.

Lastly, the HLCer is found to be easily scalable as the computation power of the HLCer is sufficiently large to predict the power flows within the given time instants for at least 50 EVs and a prediction horizon of 1 hour.

It can be concluded that the HLCer works correctly in creating setpoints for the EVSPL as long as external disturbances are predicted correctly.

7.3 Scenario III - Combining Higher- and Lower-Level Control

In this scenario Multi-Level control is the central topic. The complete control strategy is tested in terms of stability and performance. Unfortunately, only small time frames can be examined due to high computation loads. This leads to this scenario not being very realistic, as EVs will arrive and depart within a very short time frame, as well as huge differences in solar irradiance occur. Still, this scenario is very helpful in illustrating the effects of MLC as it will work the same for realistic longer time frames.

As the time frame is short, two simulations will be executed regarding the

- linear area of the charging curve, and
- non-linear area of the charging curve.

in which the last scenario will be illustrating the safety effect described in subsection 4.4.

The following objective arises;

> *The objective of scenario III is to evaluate the performance of the Multi-Level Controller on the constructed Simulink model of an EVSPL.*

Again the 'basic' conditions as defined in section 4 are used for the next simulations. The EVSPL will be controlled using SOSMC as LLCer, with the same parameters as defined in section 11. The prediction horizon will be constant at half a minute N = 6. The total simulation time implies a mere 2 minutes starting from 11:00. Three EVs arrive and depart within this time span, according to the following pattern:

Name	Brand	Q (kWh)	Q_0 (%)	Q_{des} (%)	EV_{maxin} (kW)	t_{arr} ($hh:mm:ss$)	$t_{dep,pred}$ ($hh:mm:ss$)	$t_{dep,real}$ ($hh:mm:ss$)
EV1	CHEV	18.4	41	41.20	3.3	11:00:05	11:01:39	11:01:39
EV2	NISS	24.0	79	80.20	16	11:00:17	11:01:49	11:01:49
EV3	CHEV	18.4	31	31.37	3.3	11:00:21	11:01:57	11:01:57

Tab. 27: The arrival data of the EVs in scenario III.

The BESS is initialised with a capacity of 200 kWh at 50% SOC and the DNI is shown in Figure 31.

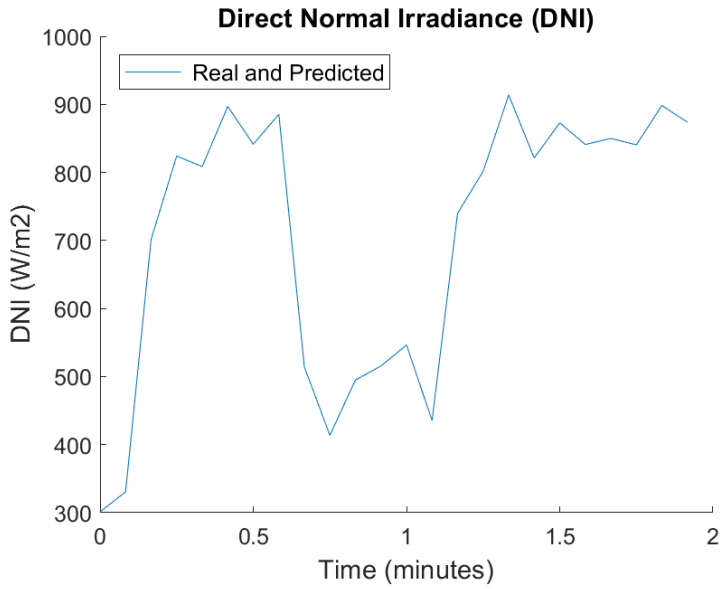

Fig. 31: The Direct Normal Irradiance (DNI) for Scenario III. The MPC model will predict the values of the irradiance perfectly as the DNI_{real} is equal to the DNI_{pred}.

A: Evaluating Linear Charging

First the overall stability in the DC network of the EVSPL will be analysed with help of Figure 32. The first observation made is that the network is clearly balanced with help of the utility grid. A drop in the PV power is recovered with an peak of power from the grid, yet this change is accompanied with the biggest voltage drop in the time span. Although this voltage drop is around 4 Volt, the overall voltage of the DC network is held within a constant boundaries of +/- 1 V which is classified as adequately.

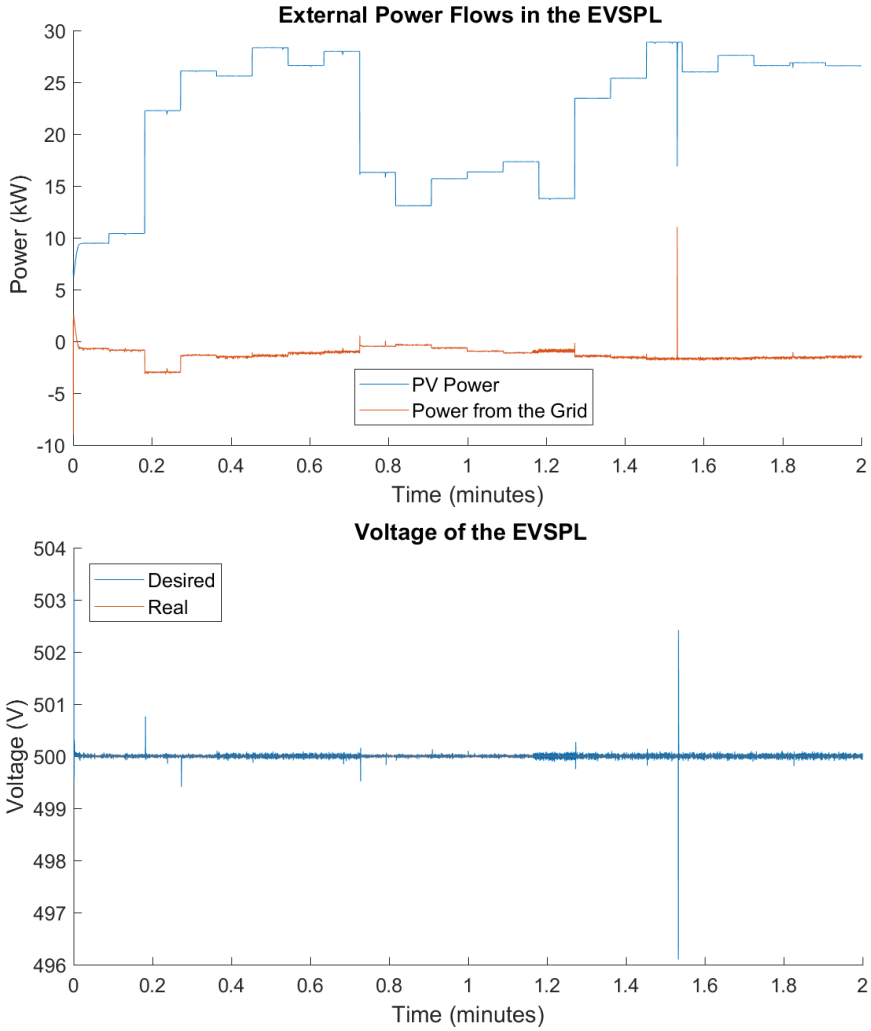

Fig. 32: The external power flows in the EVSPL, and the overall voltage of the DC network are shown in this figure.

During the charging process of the EVs, the drop in solar irradiance after around $t = 0.7$, is translated into lower desired currents for the EVs and the BESS. The LLCer is keeping this current as close as possible to the desired current, yet Figure 33 shows that the controller has difficulty to achieve this. The setpoints are clearly communicated to the LLCer, as shown by the desired currents. Nevertheless, the real current shows that the LLC has difficulty keeping the current at a very constant level and it fluctuates with $+/-2$A.

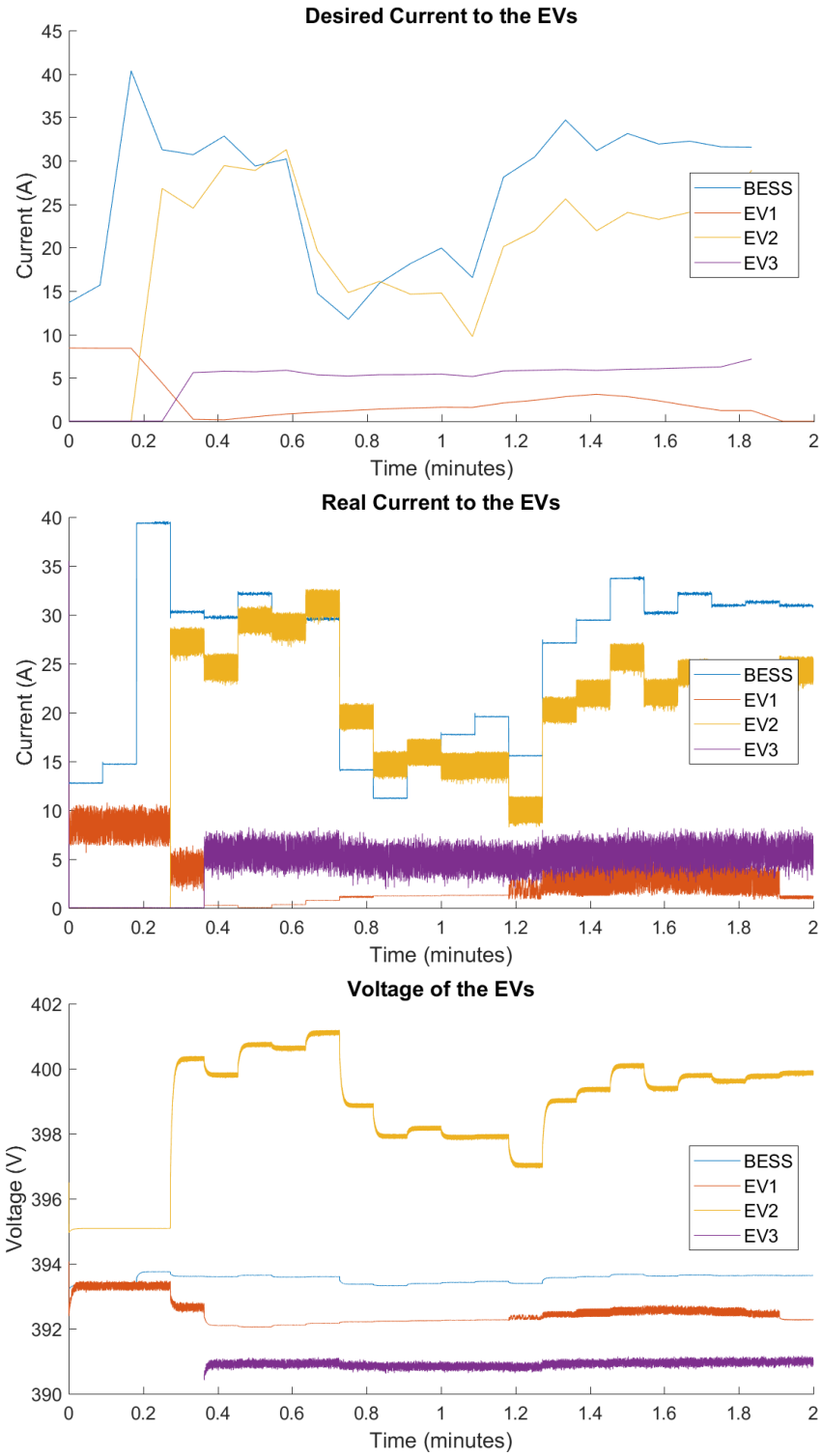

Fig. 33: This figure shows the desired current provided by the HLC and the real current of the EVs and BESS, which result from the EVSPL. The bottom subfigure shows the accompanied voltages of the currents.

A correlation is noted between the battery capacity and the overall stability of the current control. The EVs with the smallest capacity (EV 1 and EV 3), clearly show more chattering compared to e.g. the BESS with an overall capacity of almost 10 times the size of previously mentioned EVs. It should also be noted that a lot of time was spent on tuning the sliding mode controller for the BESS, in case scenario I. The reason for this is the fact that a higher battery capacity is accompanied with a lower change of voltage over time if the injected current is similar. These changes in battery voltage, create the disturbances for the current in the EVSPL. An interesting topic for further research would be implementing adaptive sliding mode control in the LLCer, which adapts to the different capacities of the batteries and the input current.

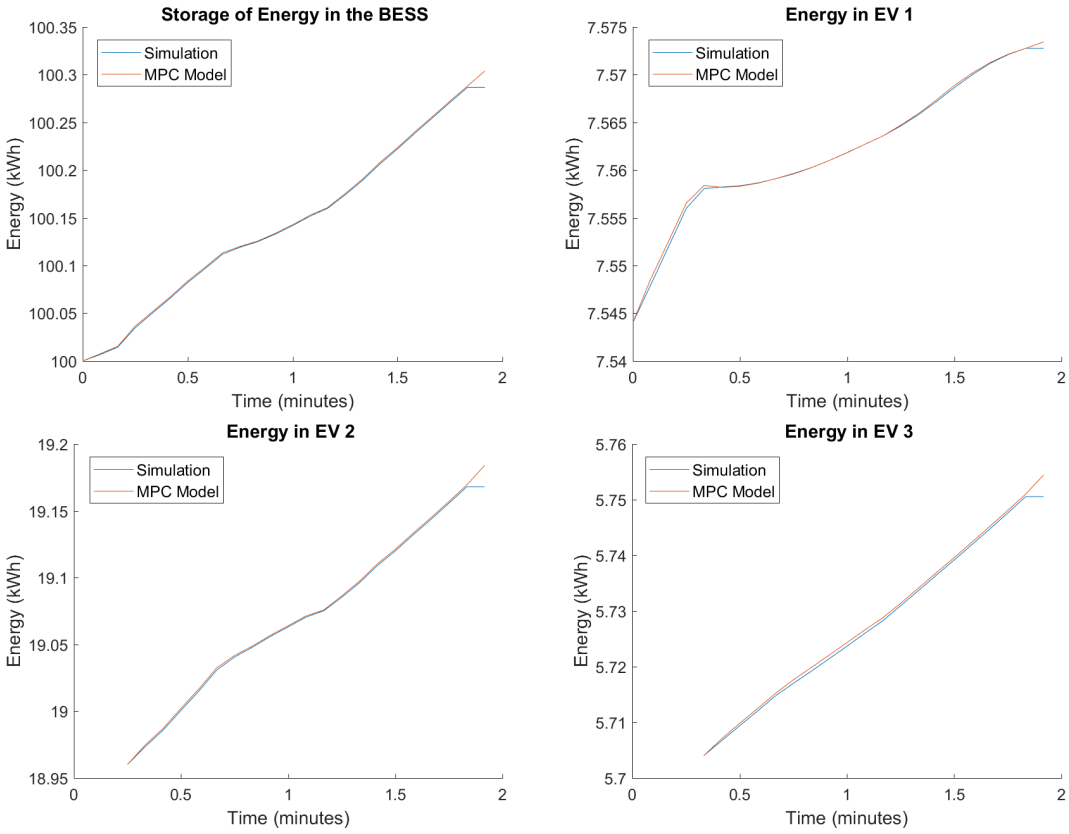

Fig. 34: The energy in the EVs and the BESS according to the MPC model and the Simulation in Simulink. The last time step is predicted differently which has to do with the end of the simulation. Although the simulation had already ended, the MPC model still had created a predicted value for the next time step. This is clearly shown in Figure 24.

Lastly, the results regarding the energy in the EVs and the BESS are predicted well for this small time frame. Only minor changes are shown in the predicted stored energy and the real stored energy provided by the EVSPL in Figure 34. This clearly shows that Multi-Level Control in an EVSPL works for the linear area of charging. This linear area is usually up to 85 – 90% of the battery capacity (Nazri and Pistoia, 2008).

B: Evaluating the Nonlinear Area of the Charging Curve

In the following simulation the effect of constant voltage control is illustrated. The same initialisation values as previous scenario are used, with the exception of the initial Q_0 of EV 1. This is done to illustrate the reaction of the EVSPL, to constant voltage charging. As the EVs' SOC becomes greater than a given value, the EVSPL switches from constant current charging to constant voltage charging as described in subsection 4.4. This safety feature is built in to protect the EVs from overcharging, as the voltage of their battery is increasing exponentially in the last part of the charging curve.

Interpretation

The results of the voltage, current, desired current and SOC over time are shown in Figure 35. As the EVs' SOC becomes greater than 85% at $t = 0.2$ minutes, the EVSPL switches from constant current charging to constant voltage charging. This is shown by a constant voltage from $t = 0.2$ in the top left subfigure, which is accompanied with a constant current, shown in the bottom right subfigure.

Although the same chattering of previous scenario occurs, another observations is made. The desired current is completely different than the actual current. This results in a difference in the expected energy in the EV by the MPC model, and the real energy in the EV, provided by the simulation results. This is shown in the bottom left subfigure in Figure 35. This is due to the fact that the sliding mode controller is not able to converge for the current and the voltage at the same time. If the time span would increase, the voltage would be kept constant and the current would slowly decrease to zero. This will make sure the batteries are not overloaded.

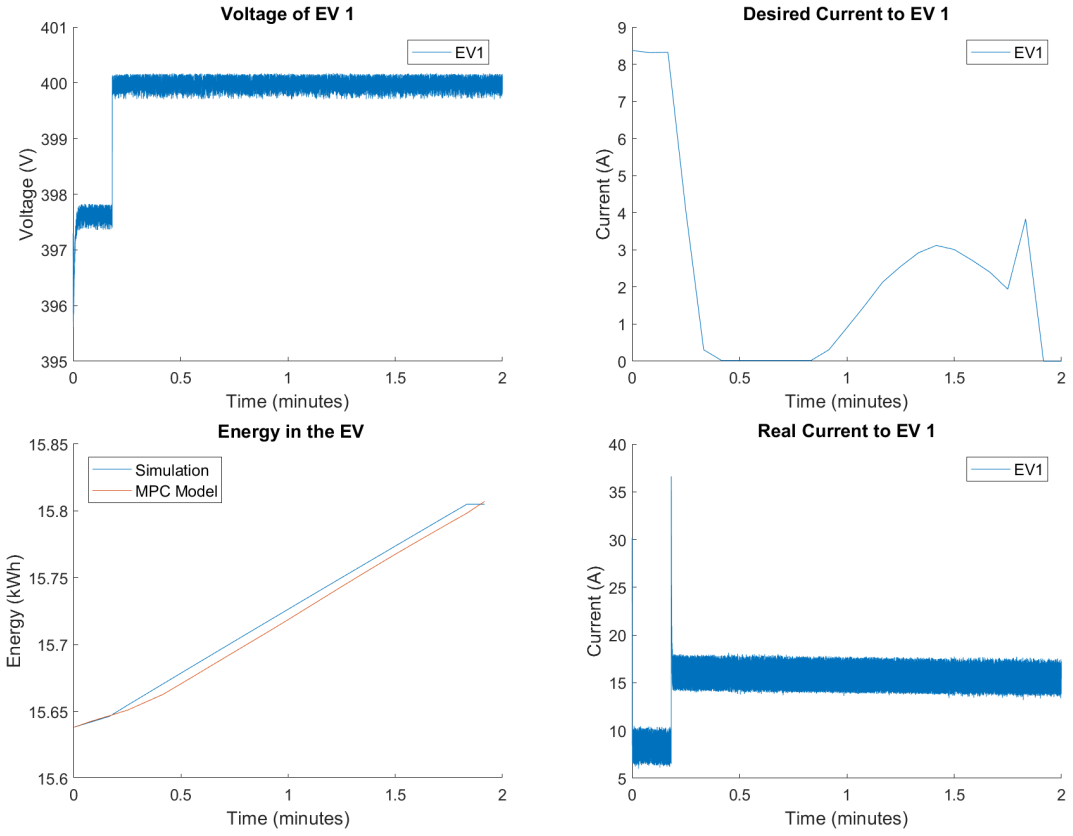

Fig. 35: All the information regarding EV 1, during the change from constant current charging, to constant voltage charging.

A topic for further research is controlling this constant voltage charging, to make sure that charging the last percentages of the battery can be controlled and predicted as well. In this simulation of the EVSPL, the shortage of energy is simply provided by the utility grid, which is shown in Figure 36. The peak which is needed to justify the change in the real current from 8A to 16A, is provided by power from the utility grid at $t = 2$.

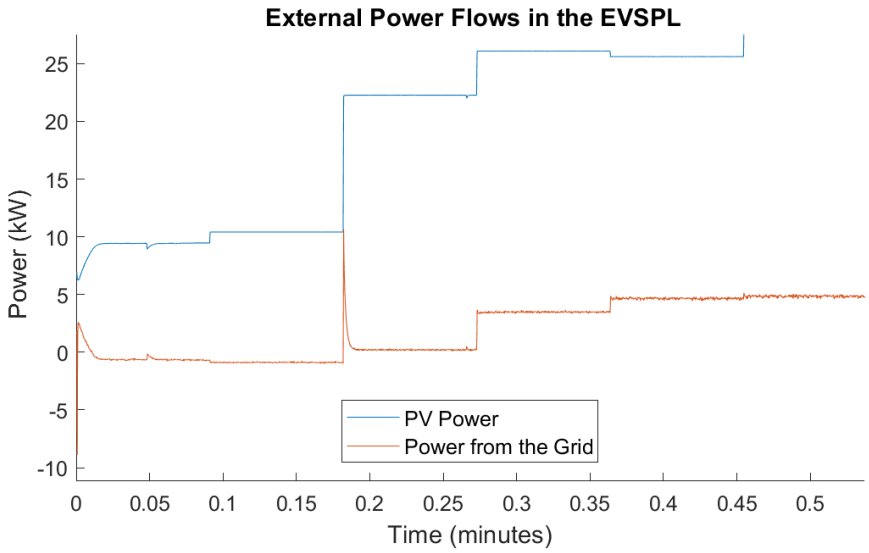

Fig. 36: The power of the grid during the change from constant current charging, to constant voltage charging.

Discussion & Conclusion

The overall simulations of the EVSPL and its control strategy have been executed. Multi-Level Control works appropriately in the EVSPL, however there are some adaptions which could improve the process.

First of all, chattering occurs at the current flows to the EVs. This has to do with the differences in the battery capacity and the change in voltage over time accompanied to this process. Introducing adaptive second-order sliding mode control, in terms of the battery capacity and the input current, might resolve this issue. A recommendation would be to further research adaptive SOSMC in combination with battery modelling.

Secondly, from around 85−90% the charging switches from constant current control to constant voltage control. This process provides safety for the possibility of overcharging the battery, however it reduces the impact of the HLCer. Possible solutions could be to improve the MPC model of the HLCer, or to create a method which translates the amount of power to a non-constant desired current. Due to time limitations, these topics are assigned to further research.

Lastly, the MLC method was tested for a very short time frame of a mere 2 minutes. The reason for this is the different time scales which are necessary to evaluate the combination of Higher- and Lower-Level Control. The LLCer needs very short time instants to execute the Pulse-Width-Modulation techniques carefully, while the HLC only shows great advantages when the disturbances of the environment are taken into account. These however, can only be predicted using average values for much bigger time instants. The limitations of computing power made it impossible to test the MLC strategy for a longer time span.

8 Limitations & Further Work

In this section, first the limitations of this thesis are discussed. The made assumptions regarding simulation time frames, the MPC model, battery modelling, and are explained. The section is finalised with the options for further research, which result from the limitations of this thesis.

First of all it should be noted that combining the Lower- and Higher-Level control strategies is a difficult task, due to enormous differences in the time scale. The LLCer requires very short time instants to provide network stability, due to the frequent switching behaviour of the DC/DC converters. In contrast, the HCLer is most purposeful for larger time instants, as it aims to predict external disturbances in the RES' behaviour. The lack of high computation power resulted in short simulation studies when Multi-Level Control was investigated. Further research should make clear whether longer time spans provide the same results.

In terms of the LLCer, second-order sliding mode control was used to provide stability to the EVSPL. As the capacity of the EVs slightly changes the behaviour of the power flows changes as well. Improvements can be made by tuning the SMC gain for different EVs and the desired current inflow. This would imply a more complicated control method referred to as 'adaptive second-order sliding mode control' (Utkin and Poznyak, 2013).

As it was not the goal of this thesis to design a detailed MPC model, a relatively simple model was used to demonstrate the effects of multi-level control. Yet, an option for further research would be to elaborate on the MPC model to create more insight in the operational issues of an EVSPL. Suggestions would be to introduce pricing strategies, implement a more realistic prediction of the solar irradiance or elaborate more on the huge variety of EVs which is constantly growing.

Furthermore, battery charging and discharging is a complex process which is accompanied with complicated battery modelling, according to an abundance of options. In this thesis, Simulink's nonlinear description of a rechargeable battery was used to model the BESS as well as the EVs' batteries. Assumptions within this model are; the use of a constant internal resistance, the absence of the Peukert effect, and the absence of self-discharge options. Although the battery model also implies temperature and ageing effect, these were neither taken into account during this thesis.

Another aspect which should be noted is the fact that during charging, the Lithium-Ion cells are usually described in multiple phases of which Constant-Current charging and Constant Voltage charging are most interesting in the field of EVs. In this thesis, the main focus is on the current charging phase, as it will charge the battery up to 85% and creates convenience for the EVSPL to control the desired power flows more accurately. The Constant Voltage charging phase should be emphasised more in future research, as it will improve the overall stability of the MG.

Lastly, but maybe most importantly for future research; is the lack of field testing in the area of EVSPLs. It is highly recommended to expand the experimentation of EV batteries in real MGs and their response on different charging strategies. Therefore, it is recommended to test the MLC strategy in a real setting.

To summarise, options for further research imply field testing, an extended simulation time span, a more detailed MPC model and a better controlled constant voltage charging phase for EVs in future EVSPLs.

9 Conclusion

In the introduction the problem was defined as the limitations of insight regarding operational issues of EVSPLs and its control. After an extended literature review, the open issues regarding the problem appeared. From the open issues, it was chosen to focus on the integration of the electrical charging in a MGs, the usage of Power Systems Analysis Tools and on V1G power flows in this thesis. This lead to the research goal of designing an easily scalable, realistic simulation model of an EVSPL, including its control strategy.

After describing the system and its control carefully, it was chosen to model the EVSPL using a PV array, a BESS, multiple EVs, a central control hub, and a connection to the utility grid. The Micro-Grid is stabilised at 500V DC using a 3-Level Bridge at the connection to the utility grid. Maximum power is generated at the PV array, using a MPPT control algorithm. The power flows to the EVs and the BESS, are controlled using DC/DC Bi-Directional converters.

A Multi-Level Control method is introduced, which combines Higher-Level Control and Lower-Level Control. The HLCer is based on the MPC methodology, and takes into account future time steps The result of the HLCer are charging setpoints for the LLCer which is responsible for stabilising the power flows using the DC/DC converters. Nonlinear second-order Sliding Mode Control in combination with Pulse-Width-Modulation is used to provide stability in the EVSPL.

In section 7 multiple scenarios are defined and executed regarding the different control methods. Scenario I elaborated on the LLCer, by providing a clear comparison study between PI Control and second-order Sliding Mode Control in terms of stability, where second-order Sliding Mode Control clearly presented the best results.

Scenario II elaborated upon the performance of the MPC model which is used by the HLC in terms of disturbances of the environment. It was concluded that in increase in the prediction horizon provided improved results, yet also higher computation power. Furthermore,the model anticipated well on external disturbances and passed the test of being scalable. Improvements can be made regarding the amount of detail in which the MPC model is designed.

Lastly, scenario III combined the Multi-Level Control method using the constructed model of the EVSPL, unfortunately only on a short time frame due to the absence of high computation power. Although slight chattering occurred during the simulations, the control method is able to keep the network adequately balanced in the linear- and nonlinear area of the charging curve.

To come back to the goal defined in section 3, a realistic model of an EVSPL, including Multi-Level control was successfully designed in this thesis. The constructed scenarios provided insights in the operational issues of the EVSPL and options for further research imply extended simulation time frames, a more detailed MPC model and a more thorough constant voltage charging phase for the EVs in future EVSPLs.

10 Appendix A: The Lay-Out of the EVSPL

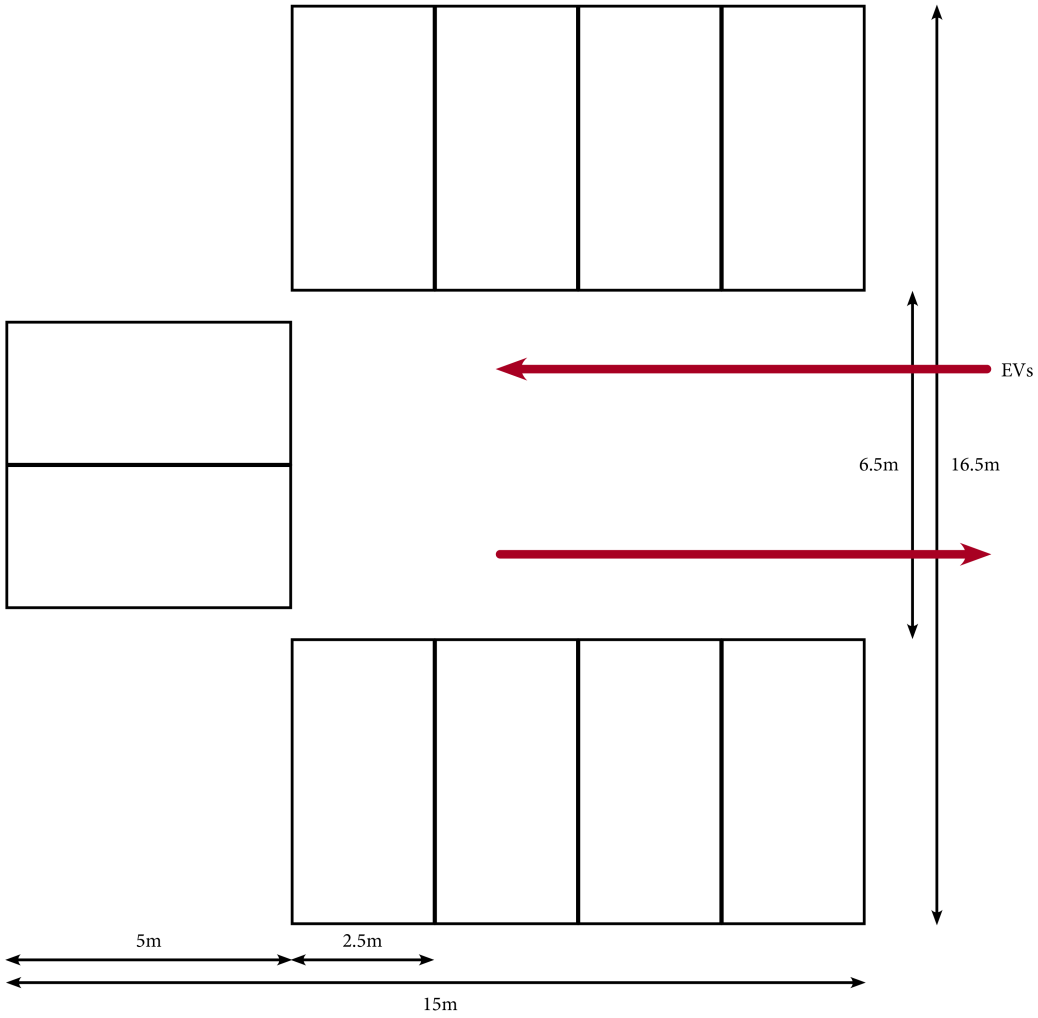

Fig. 37: The lay-out of the parking places in 'basic conditions' is shown. According to MUTCD (2009), the most convenient configuration is parking place with an angle of 90 degrees with the driving lane. The average size of one parking place is $5m$ x $2.5m$ and the driving lanes within a parking lot must at least be $6.5m$ in width.

$$\text{Surface Area of the EVSPL} = 16.5 * 15 = 247.5m^2 \tag{63}$$

11 Appendix B: Parameters of the Simulation Model in Simulink

Block	**Parameter**	**Value**	
General	Solver	Tustin	
General	Solver Fixed Step	Discrete	
General	Time Steps Control	$5 * 10^{-6}$	s
General	Time Steps Power	$1 * 10^{-6}$	s
BESS Bi-Directional Converter	f	5000	Hz
BESS Converter PI	Boost K_p	0.05	
BESS Converter PI	Boost K_i	100	
BESS Converter PI	Buck K_p	0.1	
BESS Converter PI	Buck K_i	50	
BESS Converter SMC	Boost K	2000	
BESS Converter SMC	Buck K	500	
BESS Converter SMC	Starting Condition x_0	0	
EV Bi-Directional Converter	f	5000	Hz
EV Converter SMC	K	Variable	
EV Converter SMC	Starting Condition x_0	0	
MPPT Boost Converter	K_p	1	
MPPT Boost Converter	K_i	7	
MPPT Boost Converter	f	5000	Hz
VSC Converter	Voltage K_p	7	
VSC Converter	Voltage K_i	800	
VSC Converter	Current K_p	0.3	
VSC Converter	Current K_i	20	
VSC Converter	f	$33 * 60$	Hz

Tab. 28: The parameters of the simulation model built using Simulink. The converter at the BESS has values for PI control as well as SMC, due to scenario I, as described in subsection 7.1.

The parameters for the different capacities of the batteries are shown below:

Block	Q_{max}	Buck Mode	Boost Mode
BESS	200	500	2000
TESL	100	900	-
NISS	24	700	-
CHEV	18.4	600	-

Tab. 29: The parameters for the sliding mode controller.

12 Appendix C: The Solar Irradiance

In Figure 38, the predicted direct normal irradiance can be found. This is used in the MPC model, as described in subsection 6.2. The average is shown in Figure 39. All data was retrieved from the database of the National Solar Radiation Data Base (NREL, 2010). The data encompasses the average monthly DNI in Los Angeles in the year 2010.

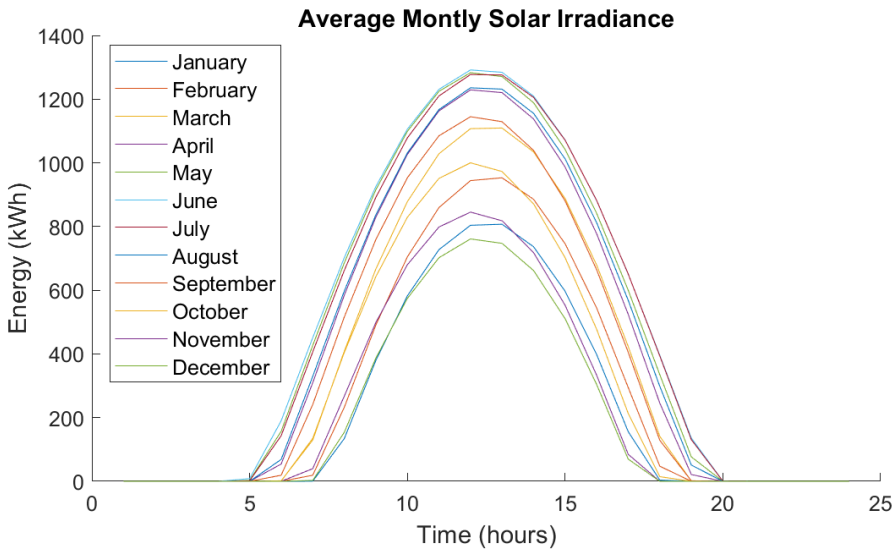

Fig. 38: The average solar irradiance for different months are shown.

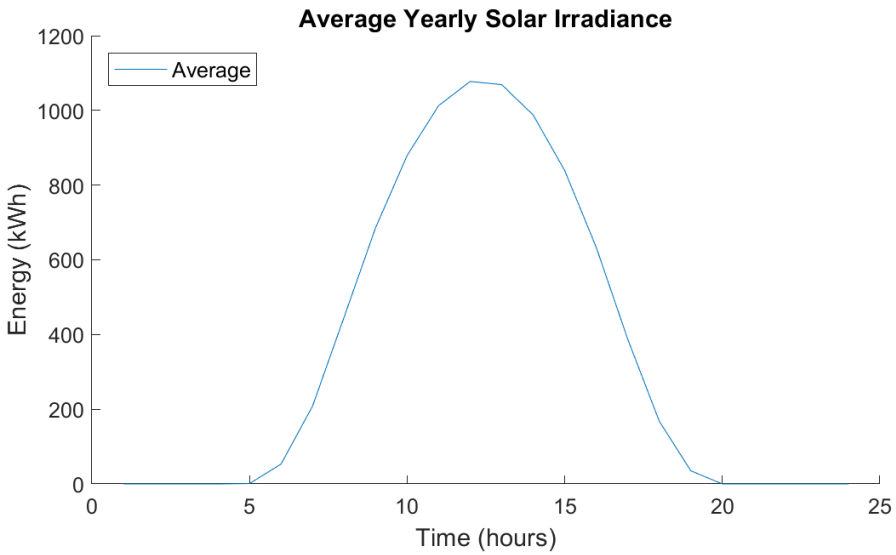

Fig. 39: The average solar yearly irradiance of 2010 is shown.

13 Appendix D: The Arrival Pattern of Scenario II

Name	Brand	Q (kWh)	Q_0 (%)	Q_{des} (%)	EV_{maxin} (kW)	t_{arr} ($hh:mm:ss$)	$t_{dep,planned}$ ($hh:mm:ss$)	$t_{dep,real}$ ($hh:mm:ss$)
EV1	CHEV	18.4	10.0	91.7	3.3	08:44:56	12:13:05	12:48:34
EV2	TESL	100	22.0	73.0	145	08:37:56	17:55:33	18:22:20
EV3	NISS	24	10.0	82.5	16	07:34:46	17:53:07	18:38:06
EV4	TESL	100	56.0	90.0	145	14:54:40	16:10:14	16:30:12
EV5	TESL	100	50.0	86.0	145	07:47:02	17:51:02	17:46:32
EV6	TESL	100	34.0	80.0	145	08:05:08	17:21:09	17:36:57
EV7	NISS	24	39.2	95.0	16	08:25:28	16:07:11	16:17:27
EV8	TESL	100	51.0	73.0	145	08:47:12	17:10:21	17:32:56
EV9	TESL	100	54.0	78.0	145	08:48:47	17:51:27	18:17:28
EV10	TESL	100	16.0	100.0	145	08:41:18	10:03:00	10:11:15
EV11	TESL	100	18.0	98.0	145	07:34:57	17:53:05	18:06:00
EV12	CHEV	18.4	53.5	70.0	3.3	08:13:01	17:12:42	17:39:51
EV13	TESL	100	63.0	92.0	145	08:02:13	12:00:19	12:25:58
EV14	NISS	24	35.0	86.7	16	08:51:43	16:35:59	16:38:40
EV15	TESL	100	29.0	99.0	145	08:37:48	17:02:11	17:37:43
EV16	NISS	24	30.8	74.2	16	08:55:12	17:03:19	17:20:51
EV17	TESL	100	27.0	78.0	145	07:47:40	17:08:21	17:19:14
EV18	NISS	24	43.3	86.7	16	07:51:01	17:37:27	18:02:34
EV19	TESL	100	44.0	92.0	145	11:30:32	16:45:15	16:59:21
EV20	NISS	24	55.8	70.0	16	08:23:15	16:36:10	17:17:09
EV21	CHEV	18.4	58.9	80.9	3.3	07:53:51	16:22:05	16:15:37
EV22	NISS	24	22.5	95.0	16	08:59:16	17:51:59	17:56:01
EV23	NISS	24	26.7	78.3	16	08:09:43	17:54:30	18:00:53
EV24	NISS	24	39.2	95.0	16	07:13:14	17:28:49	17:40:24
EV25	CHEV	18.4	58.9	86.3	3.3	07:30:22	17:09:36	17:23:58
EV26	TESL	100	63.0	92.0	145	08:02:13	12:00:19	12:25:58
EV27	NISS	24	35.0	86.7	16	08:51:43	16:35:59	16:38:40
EV28	TESL	100	29.0	99.0	145	08:37:48	17:02:11	17:37:43
EV29	NISS	24	30.8	74.2	16	08:55:12	17:03:19	17:20:51
EV30	TESL	100	27.0	78.0	145	07:47:40	17:08:21	17:19:14
EV31	NISS	24	43.3	86.7	16	07:51:01	17:37:27	18:02:34
EV32	TESL	100	44.0	92.0	145	11:30:32	16:45:15	16:59:21
EV33	NISS	24	55.8	70.0	16	08:23:15	16:36:10	17:17:09
EV34	CHEV	18.4	58.9	80.9	3.3	07:53:51	16:22:05	16:15:37
EV35	NISS	24	22.5	95.0	16	08:59:16	17:51:59	17:56:01
EV36	NISS	24	26.7	78.3	16	08:09:43	17:54:30	18:00:53
EV37	NISS	24	39.2	95.0	16	07:13:14	17:28:49	17:40:24
EV38	CHEV	18.4	58.9	86.3	3.3	07:30:22	17:09:36	17:23:58
EV39	TESL	100	27.0	78.0	145	07:47:40	17:08:21	17:19:14
EV40	NISS	24	43.3	86.7	16	07:51:01	17:37:27	18:02:34
EV41	TESL	100	44.0	92.0	145	11:30:32	16:45:15	16:59:21
EV42	TESL	100	56.0	90.0	145	14:54:40	16:10:14	16:30:12
EV43	TESL	100	50.0	86.0	145	07:47:02	17:51:02	17:46:32
EV44	NISS	24	39.2	95.0	16	07:13:14	17:28:49	17:40:24
EV45	NISS	24	22.5	95.0	16	08:59:16	17:51:59	17:56:01
EV46	NISS	24	26.7	78.3	16	08:09:43	17:54:30	18:00:53
EV47	NISS	24	39.2	95.0	16	07:13:14	17:28:49	17:40:24
EV48	CHEV	18.4	58.9	86.3	3.3	07:30:22	17:09:36	17:23:58
EV49	TESL	100	63.0	92.0	145	08:02:13	12:00:19	12:25:58
EV50	NISS	24	39.2	95.0	16	07:13:14	17:28:49	17:40:24

Tab. 30: The arrival data of the EVs in scenario II.

References

Arcus, C. (2016). A tale of 3 battery packs. https://cleantechnica.com/2016/01/06/a-tale-of-3-battery-packs/.

Babic, J., Carvalho, A., Ketter, W., and Podobnik, V. (2016). Modelling electric vehicle owners' willingness to pay for a charging service. In *Proceedings of the Erasmus Energy Forum*, pages 1–8.

Babic, J., Carvalho, A., Ketter, W., and Podobnik, V. (2017). Electricity trading agent for ev-enabled parking lots. In *International Workshop on Agent-Mediated Electronic Commerce and Trading Agents Design and Analysis*, pages 35–49. Springer.

Bartolini, G., Ferrara, A., and Usai, E. (1998a). Chattering avoidance by second-order sliding mode control. *IEEE transactions on Automatic Control*, 43(2):241–246.

Bartolini, G., Ferrara, A., and Usai, E. (1998b). On boundary layer dimension reduction in sliding mode control of siso uncertain nonlinear systems. In *Control Applications, 1998. Proceedings of the 1998 IEEE International Conference on*, volume 1, pages 242–247. IEEE.

Bhatti, A. R., Salam, Z., Aziz, M. J. B. A., Yee, K. P., and Ashique, R. H. (2016). Electric vehicles charging using photovoltaic: Status and technological review. *Renewable and Sustainable Energy Reviews*, 54:34–47.

Birnie, D. P. (2009). Solar-to-vehicle (s2v) systems for powering commuters of the future. *Journal of Power Sources*, 186(2):539 – 542.

Camacho, E. F. and Alba, C. B. (2013). *Model predictive control*. Springer Science & Business Media.

Chakraborty, S., Simões, M. G., and Kramer, W. E. (2013). Power electronics for renewable and distributed energy systems. *A Sourcebook of Topologies, Control and Integration*, 99:100.

Chan, P. W. (2010). Dc-dc boost converter with constant output voltage for grid connected photovoltaic application system. In *Industrial Electronic Seminar*.

Chevrolet (2017). Configure chevrolet volt. http://www.chevrolet.com/byo-vc/client/en/US/chevrolet/volt/2018/volt/trim.

Cucuzzella, M., Lazzari, R., Trip, S., Rosti, S., Sandroni, C., and Ferrara, A. (2018). Sliding mode voltage control of boost converters in dc microgrids. *Control Engineering Practice*, 73:161–170.

Cucuzzella, M., Trip, S., De Persis, C., Ferrara, A., and van der Schaft, A. (2017). A robust consensus algorithm for current sharing and voltage regulation in dc microgrids. *arXiv preprint arXiv:1708.04608*.

Dhameja, S. (2001). *Electric vehicle battery systems*. Newnes.

Di Giorgio, A., Liberati, F., and Canale, S. (2014). Electric vehicles charging control in a smart grid: A model predictive control approach. *Control Engineering Practice*, 22:147–162.

EIA (2014). Technology solar roadmap 2014. -.

EIA (2017). World energy outlook 2017. -.

Elsayed, A. T., Mohamed, A. A., and Mohammed, O. A. (2015). Dc microgrids and distribution systems: An overview. *Electric Power Systems Research*, 119:407–417.

Fazelpour, F., Vafaeipour, M., Rahbari, O., and Rosen, M. A. (2014). Intelligent optimization to integrate a plug-in hybrid electric vehicle smart parking lot with renewable energy resources and enhance grid characteristics. *Energy Conversion and Management*, 77:250–261.

Gan, L., Topcu, U., and Low, S. H. (2013). Optimal decentralized protocol for electric vehicle charging. *IEEE Transactions on Power Systems*, 28(2):940–951.

García-Villalobos, J., Zamora, I., San Martín, J., Asensio, F., and Aperribay, V. (2014). Plug-in electric vehicles in electric distribution networks: A review of smart charging approaches. *Renewable and Sustainable Energy Reviews*, 38:717–731.

Gearheads (2017). World's top 10 best-selling electric vehicles. https://gearheads.org/worlds-top-10-best-selling-electric-vehicles/.

Goli, P. and Shireen, W. (2014). Pv powered smart charging station for phevs. *Renewable Energy*, 66:280–287.

Halvgaard, R., Poulsen, N. K., Madsen, H., Jørgensen, J. B., Marra, F., and Bondy, D. E. M. (2012). Electric vehicle charge planning using economic model predictive control. In *Electric Vehicle Conference (IEVC), 2012 IEEE International*, pages 1–6. IEEE.

Hamilton, C., Gamboa, G., Elmes, J., Kerley, R., Arias, A., Pepper, M., Shen, J., and Batarseh, I. (2010). System architecture of a modular direct-dc pv charging station for plug-in electric vehicles. In *IECON 2010-36th Annual Conference on IEEE Industrial Electronics Society*, pages 2516–2520. IEEE.

Hatziargyriou, N. et al. (2014). *Microgrids: architectures and control*. Wiley Online Library.

Holmes, D. G. and Lipo, T. A. (2003). *Pulse width modulation for power converters: principles and practice*, volume 18. John Wiley & Sons.

Honarmand, M., Zakariazadeh, A., and Jadid, S. (2014a). Integrated scheduling of renewable generation and electric vehicles parking lot in a smart microgrid. *Energy Conversion and Management*, 86:745–755.

Honarmand, M., Zakariazadeh, A., and Jadid, S. (2014b). Optimal scheduling of electric vehicles in an intelligent parking lot considering vehicle-to-grid concept and battery condition. *Energy*, 65:572–579.

Honarmand, M., Zakariazadeh, A., and Jadid, S. (2015). Self-scheduling of electric vehicles in an intelligent parking lot using stochastic optimization. *Journal of the Franklin Institute*, 352(2):449–467.

Incremona, G. P., Cucuzzella, M., and Ferrara, A. (2016). Adaptive suboptimal second-order sliding mode control for microgrids. *International Journal of Control*, 89(9):1849–1867.

Justo, J. J., Mwasilu, F., Lee, J., and Jung, J.-W. (2013). Ac-microgrids versus dc-microgrids with distributed energy resources: A review. *Renewable and Sustainable Energy Reviews*, 24:387–405.

Kazimierczuk, M. K. (2015). *Pulse-width modulated DC-DC power converters*. John Wiley & Sons.

Knezović, K., Martinenas, S., Andersen, P. B., Zecchino, A., and Marinelli, M. (2017). Enhancing the role of electric vehicles in the power grid: field validation of multiple ancillary services. *IEEE Transactions on Transportation Electrification*, 3(1):201–209.

Lai, J.-S. and Chen, D. (1993). Design consideration for power factor correction boost converter operating at the boundary of continuous conduction mode and discontinuous conduction mode. In *Applied Power Electronics Conference and Exposition, 1993. APEC'93. Conference Proceedings 1993., Eighth Annual*, pages 267–273. IEEE.

Ma, J. and Horie, M. (2017). The leaf is the world's best-selling electric car. now, nissan needs to catch up with tesla. https://www.bloomberg.com/news/articles/2017-08-29/the-leaf-is-the-world-s-best-selling-electric-car-now-nissan-needs-to-catch-up-with-tesla.

Mathworks (2017a). Implement generic battery model. https://nl.mathworks.com/help/physmod/sps/powersys/ref/battery.html.

Mathworks (2017b). Implement pv array modules. https://nl.mathworks.com/help/physmod/sps/powersys/ref/pvarray.html?s_tid=srchtitle.

Mathworks (2017c). Simscape power systems. https://nl.mathworks.com/products/simpower.html.

Mohamed, A., Salehi, V., Ma, T., and Mohammed, O. (2014). Real-time energy management algorithm for plug-in hybrid electric vehicle charging parks involving sustainable energy. *IEEE Transactions on Sustainable Energy*, 5(2):577–586.

Moradijoz, M., Moghaddam, M. P., Haghifam, M., and Alishahi, E. (2013). A multi-objective optimization problem for allocating parking lots in a distribution network. *International Journal of Electrical Power & Energy Systems*, 46:115–122.

MUTCD (2009). Manual and uniform traffic control devices. https://mutcd.fhwa.dot.gov/htm/2009/html_index.htm.

Mwasilu, F., Justo, J. J., Kim, E.-K., Do, T. D., and Jung, J.-W. (2014). Electric vehicles and smart grid interaction: A review on vehicle to grid and renewable energy sources integration. *Renewable and Sustainable Energy Reviews*, 34:501–516.

Naceur, K. and Gagné, J. (2017). Global EV Outlook 2017; Two million and counting.

Nazri, G.-A. and Pistoia, G. (2008). *Lithium batteries: science and technology*. Springer Science & Business Media.

Nissan (2017). Battery performance nissan leaf. https://www.nissan.co.uk/vehicles/new-vehicles/leaf/battery-performance.html.

Nitta, N., Wu, F., Lee, J. T., and Yushin, G. (2015). Li-ion battery materials: present and future. *Materials today*, 18(5):252–264.

NREL (2010). National Solar Radiation Data Base.

Nunes, P., Farias, T., and Brito, M. C. (2015). Day charging electric vehicles with excess solar electricity for a sustainable energy system. *Energy*, 80:263–274.

Nunes, P., Figueiredo, R., and Brito, M. C. (2016). The use of parking lots to solar-charge electric vehicles. *Renewable and Sustainable Energy Reviews*, 66:679–693.

Pahasa, J. and Ngamroo, I. (2015). Phevs bidirectional charging/discharging and soc control for microgrid frequency stabilization using multiple mpc. *IEEE Transactions on Smart Grid*, 6(2):526–533.

Pahasa, J. and Ngamroo, I. (2016). Coordinated control of wind turbine blade pitch angle and phevs using mpcs for load frequency control of microgrid. *IEEE Systems Journal*, 10(1):97–105.

Pierre Giroux, G. S. (2012). Grid-connected pv array. https://nl.mathworks.com/matlabcentral/fileexchange/34752-grid-connected-pv-array.

Preetham, G. and Shireen, W. (2012). Photovoltaic charging station for plug-in hybrid electric vehicles in a smart grid environment. In *Innovative Smart Grid Technologies (ISGT), 2012 IEEE PES*, pages 1–8. IEEE.

Rahbari, O., Vafaeipour, M., Omar, N., Rosen, M. A., Hegazy, O., Timmermans, J.-M., Heibati, M., and Van Den Bossche, P. (2017). An optimal versatile control approach for plug-in electric vehicles to integrate renewable energy sources and smart grids. *Energy*.

Richardson, D. B. (2013). Electric vehicles and the electric grid: A review of modeling approaches, impacts, and renewable energy integration. *Renewable and Sustainable Energy Reviews*, 19:247–254.

Robinson, J., Brase, G., Griswold, W., Jackson, C., and Erickson, L. (2014). Business models for solar powered charging stations to develop infrastructure for electric vehicles. *Sustainability*, 6(10):7358–7387.

Sahan, Z. (2017). Electric car charging capabilities — comparison of 27 models. https://evobsession.com/electric-car-charging-capabilities-comparison-of-27-models/.

Saleh, M., Esa, Y., Mhandi, Y., Brandauer, W., and Mohamed, A. (2016). Design and implementation of ccny dc microgrid testbed. In *Industry Applications Society Annual Meeting, 2016 IEEE*, pages 1–7. IEEE.

Shtessel, Y., Edwards, C., Fridman, L., and Levant, A. (2014). *Sliding mode control and observation*, volume 10. Springer.

Sira-Ramirez, H. J. and Silva-Ortigoza, R. (2006). *Control design techniques in power electronics devices*. Springer Science & Business Media.

Su, W., Wang, J., Zhang, K., and Huang, A. Q. (2014). Model predictive control-based power dispatch for distribution system considering plug-in electric vehicle uncertainty. *Electric Power Systems Research*, 106:29–35.

Sultana, W. R., Sahoo, S. K., Sukchai, S., Yamuna, S., and Venkatesh, D. (2017). A review on state of art development of model predictive control for renewable energy applications. *Renewable and Sustainable Energy Reviews*, 76:391–406.

Tesla (2017). Configure tesla model s. https://www.tesla.com/nl_NL/models/design.

Top10Reviews (2017). The best solar panels. http://www.toptenreviews.com/home/smart-home/best-solar-panels/.

Traube, J., Lu, F., and Maksimovic, D. (2012). Photovoltaic power system with integrated electric vehicle dc charger and enhanced grid support. In *Power Electronics and Motion Control Conference (EPE/PEMC), 2012 15th International*, pages LS1d–5. IEEE.

Tremblay, O., Dessaint, L.-A., and Dekkiche, A.-I. (2007). A generic battery model for the dynamic simulation of hybrid electric vehicles. In *Vehicle Power and Propulsion Conference, 2007. VPPC 2007. IEEE*, pages 284–289. Ieee.

Tulpule, P. J., Marano, V., Yurkovich, S., and Rizzoni, G. (2013). Economic and environmental impacts of a pv powered workplace parking garage charging station. *Applied Energy*, 108:323–332.

Utkin, V. I. and Poznyak, A. S. (2013). Adaptive sliding mode control. In *Advances in sliding mode control*, pages 21–53. Springer.

Visioli, A. (2006). *Practical PID control*. Springer Science & Business Media.

Widén, J., Carpman, N., Castellucci, V., Lingfors, D., Olauson, J., Remouit, F., Bergkvist, M., Grabbe, M., and Waters, R. (2015). Variability assessment and forecasting of renewables: A review for solar, wind, wave and tidal resources. *Renewable and Sustainable Energy Reviews*, 44:356–375.

Wieringa, R. J. (2014). *Design Science Methodology for Information Systems and Software Engineering*. Springer.

Yan, J., Xu, G., Qian, H., Xu, Y., and Song, Z. (2011). Model predictive control-based fast charging for vehicular batteries. *Energies*, 4(8):1178–1196.

Yilmaz, M. and Krein, P. T. (2013). Review of battery charger topologies, charging power levels, and infrastructure for plug-in electric and hybrid vehicles. *IEEE Transactions on Power Electronics*, 28(5):2151–2169.

Zakariazadeh, A., Jadid, S., and Siano, P. (2014). Multi-objective scheduling of electric vehicles in smart distribution system. *Energy Conversion and Management*, 79:43–53.

Zakariazadeh, A., Jadid, S., and Siano, P. (2015). Integrated operation of electric vehicles and renewable generation in a smart distribution system. *Energy Conversion and Management*, 89:99–110.